THE DECOMPOSITION OF AMMONIA ON TUNGSTEN SURFACES

THE DECOMPOSITION OF AMMONIA ON TUNGSTEN SURFACES

by

YU KWANG PENG, DIPL. CHEM.

A Thesis

Submitted to the School of Graduate Studies

in Partial Fulfilment of the Requirements

for the Degree

Doctor of Philosophy

McMaster University

(February) 1973

DOCTOR OF PHILOSOPHY
(Chemistry)

McMASTER UNIVERSITY
Hamilton, Ontario.

TITLE: The Decomposition of Ammonia on Tungsten Surfaces

AUTHOR: Yu Kwang Peng, B.Sc. (Cheng Kung University)
Dipl. Chem. (Technical University Hannover, Germany)

SUPERVISOR: Professor P. T. Dawson

NUMBER OF PAGES: XV, 208

SCOPE AND CONTENTS:

This thesis presents an experimental study of the decomposition of ammonia on tungsten surfaces. The investigations were made at ammonia pressures between 10^{-7} and 10^{-2} torr, and at temperatures between 200 and 800^{o}K by employing thermal desorption mass spectrometry and field emission microscopy. The surface species formed during the interaction were first isolated and the rate parameters for the formation and desorption of these species were determined. The properties of the adlayer of these species were also studied. Based on the rate parameters for the formation and desorption of these species a satisfactory mechanism for the decomposition of ammonia on tungsten surfaces has been deduced.

ACKNOWLEDGEMENTS

The author wishes to express his most sincere gratitude to his supervisor, Professor P. T. Dawson, for his guidance and encouragement throughout the course of this work, and for his valuable criticisms and suggestions during the preparation of this thesis.

The author wishes to thank Professors R. B. Anderson and C. Calvo for their helpful suggestions and reading of the manuscript.

The author also wishes to thank his wife, Anita, for her patience and constant encouragement.

Finally, the author wishes to acknowledge the receipt of financial support from the Chemistry Department for all the time spent in this university.

TABLE OF CONTENTS

LIST OF FIGURES

LIST OF TABLES

CHAPTER 1

INTRODUCTION

1.1 General.

The decomposition of ammonia on tungsten surfaces has been studied for over forty years. It is generally accepted that the decomposition is kinetically zero order with respect to ammonia and that there exists a kinetic hydrogen isotope effect, i.e. the decomposition rates of ammonia and deutero-ammonia are different. However, no satisfactory mechanism has yet been described to account for these observations. In the earlier studies, due to limitations of experimental technique, the surface processes were inferred from the rates of disappearance and appearance of reactants and products. The recent enormous improvement in experimental techniques enables one to study the reaction on well defined surfaces in ultra-high vacuum and to study the surface species directly.

In general, the overall mechanism of a reaction consists of several reaction steps; the first task of the study is thus to separate the complex reaction into its components and to investigate each individual step. The flash desorption technique makes this kind of study possible by investigating the surface species formed under different reaction conditions. This technique consists of following partial

pressure changes when the sample is heated at the end of an adsorption period, and yields information concerning the different binding states and the kinetics of adsorption and desorption. The properties of the species detected by the flash desorption method can be further investigated by employing the field electron emission microscopy which enables one to observe the surface directly and to follow rapid changes in the adsorbed layer. The combination of these two techniques thus offers a powerful tool for catalytic studies, and should lead to a thorough understanding of surface reactions.

In this work, ammonia decomposition on tungsten surfaces is studied by employing these two techniques. This is achieved by investigating the individual surface species formed under widely different decomposition conditions.

1.2 Current status of studies on the interaction of ammonia with tungsten surfaces.

The first systematic study of ammonia decomposition on tungsten surfaces was carried out by Hinshelwood and Burke [1]. They showed that at temperatures between 900 to 1200^{o}K the decomposition was zero order with respect to ammonia and that rate was not influenced by the decomposition products. These results, subsequently confirmed by many workers [2-4], have been interpreted as being due to

the saturation of the surface with ammonia.

On the other hand, Frankenburger and Hodler [5] showed that a rapid first step of the decomposition was the formation of a surface nitride which took place at temperature as low as 363°K and was followed by imide formation at higher coverages with the concurrent adsorption of increasing amounts of undecomposed ammonia

$$W_x + 2NH_3 \rightarrow W_xN_2 + 3H_2$$

$$W_x + NH_3 \rightarrow W_xNH + H_2$$

At lower temperatures (363 to 523°K) this nitride and imide formation was the only step and decomposition ceased after it was completed.

The observations of Jungers and Taylor [6] and also of Barrer [7] made an important advance in the understanding of this reaction. They showed the existence of a kinetic isotope effect in the decomposition rates of ammonia and deutero-ammonia at ~ 1000°K; NH_3 decomposed 1.6 times faster than ND_3. Since both reactions are zero order with respect to ammonia and hydrogen, the difference in rate was ascribed to the greater stability of the ND_3 molecule on the surface. A difference in zero point energies of 900 cals between NH_3 and ND_3 would account for the difference in rates. Thus, the rate determining step was identified as the breaking of an N-H (or N-D) bond and not the desorption of nitrogen.

More recently, Tamaru[8] has

measured the rate of decomposition between 548 and 873°K. Below 723°K, no nitrogen desorption was observed and the surface was covered with about a monolayer of nitrogen plus some hydrogen. For temperatures above 773°K, nitrogen was produced in the ambient. In addition, practically no hydrogen containing species was inferred to be present on the surface at 873°K, which would invalidate the interpretation of the zero order kinetics at higher temperatures as being due to the saturated adsorption of NH_3 or NH. The rate of decomposition at 823 and 873°K was claimed to equal the rate of nitrogen desorption at the same temperature and coverage of nitrogen. This led Tamaru to conclude that the decomposition was a consecutive reaction of nitride formation and nitrogen desorption and that nitrogen desorption was the rate limiting step. In order to account for the isotope effect, it was suggested that extent of nitriding, and therefore the rate of desorption, differed for NH_3 and ND_3.

In even more recent work, instead of deducing the surface processes from the rate of disappearance and appearance of reactants and products, emphasis has been on trying to identify the adsorbed species directly using well defined surfaces and different techniques such as field electron emission microscopy [9], low energy electron diffraction (LEED) [10,11] and flash desorption spectrometry [12].

In the field emission study of ammonia decomposition on tungsten, Dawson and Hansen [9] found that ammonia

adsorption at 200°K produced an immobile deposit which decomposed over the temperature interval 200-400°K to leave a β-nitrogen adlayer which has a surface stoichiometry, W_2N. This decomposition sequence, implying β-nitrogen desorption rate limiting, was unacceptable since the desorption rate is too slow [13]. New surface species which were tentatively assigned stoichiometries such as $W_2\overset{+}{N}NH_3$ and W_2NNH_2 were observed when ammonia interaction took place at higher temperatures, 500°K for example. The observed variation in work function with temperature was taken to indicate that the species W_2NNH_2, which gave rise to a high work function, decomposed at temperature ∿ 900°K, i.e. in the range of the effective catalysis of the ammonia decomposition by tungsten. This led them to conclude that the rate limiting step in the overall decomposition mechanism was the decomposition of this surface species

$$W_2NNH_2 \rightarrow 2W + N_2(g) + H_2(g)$$

The decomposition of ammonia on a single-crystal tungsten {100} plane has recently been studied at pressures below 10^{-7} torr with a combination of techniques, LEED and flash desorption spectrometry, by Estrup and Anderson [10]. They observed that the adsorption of ammonia at 300°K was nondissociative and that raising the temperature to ∿ 800°K after saturation resulted in dissociation of ammonia and desorption of hydrogen, leaving behind half a monolayer of

NH_2 in a C(2x2) structure (an adsorbed overlayer with double the spacing of the substrate and a centering adatom). This structure could be destroyed rapidly at $\sim$ 1375°K with desorption of nitrogen and hydrogen. In addition, repeated ammonia adsorption at 300°K with intermittent heating to 800°K or ammonia interaction at 800°K caused NH_2 surface concentration to increase to $\sim$ one monolayer. During this process a change from a C(2x2) to a (1x1) structure (one nitrogen atom per surface tungsten atom) was observed. This completed NH_2 adlayer decomposed at temperatures higher than 1100°K and gave rise to the desorption of hydrogen and nitrogen. Similar experiments have been carried out on the W{211} plane by May et al. [11] and the same conclusions were drawn; the decomposition of NH_2 surface species was the rate limiting step. However, since both experiments were carried out in a continuous NH_3 ambient, these results have been questioned and criticized [14].

More recently, in a flash desorption study of ammonia decomposition on tungsten, Matsushita and Hansen [12] showed that repeated ammonia adsorption at 300°K with intermittent heating to 870°K caused an increase in nitrogen surface concentration and a new surface species designated as x-nitrogen was observed. The desorption of x-nitrogen commenced at $\sim$ 870°K with a peak maximum at $\sim$ 1100°K. It was also shown that some of the field emission characteristics of the species obtained by ammonia adsorption [9] could be reproduced

by adsorption of activated nitrogen gas alone [15]. Thus, it was claimed that the species observed in the field emission experiment [9], W_2NNH_2, and that observed in the LEED study [10], WNH_2, were in fact the x-nitrogen. Based on the agreement between the average rate of x-nitrogen desorption measured and rates of ammonia decomposition, they concluded that the desorption of x-nitrogen was the rate limiting step in the decomposition of ammonia on tungsten surfaces.

Though the interpretation of Matsushita and Hansen [12] appears straight-forward, it is not apparent how the isotope effect can be explained by assuming N_2-desorption to be rate limiting. A satisfactory mechanism should be able to explain the zero order reaction and the hydrogen isotope effect. All these studies have thus led to conflicting opinions as to the rate determining step in the decomposition of ammonia on tungsten surfaces. Though recent studies were carried out on well defined surfaces in a ultra-high vacuum system, the proposed mechanisms are no more satisfactory than those obtained in earlier studies.

1.3 Scope of the present work.

The kinetics and mechanism of the decomposition of ammonia on tungsten surfaces has been deduced from a study of the interaction of ammonia gas, at pressures between 10^{-7} and 10^{-2} torr, with tungsten surfaces at temperatures between

200 and 800°K. The study of this interaction under such a large range of conditions is necessary since the species formed at high temperature, which is important for the decomposition process, may not be formed at low temperature and vice versa. The species formed during the interaction were first isolated by choosing the suitable interaction conditions and the rate parameters for the formation and desorption of these species were determined individually, either directly or indirectly. The properties of the adlayer of these species were also studied. Based on the rate parameters for the formation and desorption of these species a satisfactory mechanism for the decomposition of ammonia on tungsten surfaces has been deduced.

CHAPTER 2

FLASH DESORPTION SPECTROMETRY AND FIELD ELECTRON EMISSION MICROSCOPY

2.1 Ultra-high vacuum.

The applicability of modern techniques such as flash desorption spectrometry and field electron emission microscopy in the study of the surface processes is based on the ability to establish and maintain pressures in the ultra-high vacuum range, namely below 10^{-9} torr. In these methods, a sample with a small surface area is generally used, thus even a small amount of contaminant in the system can markedly alter the adsorption characteristics of the sample under study.

It can be shown from the kinetic theory that at a pressure of 10^{-6} torr, it takes only one second to have the sample surface covered with one monolayer of contaminant, if the sticking probability is unity. Thus under this condition the experiment must be completed in a matter of one milli-second to ensure a meaningful result. On the other hand, if the pressure is at $\sim 10^{-10}$ torr, clean surfaces can be maintained for a period of several hours. The necessity of ultra-high vacuum conditions for the study of adsorption phenomena is therefore obvious.

Generally, a pressure in ultra-high vacuum range

can be easily obtained by high temperature bake-out during the pumping to reduce the desorption of gases from the walls at room temperature or by immersing the entire apparatus in liquid hydrogen or helium, thus reducing the vapor pressures of all gases except hydrogen and helium to values $\sim 10^{-13}$ torr.

2.2 Flash desorption spectrometry.

Flash desorption spectrometry has been widely applied for obtaining information about the kinetics of adsorption and desorption. This method consists of following partial pressure changes, when the sample is heated at the end of an adsorption period. If the temperature-time relationship for the sample heating is known, the pressure versus time curve, i.e. desorption spectrum, can be analyzed to obtain information about the number of the various binding states, the population of the individual binding states, and the order and the rate constant of the desorption process.

2.2.1 Single binding state with constant activation energy.

In order to simplify the analysis of the desorption spectra, the heating of the sample is generally achieved by employing either a linear, slow heating [16] or a hyperbolic, fast heating rate [17]. Whereas the former produces highly resolved desorption spectra, the latter produces a uniform sample temperature. In this work, since high resolution is required to avoid the overlap between surface processes and gas phase processes, a linear, slow heating rate

has been employed extensively.

On heating the sample, the rate at which the number of molecules in the gas phase changes depends on the course of the desorption, the temperature-time relation and the rate of removal of gases from the system by pumping, if the desorption of gases from the walls and readsorption on the sample are negligible. The rate of change of the number of molecules in the gas phase in desorption is therefore given by

$$\frac{dN}{dt} = -A\frac{dn}{dt} - \frac{S}{V}N \qquad (1)$$

where N is the number of molecules in the gas phase, $-A\frac{dn}{dt}$ the number of molecules released from the sample with area A per second, S the pumping speed, and V the volume of the system. Alternatively equation (1) can be written as

$$-A\frac{dn}{dt} = \frac{dN}{dt} + \frac{N}{\tau} \qquad (2)$$

where $\tau = V/S$ is a characteristic pumping time. At one extreme of negligible pumping, $\tau \to \infty$, the desorption rate is proportional to the first derivative of the number of molecules in the gas phase versus time. For the other extreme of high pumping speed, $\tau \to 0$, the desorption rate becomes proportional to the number of molecules in the gas phase, hence to the pressure of the system. Under this condition, the pressure versus time curve can therefore be used directly as a desorption rate curve for the evaluation of kinetic

parameters.

The rate of desorption from unit surface area can be represented by an Arrhenius equation,

$$-\frac{dn}{dt} = \nu_x \exp\left(-\frac{E^{\ddagger}}{RT}\right) \cdot n^x \qquad (3)$$

where ν_x is the frequency factor, n the surface coverage in molecules cm^{-2}, x the order of the desorption process, and $E^{\ddagger}$ the activation energy for desorption. During desorption with a linear heating rate b, i.e. $T = T_o + bt$, equation (3) can be written as

$$-\frac{dn}{dt} = \nu_x \exp\left[-\frac{E^{\ddagger}}{R(T_o+bt)}\right] \cdot n^x \qquad (4)$$

If ν_x and $E^{\ddagger}$ are independent of surface coverage, n, the temperature, T_m, at which the rate of desorption is a maximum can be determined. Taking the derivative of equation (4) with respect to t, and setting $\frac{d^2n}{dt^2} = 0$, one obtains

$$\frac{E^{\ddagger}}{RT_m^2} = \frac{\nu_1}{b} \exp\left(-\frac{E^{\ddagger}}{RT_m}\right) \text{ for } x = 1 \qquad (5)$$

$$\frac{E^{\ddagger}}{RT_m^2} = \frac{2n_m\nu_2}{b} \exp\left(-\frac{E^{\ddagger}}{RT_m}\right) \text{ for } x = 2 \qquad (6)$$

where n_m is the surface coverage at $T = T_m$. Since for a second order reaction n_m is approximately equal to one-half of the initial surface coverage n_o [16], equation (6) can be

written as

$$\frac{E^{\ddagger}}{RT_m^2} = \frac{n_o \nu_2}{b} \exp\left(-\frac{E^{\ddagger}}{RT_m}\right) \text{ for } x = 2 \qquad (7)$$

From equations (5) and (7), it is seen that for a first order rate process T_m is independent of initial surface coverage, whereas for a second order rate process T_m depends on the coverage. Thus, the order of the desorption process can be determined from the behaviour of the maximum in the desorption spectrum with coverage. The activation energy for desorption, $E^{\ddagger}$, can be determined from the variation of T_m with heating rate, b. After expressing T_m^2/b of equation (5) and (7) in terms of the remaining parameters, and taking the derivative of $\ell n(T_m^2/b)$ with respect to $1/T_m$, one obtains for a first order desorption process, or a second order process with constant initial coverage,

$$\frac{d\ \ell n(T_m^2/b)}{d(1/T_m)} = \frac{E^{\ddagger}}{R} \qquad (8)$$

The activation energy, $E^{\ddagger}$, can therefore be determined from the slope of a plot of $\ell n(T_m^2/b)$ versus $1/T_m$. The frequency factor, ν_x, can be found by substituting $E^{\ddagger}$ into equation (5) or (7).

2.2.2. Single binding state with activation energy dependent on coverage.

The analysis of desorption spectra described in the

previous section is based on the assumption that $E^{\ddagger}$ and ν_x are both independent of surface coverage. In many cases, however, a variation of $E^{\ddagger}$ with coverage has been observed. For such cases, equation (3) which describes the rate of desorption has to be replaced by

$$- \frac{dn}{dt} = \nu_x \exp\left(- \frac{E^{\ddagger}(\theta)}{RT} \right) \cdot n^x \qquad (9)$$

where θ is the surface coverage, expressed as a fraction of one monolayer.

The dependence of $E^{\ddagger}$ upon θ varies from system to system, however, for many cases a linear dependence is a good approximation. If one assumes $E^{\ddagger} = E_o^{\ddagger} - \alpha\theta$, where $E_o^{\ddagger}$ is the activation energy of desorption at zero coverage, equation (9) becomes

$$- \frac{dn}{dt} = \nu_x \exp\left[- \frac{(E_o^{\ddagger} - \alpha\theta)}{RT} \right] \cdot n^x \qquad (10)$$

Applying the same procedure as used in previous section, we have derived the following expression for the peak maximum temperature, T_m,

$$\ell n \left(\frac{T_m^2}{b} \right) = \frac{E_o^{\ddagger} - \alpha\theta_m}{RT_m} + \ell n \frac{E_o^{\ddagger} - \alpha\theta_m}{\nu_x R} - \ell n \left[N_m^{x-1} \left(\frac{\alpha\theta_m}{RT_m} + x \right) \right] \qquad (11)$$

where θ_m is the surface coverage at $T = T_m$. Thus, assuming

θ_m is independent of T_m which should be satisfactory for fixed initial coverage, one finds that,

$$\frac{d\ell n(T_m^2/b)}{d(1/T_m)} = \frac{E_o^{\ddagger}-\alpha\theta_m}{R} - \left(\frac{1}{T_m} + \frac{Rx}{\alpha\theta_m}\right)^{-1} \qquad (12)$$

If the last term can be neglected, $E_o^{\ddagger}-\alpha\theta_m$ can be obtained directly from the plot of $\ell n(T_m^2/b)$ versus $1/T_m$, and the value obtained will then correspond to the activation energy of desorption at $\theta=\theta_m$, which is approximately equal to half of the initial surface coverage. Since $E_o^{\ddagger}-\alpha\theta_m$ is a function of θ_m, hence the initial surface coverage, $E_o^{\ddagger}$ and α can be determined from the values of $E_o^{\ddagger}-\alpha\theta_m$ at two different initial surface coverages.

Furthermore, it is seen from equation (11) that regardless of whether the desorption process follows first order or second order kinetics, the maximum in the desorption rate curve will vary with coverage, and T_m will decrease with increasing coverage. The observation of the shift of T_m with coverage thus indicates that the desorption may be second order with constant activation energy, as noted in previous section, or first order with an activation energy dependent on coverage. These two cases, however, can be distinguished by plotting log $(n_o T_m^2)$ against $1/T_m$, since only the second order desorption process with constant activation energy will yield a straight line (see equation (7)).

2.2.3 Multiple binding states.

When multiple binding states are present on the surface, the analysis of desorption spectra may become very complicated. In the case where each binding state has widely different kinetic parameters from the others, the desorption spectrum will consist of well resolved peaks. Since each peak corresponds to an individual binding state, the method described in previous section can be applied to each peak independently for the determination of kinetic parameters.

If the kinetic parameters are similar for each binding state, overlap between the desorption peaks will occur extensively so that these peak maximum temperatures will no longer correspond to the temperatures at which the rate of desorption of individual binding state is a maximum. The desorption spectrum in this case merely reflect the sum of the desorption rates of individual binding states, which is

$$\text{rate} = \sum_i \nu_i \exp\left(-\frac{E_i^{\ddagger}}{RT}\right) \cdot n_i^x \qquad (13)$$

The analysis of the desorption spectra according to equation (13) can be achieved only by computer fitting.

2.3 Field electron emission microscopy.

Flash desorption is one of the most fruitful techniques for obtaining information about the existence of

different binding states and the kinetics of adsorption and desorption. However, the adsorbed layer has to be destroyed in generating this information and therefore the properties and the structure of the adsorbed layer cannot be obtained by this technique.

There are many techniques which yield information about this adsorbed layer by direct observation. Among them field electron emission microscopy is one of the most useful techniques; it enables one to "see" the surface and to follow rapid changes in the adsorbed layer.

2.3.1 Field electron emission from metals.

Field electron emission, also known as cold emission, is defined as the emission of electrons from the surface under the influence of a high electrostatic field.

In the absence of an external field, electrons in the metal are confronted by a large, infinitely thick potential barrier, as shown in Figure 1A, line a, and escape is possible only over the barrier. The presence of a field at the surface, however, modifies the barrier, as shown in Figure 1A, line b, and electrons approaching the surface are confronted by a potential barrier of finite width. If the barrier is sufficiently low and thin, unexcited electrons can escape from the surface by tunneling through the barrier. Based on the uncertainty principle, tunneling will be expected to occur if the momentum uncertainty Δp

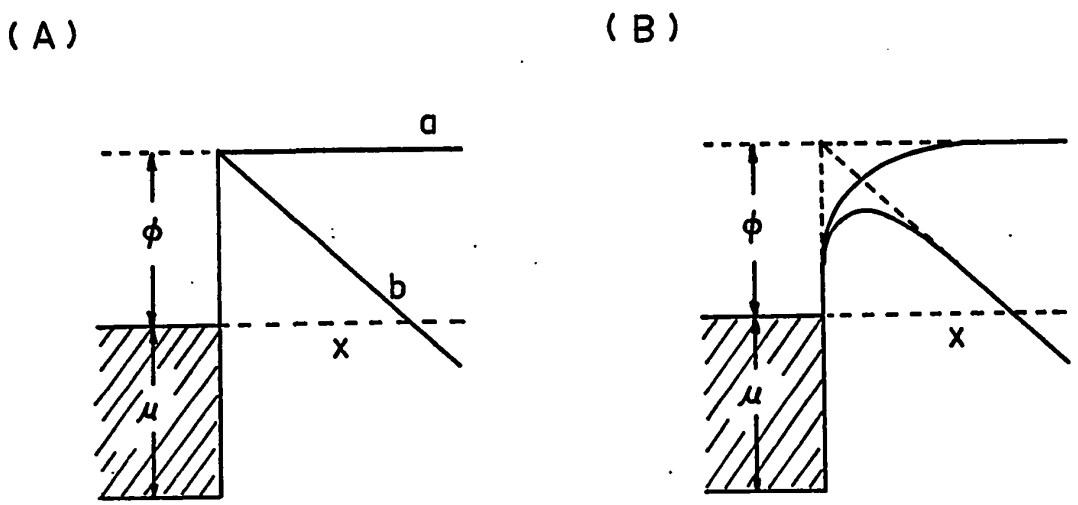

Fig. 1. Potential energy diagrams for electrons at a metal surface in the presence of an applied field: (A) without image potential; (B) with image potential included. ϕ = work function, μ = Fermi energy.

corresponds to the barrier height ϕ, $\Delta p \sim (2m\phi)^{1/2}$ and the uncertainty in position Δx corresponds to the barrier width ϕ/Fe. The applied field strength F necessary to produce field emission must therefore be of the order of $(2m\phi^3)^{1/2}/\hbar e$, where $\hbar = h/2\pi$, h is Planck's constant and m the mass of the electron. For a clean tungsten surface for which $\phi \sim 4.5$ev, the required value of F is $\sim 5\times10^7$v/cm.

Owing to the image potential which arises from the attraction of the electron to its positive image in the surface, the abrupt potential step, as shown in Figure 1A, in fact can not be expected at the surface. A more realistic model of the potential barrier thus includes the image potential $-e^2/4x$ for an electron distant x from a metal surface. The effect of this potential is to reduce the effective barrier area as shown in Figure 1B. This may be thought of as an increase in field or a decrease in work function.

For a specific model of the emission process, where electrons are assumed to tunnel out of a metal through the potential barrier shown in Figure 1B, namely a potential barrier formed by superimposing a high field on an image potential, a relationship which gives the dependence of the emission current I upon applied field F and work function ϕ has been derived [18]. This relationship, known as Fowler-Nordheim equation with image correction, reads

$$I = 6.2\times10^{-6} \cdot \frac{(\mu/\phi)^{1/2}}{\alpha^2(\phi+\mu)} \cdot F^2 \cdot \exp\left(-6.8\times10^7 \phi^{3/2} \frac{\alpha}{F}\right) \qquad (14)$$

where α is the image correction term and is a function of F and ϕ, and μ is the Fermi energy. In spite of the simplicity of the model, equation (14) has been found to satisfactorily describe field emission from clean metals.

2.3.2 Work function of the clean surface.

The work function ϕ, which is the energy difference between Fermi level and the potential energy of the electrons in the vacuum, includes in addition to the inner work function, i.e. the intrinsic partial free energy of "solution" of electrons in the metal, a contribution due to the electrostatic double layer present at the surface, which is also known as the outer work function. While the inner work function is a function only of the internal state of the metal, the outer work function depends on the condition of its surface and on the external conditions and is responsible for the crystallographic anisotropy in work function.

The surface double layer at the clean surface arises from the fact that the electron charge density does not terminate abruptly at the surface, instead, decays gradually [19]. This spill-over of electrons gives rise to a double layer with negative end outward on closely packed planes and positive end outward on loosely packed planes. Very closely packed planes will therefore have high work functions and loosely packed planes low work functions [20].

2.3.3 Field electron emission microscope.

The field emission microscope is an important

application of cold emission. A schematic diagram of the microscope is shown in Figure 2. The microscope consists of a point emitter and a spherical anode which is usually in the form of a fluorescent screen. The field F at the surface of a free sphere of radius r and potential V is

$$F = V/r \tag{15a}$$

At the surface of an actual tip the field is reduced from this value by the presence of the emitter shank, but is given to a very good approximation by

$$F = V/kr \tag{15b}$$

where $k \sim 5$ near the apex and increases with polar angle [18]. Thus, the fields necessary, i.e. $3\text{-}7\times10^{7}$ volts cm^{-1}, can be obtained with voltages of the order of 3-7 kV for emitters of 2000 Å radius.

The electrons tunneling through the barrier are accelerated towards the fluorescent screen along the lines of force, and produce there a greatly magnified image of the emitter as shown in Figure 3. However, since the emitter shank not only decreases the field near the apex but also compresses the lines of force, the magnification is given by d/cr, instead of d/r, where r is the emitter radius, d the emitter-to-screen distance, and $c \sim 1.5$ the compression factor. The

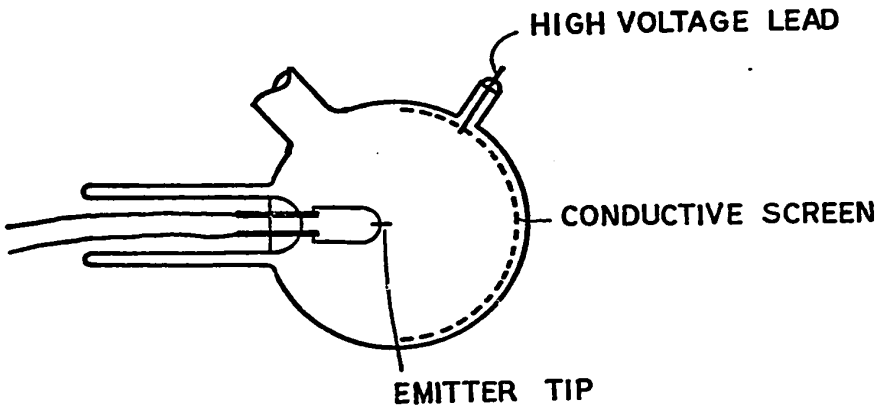

Fig. 2. Schematic diagram of field emission microscope.

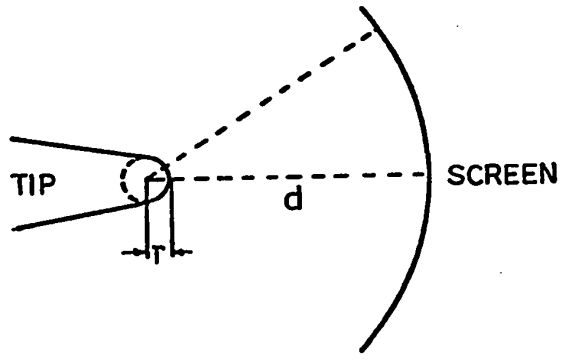

Fig. 3. Schematic diagram of electron trajectories in a field emission tube, showing mechanism of image formation.

resultant deformation of the image is axially symmetric and almost uniform over the visible portion of the emitter, so that almost uniform magnifications of the order of 10^5-10^6 can be obtained. The resolution of the microscope is limited to ~20 Å by the transverse momenta of the electrons leaving the emitter surface.

The emitter, because of its small size compared with the wire grains, is generally part of a single crystal, and its surface is made up of a variety of crystal planes. Since the work function depends on orientation, the emission pattern shows an emission anisotropy. According to the symmetry of the patterns and angular separations of the various planes, crystallographic indices can be assigned unambiguously. The typical emission pattern from clean tungsten emitter is shown in Figure 4 where the dark area corresponds to crystal planes with higher work functions.

2.3.4 Work function change and its measurement.

When a molecule or an atom is adsorbed on a surface, charge redistribution occurs. A dipole moment is therefore associated with each adsorbed molecule or atom, and the surface double layer, such as that present on a clean surface, will arise from the adsorbed layer. If the dipole moment μ of a single adsorbed molecule or atom varies negligibly with coverage, this adsorbed layer will contribute a term $\Delta\phi$ to the work function, $\Delta\phi = 2\pi\mu N_s\theta$, where N_s is the

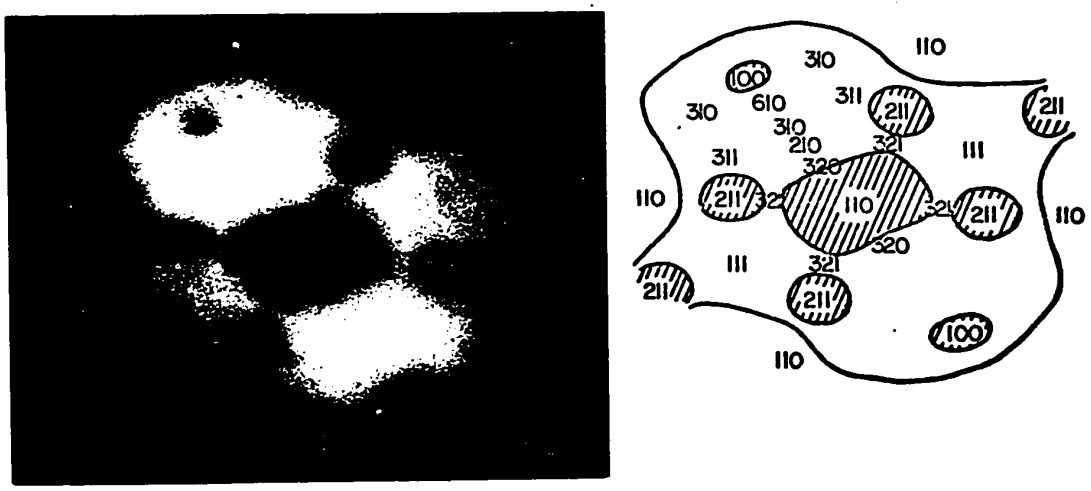

Fig. 4. Field emission pattern of clean tungsten indexed crystallographically.

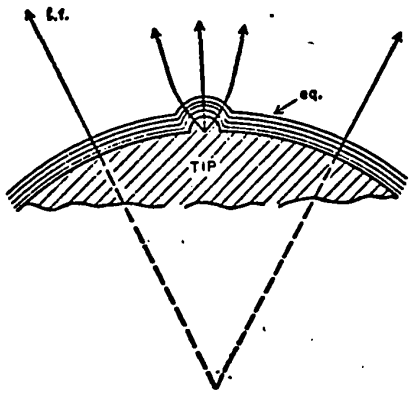

Fig. 5. Schematic diagram indicating lens effect of conducting humps on a tip surface. l.f., lines of force; eq, equipotentials.

maximum number of adsorption sites per unit area and θ the fraction of sites which are filled. Molecules and atoms, which produce dipoles with their negative end outward on adsorption, will therefore raise the work function and vice versa.

Based on Fowler-Nordheim equation (14), the field emission microscope can be used for measuring the work function of a clean metal, provided that the emitter radius and the constant k in equation (15b) are known. In the study of adsorption and surface reaction, however, instead of the absolute value of work function, the work function changes, $\Delta\phi$, are usually sufficient. The emitter radius therefore does not have to be evaluated explicitly.

Since the field F is related to the applied voltage V and the radius r of the emitter by equation (15b), the Fowler-Nordheim equation can be abbreviated in the form

$$I = AV^2 \exp(-B\phi^{3/2}/V) \qquad (16)$$

where the pre-exponential term A is a function of emitter configuration, work function and of the emitting area, and $B = 0.68\beta$, β being the voltage/field proportionality factor.

Provided the work function ϕ and the terms A and B are insensitive to changes in the applied field, the slope of the Fowler-Nordheim plot, $\ell n(I/V^2)$ against $1/V$, is given

by

$$\frac{d\ \ell n(I/V^2)}{d(1/V)} = - B\phi^{3/2} \qquad (17)$$

The change in the slope on adsorption thus can be used for evaluating the value of $\Delta\phi$, the work function change. In order to follow the work function change on adsorption the current-voltage relation must therefore be determined.

Though the Fowler-Nordheim equation is based on a simple one dimensional image potential and does not account for the presence of discrete atoms on the surface, the application of this equation for the determination of $\Delta\phi$ on adsorption does not give rise to serious errors, if the work function changes are derived from the field dependence of the emission current and not from its absolute value [21]. For a reliable measurement, however, it is essential that the applied field is not too high so that the thickness of the barrier still exceeds a few atomic diameters.

Furthermore, the work function determined from the current-voltage relation of the emitter is in fact an average quantity, since the emitter is made up of variety of crystal planes with different work functions. The emission current measured is the sum of the currents from individual crystal planes. If each plane is denoted by the subscript i, the total emission I is represented by

$$I = \sum_i I_i = V^2 \sum_i A_i \exp(-B_i \phi_i^{3/2}/V) \qquad (18)$$

where I_i is the current emitted by the i plane.

If the terms B_i are the same for all planes, the slope S of the Fowler-Nordheim plot would correspond to

$$S = - \frac{B \sum_i I_i \phi^{3/2}}{\sum_i I_i} \qquad (19)$$

Since I_i depends exponentially on $-\phi^{3/2}$, the slope is heavily weighted in favor of the low work function planes. Thus only the planes of lowest work function will contribute significantly to the average work function.

On adsorption, if the work function is raised, i.e. emission is lowered, the planes on which adsorption occurs will therefore not contribute to the work function measurement and would gradually become invisible as adsorption proceeds. On the other hand, if adsorption lowers the work function, the planes on which adsorption occurs will dominate in work function measurement and could become the only visible area in the emission patterns.

Emission anisotropies arise not only from work function differences but also from local variations in field. These occur whenever the local curvature differs from that of the main emitter. Thus, surface overgrowths and hump formation cause not only a local field enhancement and increased emission but also a higher local magnification as shown in Figure 5. All these complicate the interpretation of observed emission patterns and work function changes; a

knowledge about the changes in the pre-exponential term, A, is often found necessary for a correct interpretation of the results.

CHAPTER 3

EXPERIMENTAL METHODS

3.1 Materials.

The tungsten used in this work was supplied by Philips Elmet Corporation. The cleaning of the tungsten filaments used in flash desorption studies was achieved by heating at 2500°K for several hours in an oxygen atmosphere at a pressure of 10^{-6} torr, and by further heating at 3000°K under ultra-high-vacuum conditions for a prolonged period.

The anhydrous ammonia, hydrogen, deuterium and carbon monoxide were obtained from the Matheson Company. In the flash desorption experiments which were carried out before the field emission experiments, ammonia specified with 99.99% purity was further purified by vacuum distillation between cold fingers maintained at 195° and 77°K with an ultimate pressure of 5×10^{-4} torr. In preliminary field emission experiments, however, it was found that after purifed ammonia was introduced into the system, a clean emission pattern could not be obtained even by flashing the tip to 2500°K. A trace of impurities which was not detected by the mass spectrometer in flash desorption experiments was therefore present in the ammonia purified in this manner. To obtain ammonia with higher purity, the purification was carried out on an ultra-high vacuum line which also incorporated a nickel getter to trap impurities. The purified ammonia for use in field emission experiments was collected in a Pyrex flask

with a break-seal. Hydrogen and deuterium were also purified before use by diffusion through palladium, the deuterium was specified as 99.5% isotopic purity. Carbon monoxide with 99.9% purity was supplied in a Pyrex flask with a break-seal and was used without further purification.

Nitrogen $^{28}N_2$ was obtained from the Air Reduction Company and nitrogen $^{30}N_2$, with a specified isotopic purity of 99%, from the Isomet Corporation. Both isotopes were supplied in Pyrex flasks with break-seals and were stored over Ni-getters to remove possible traces of CO impurity.

3.2 Flash desorption experiments.

3.2.1 Decomposition of ammonia.

Apparatus

The ultra-high vacuum system, shown in Figure 6, was mounted on a vertical sheet of Marinite so that it was possible to bake out the sytem during the pump down period. The purpose of this bake-out procedure is to drive off the gases adsorbed strongly on the walls and to obtain a much lower ultimate pressure at room temperature.

The reaction vessel R, a 300ml Pyrex flask, was connected to the quadrupole mass spectrometer M through a large diameter (40 mm) tubing with a regular curvature to ensure a high conductance path for desorbed gases. To avoid exposure of the mass spectrometer to gas at high pressure during dosing, it was separated from the reaction vessel by

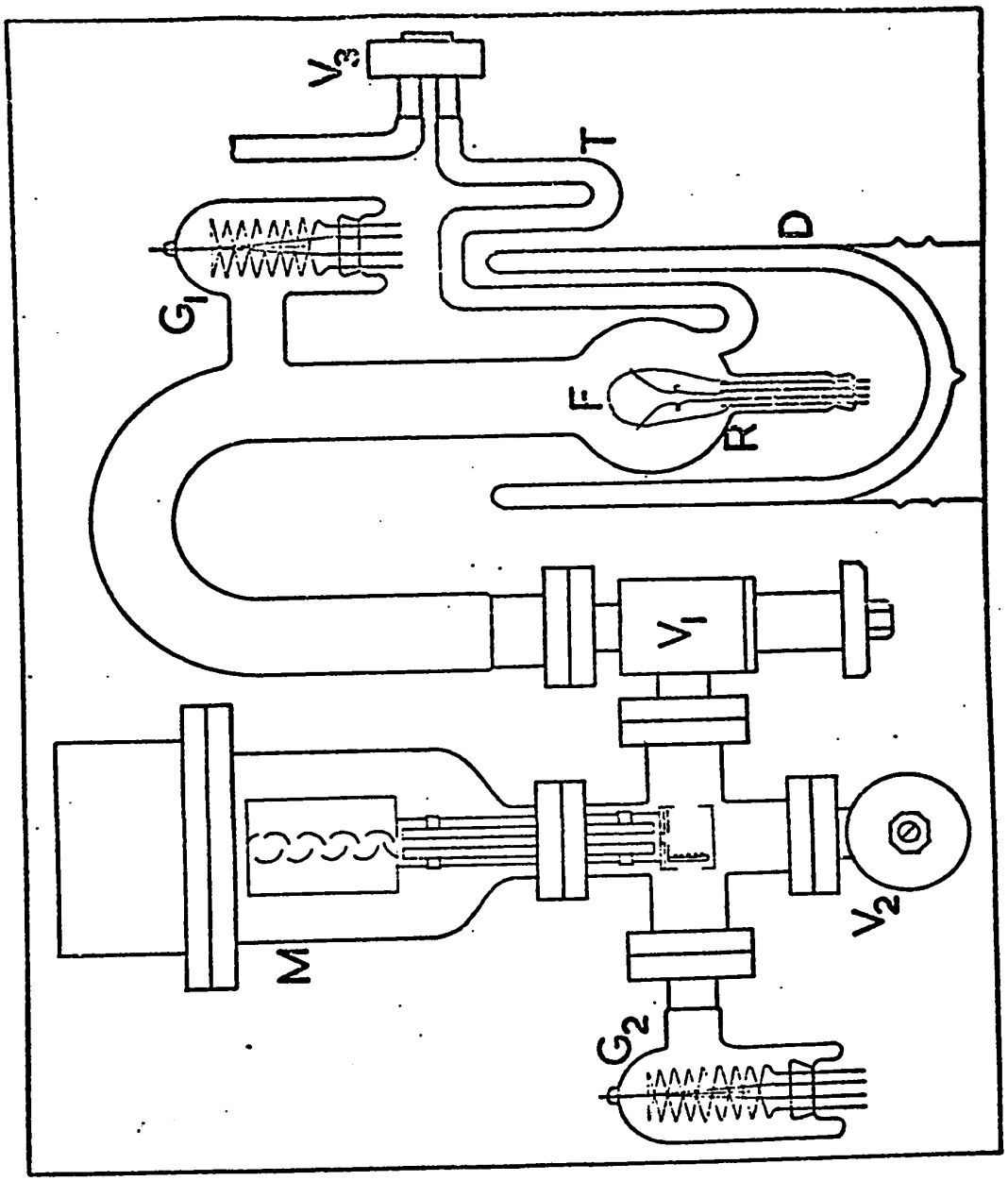

Fig. 6. Ultra-high vacuum system used for thermal desorption studies of ammonia decomposition.

a one-inch metal valve V_1. The system was evacuated through one-inch valve V_2 by a 20ℓ/sec Ultek Differential Ion pump. Purified ammonia, nitrogen and hydrogen could be introduced from storage bulbs via half-inch metal valve V_3.

The sample filament F was a 12 cm long piece of 10 mil tungsten wire, on which two 3 mil tungsten sensing leads were spot welded. The filament temperature was controlled using a Kelvin double-bridge [22]. The resistance, and hence the temperature, of the centre section of the filament was determined by measuring the potential drop across the sensing leads for a known current.

The pressure of the system was measured using ionization gauge G_1 or G_2. The quadrupole mass spectrometer was an Ultek/EAI Quad 150, modified to permit variation of the electron accelerating voltage; the ionizer was operated at 60 eV and 50 μA emission current. All the gauges and the mass spectrometer were provided with low work function filaments, to reduce the decomposition of ammonia on hot gauge filaments to a minimum. The recording system was able to monitor the desorption spectra of three different mass to charge ratios simultanously. Thermal desorption spectra were obtained using a linear slow heating rate, which was obtained by using a motorized potentiometer as the comparison resistor in a Kelvin double-bridge temperature control circuit.

Procedure.

After the system was pumped down to $\sim 10^{-3}$ torr, it was isolated from mechanical pump and the ion pump was started. Generally, it would take several hours before a pressure of $\sim 5\times10^{-7}$ torr was reached and the bake-out process could be started. In the initial stage of the bake-out, the oven temperature was raised slowly so that the pressure of the system did not exceed 5×10^{-4} torr, a value which would trigger the automatic shut-off of the ion pump. After maintaining the system at 400°C for about 10 hours with intermittent outgasing of the gauges, the oven was turned off. A pressure less than 10^{-9} torr was obtained after the system cooled down to room temperature.

The introduction of ammonia into the reaction vessel was achieved by expansion from a small volume at 40-torr pressure. The reactant pressure was only measured in check experiments using ionization gauge G_1 (or a Millitorr gauge) to avoid the decomposition of ammonia on hot gauge filaments. Possible carbon monoxide contamination of the sample surface was checked by monitoring the mass 12 ion current and found to be negligible even after an exposure of 6 torr-sec.

Handling ammonia in an ultra-high vacuum apparatus is exceedingly difficult as a result of the strong adsorption of this gas by the walls of the system and the subsequent slow desorption. Adsorption by the walls of the system makes

it impossible to quickly adjust the pressure in the system to a constant low value, and the subsequent slow desorption makes reattainment of ultra-high vacuum a problem. Experiments performed in a continuous ammonia atmosphere have been reported [10,11] and criticized [14], because it is impossible to control the adsorption conditions, and also during thermal desorption pressure peaks can arise by decomposition of gaseous ammonia on the sample. To overcome these difficulties the following four methods have been employed in these experiments.

Method I.

After dosing the sample with ammonia, the reaction cell was cooled to 77°K by surrounding it with liquid nitrogen contained in Dewar flask D. The saturation vapour pressure of ammonia at 77°K is of the order 10^{-11} torr so this technique adequately prevents interaction of gaseous ammonia with the sample during thermal desorption. This method was always used when flash cleaning the sample filament between experiments. Some of the consequences of this method are illustrated in Figure 7. Curve (a) shows the thermal desorption spectrum obtained with the reaction vessel at room temperature, after hydrogen had been adsorbed for 5 minutes at a pressure of 5×10^{-8} torr. Curve (b) shows the same spectrum obtained with the reaction vessel cooled to 77°K. The differences caused by the increased residence time for hydrogen molecules on the cold glass wall are so small that

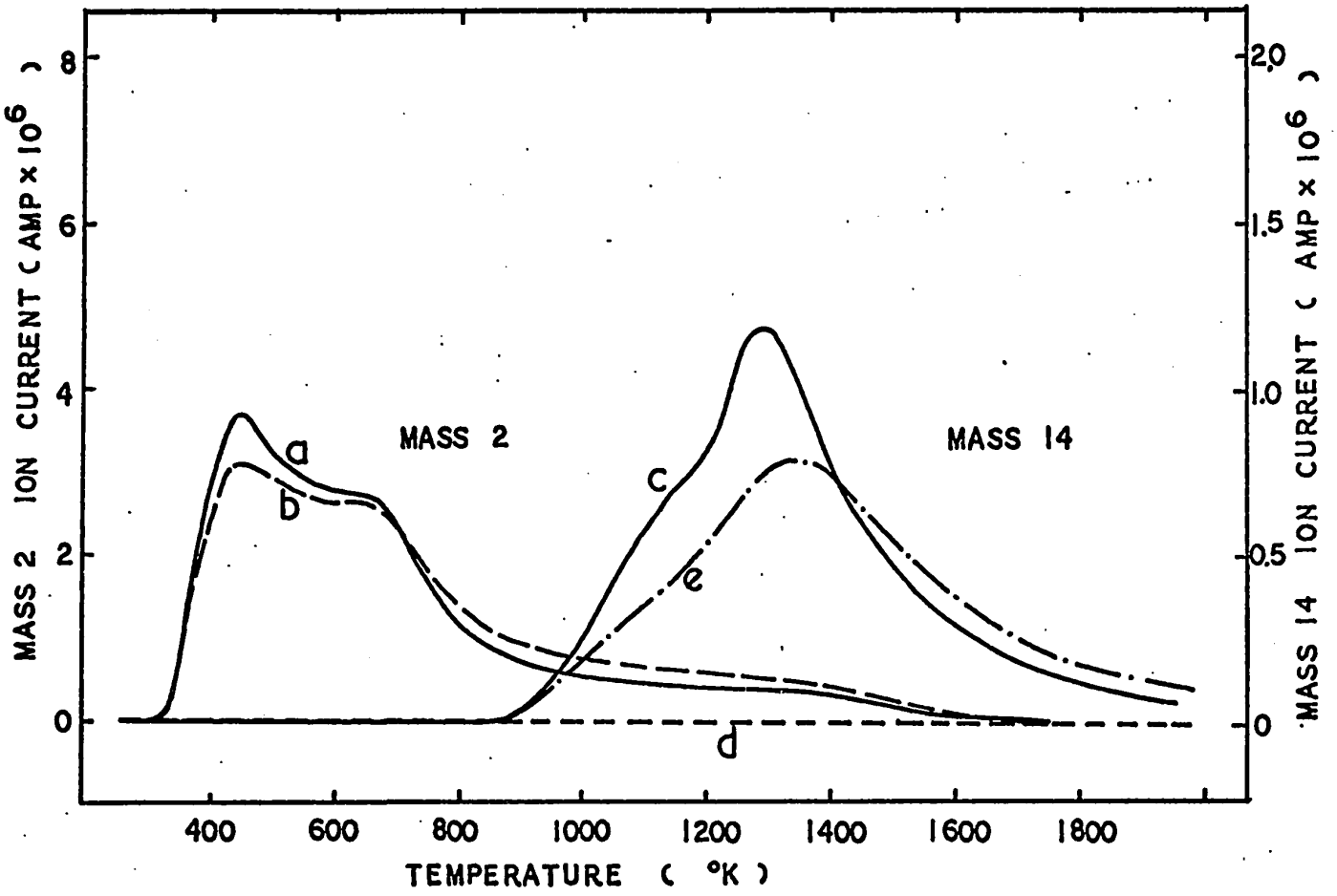

Fig. 7. Hydrogen desorption spectra obtained from adsorption of hydrogen at 5×10^{-8} torr for 5 minutes with the reaction vessel at room temperature (curve a), and 77°K (curve b). The nitrogen desorption spectra were obtained from ammonia adsorption at 5×10^{-8} torr for 10 minutes with the reaction vessel at room temperature (curve c), 77°K (curve d), and covered with a thick (ca. 25 Å) ammonia layer at 77°K (curve e).

Method I should be qualitatively quite adequate for mass 2 desorption spectra. The mass 14 spectra, (c), (d) and (e) were all obtained from ammonia adsorbed at 700°K for 10 minutes at a pressure of 5×10^{-8} torr. For spectrum (c) the reaction vessel was at 300°K and consequently interaction of ammonia gas with the sample occurred during thermal desorption. However, cooling the reaction cell to 77°K (Method I) to eliminate this problem produced spectrum (d) showing that the residence time of the nitrogen on the cold glass walls is very long on the time scale of the experiment and Method I is useless for nitrogen desorption spectra.

Method II.

If, after adsorption is complete and before cooling the reaction cell to 77°K, the reaction cell is filled with ammonia to a pressure of 0.1 torr, a nitrogen desorption spectrum can be observed, Figure 7(e). Apparently an ammonia layer on the cell wall of average thickness 25 Å causes a large decrease in the residence time of nitrogen molecules on the glass wall. The appearance of desorbed nitrogen in the mass spectrometer is slightly delayed but certainly Method II can be used to obtain qualitative nitrogen desorption spectra without the complications caused by decomposition of gaseous ammonia on the filament during the flash.

Method III.

After dosing, the gas phase ammonia pressure is

reduced to about 5×10^{-7} torr by condensing in trap T at $77^{o}K$ for 30 minutes and pumping. During thermal desorption the cell is at room temperature, thus no correction is required for delayed pressure bursts and the spectrum can be interpreted kinetically. However, decomposition of the gas phase ammonia on the filament becomes appreciable above $1000^{o}K$ and the desorption spectra must be corrected for this effect. This has been achieved by immediately repeating the experiment for a $300^{o}K$ adsorption under the same conditions and preflashing to $800^{o}K$ (Figure 16).

Method IV.

An alternative method is to pump out the reaction vessel and then cool it to $77^{o}K$, remove the liquid nitrogen coolant and allow the reaction vessel to warm for 20 seconds before commencing the thermal desorption. The wall temperature is adequate to reduce the residence time of nitrogen but not high enough to permit appreciable ammonia desorption from the reaction vessel wall (Figure 23 and 24).

In the experiment where the state of desorbing hydrogen was investigated the set-up shown in Figure 6 was rearranged so that a line of sight existed between the sample filament and the mass spectrometer (Figure 8). The recording system was also modified so that mass 1 and mass 2 could be monitored simultaneously but with different sensitivities. In this experiment a 10 times higher sensitivity was used for mass 1 than that used for mass 2.

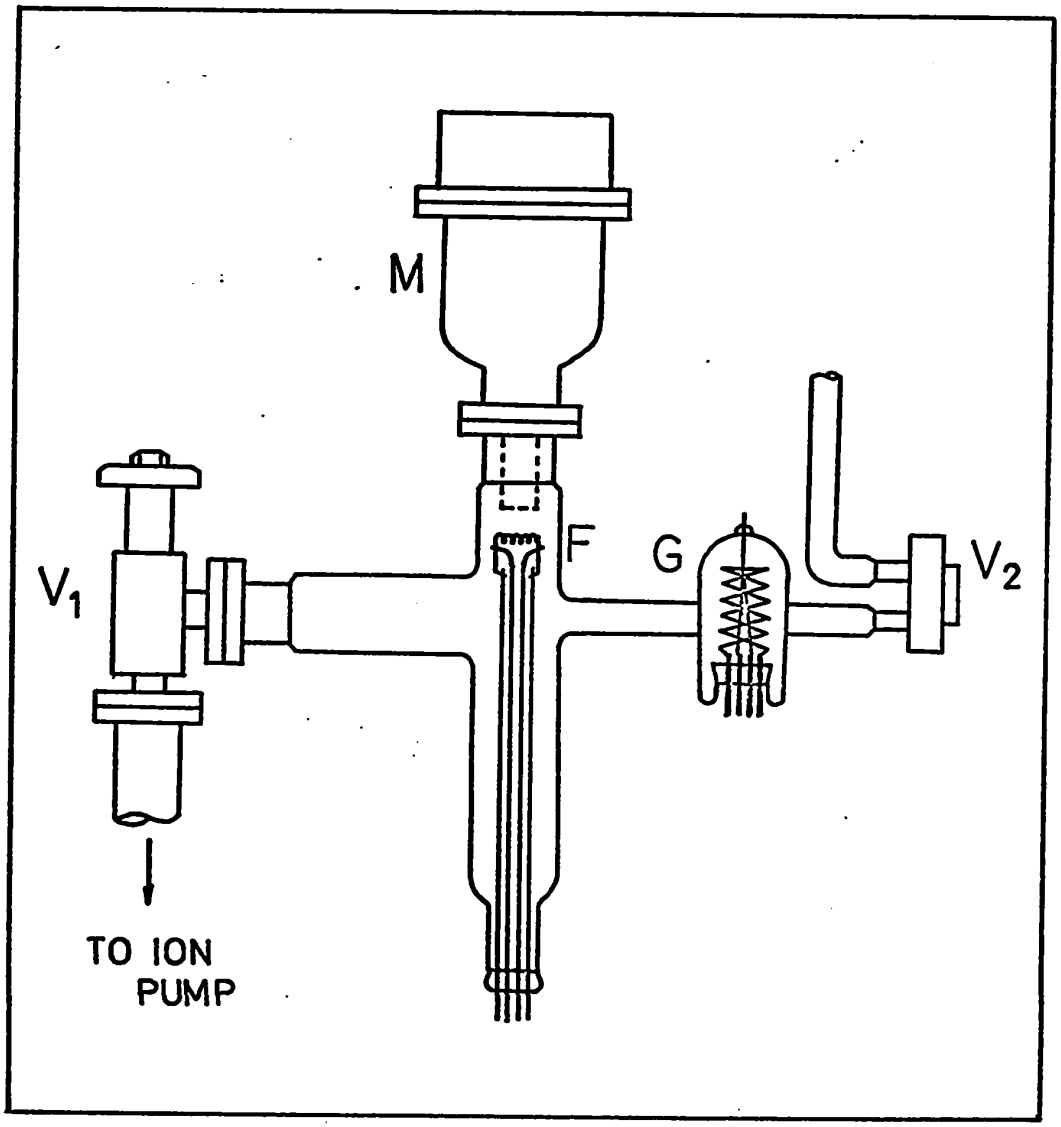

Fig. 8. Ultra-high vacuum system with a line of sight between the sample filament F and the mass spectrometer M.

3.2.2 Activated nitrogen adsorption.

Apparatus.

The ultra-high vacuum system shown in Figure 9 differs from that used in ammonia decomposition experiments only by having the reaction vessel R and the mass spectrometer M as close as possible. This arrangement enabled one to follow the instantaneous pressure change of the system either by using mass spectrometer M or ionization gauge G_1 which was directly connected to the reaction vessel through short tubing of large diameter. The ability to measure instantanous pressure changes was necessary since the overlap between multiple binding states was extensive. Even with very slow heating rates the desorption spectra were not resolved and a fast heating rate had to be used to determine the kinetic parameters. Whereas the slow linear heating rate was obtained using the Kelvin double-bridge, fast heating rates were obtained using a constant-current power supply. In addition to an x-y recorder, an oscilloscope was also used for recording the fast desorption spectra. The operating conditions of the mass spectrometer were identical to those employed in the previous experiments. The activated nitrogen was obtained by electron bombardment of gas phase nitrogen molecules using ionization gauge G_1.

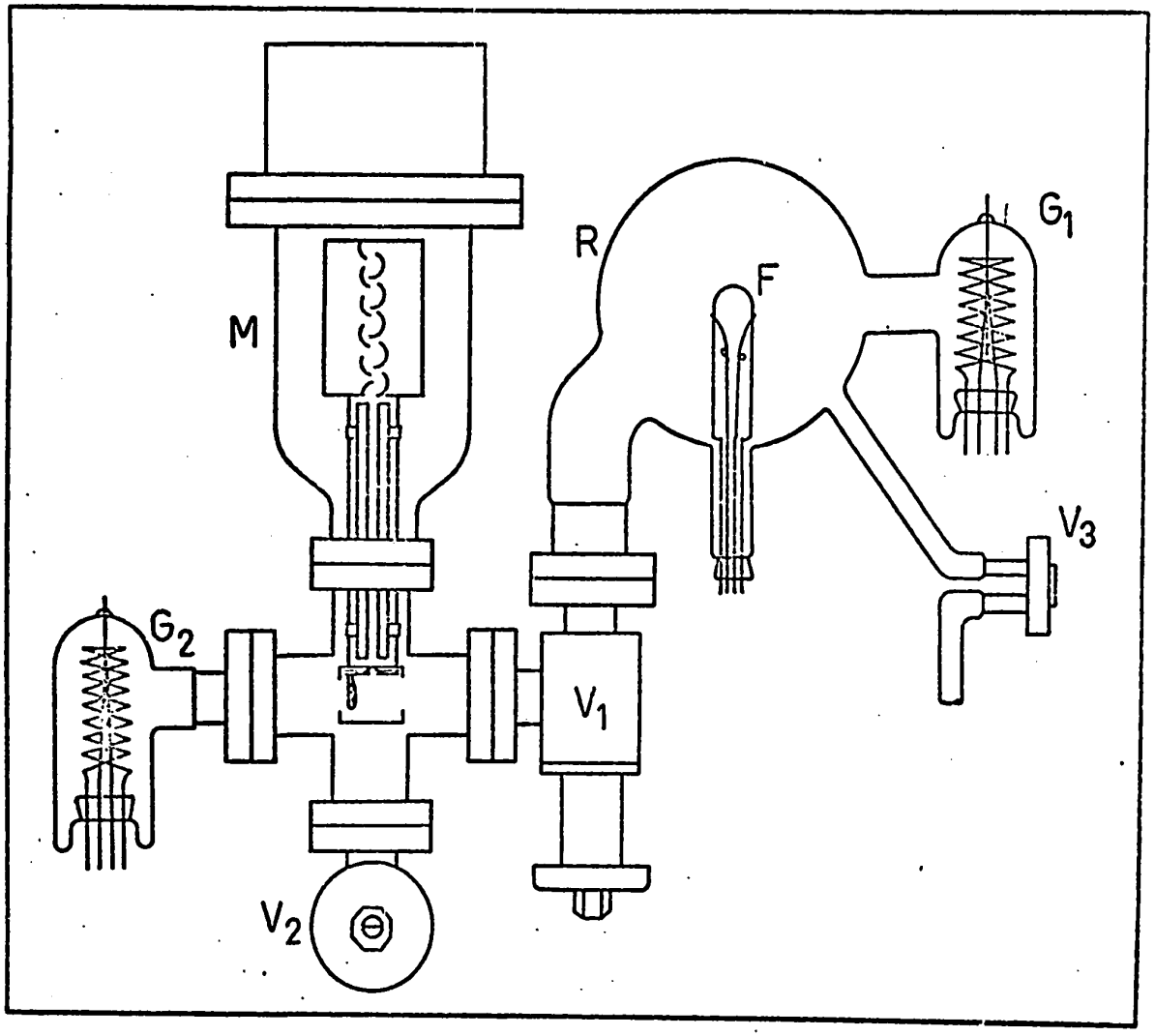

Fig. 9. Ultra-high vacuum system used for the studies of activated nitrogen adsorption.

Procedure.

The system was pumped down to a pressure less than 10^{-9} torr in the usual manner. After flash-cleaning the sample filament, it was held at $\sim 2000^{o}K$ where no adsorption could occur. The ionization gauge controller was adjusted to give an emission current of 5 mA in gauge G_1 for bombardment and activation of gas phase nitrogen and operated at a grid voltage of 160V. Nitrogen was introduced slowly through valve V_3 into reaction vessel R until the pressure reached a steady value of 2×10^{-6} torr with valve V_1 opened slightly. The sample filament was then cooled to allow the adsorption to take place. No biasing potential was applied to the sample filament during adsorption which was always at $300^{o}K$. After adsorption, the nitrogen gas flow was stopped, the system was pumped down and the sample filament was flashed at the desired heating rate.

Carbon monoxide contamination, always a possible complication, was checked by monitoring the mass 12 ion current and found to be negligible even after an exposure of 140 torr-sec.

3.3 Field emission experiments.

Apparatus.

The attainment and maintenance of a pressure less than 10^{-9} torr in a field emission microscope is generally achieved by immersing the entire sealed-off microscope in a liquid hydrogen or helium cryostat. In this case, dosing of

the field emitter with gas is usually achieved by evaporating the gas from a small cold finger. Though this method is simple and straight-forward, it is not possible to dose the emitter under high pressure and obtain either reproducible or measured doses. In the study of the interaction of ammonia with tungsten, better controlled dosing conditions are required, especially in the pressure range between 10^{-4} and 10^{-2} torr. It is essential to be able to reproduce the dosing conditions used in the flash desorption experiments. In addition, a short recycling time for the system to warm up from liquid helium temperature to room temperature is also required.

A set-up which satisfies these requirements is shown in Figure 10, which consists of the microscope A, a liquid helium cold finger B and pumping system C. The microscope was constructed from a 200 mℓ Pyrex flask. The inside walls of the flask was coated with a conductive SnO_2 layer which was produced by passing a mixture of $SnCl_4$ vapour and dry air into the flask heated at 400°C. On top of this SnO_2 layer a phophor screen was deposited on one half of the flask using phosphoric acid as a binder [18]. The high voltage lead f was connected to this conductive layer with a spring connection. The emitter assembly e was made up of a tungsten loop with the field emitter and sensing leads spot welded to it. An emitter with a diameter less than 1000 Å was

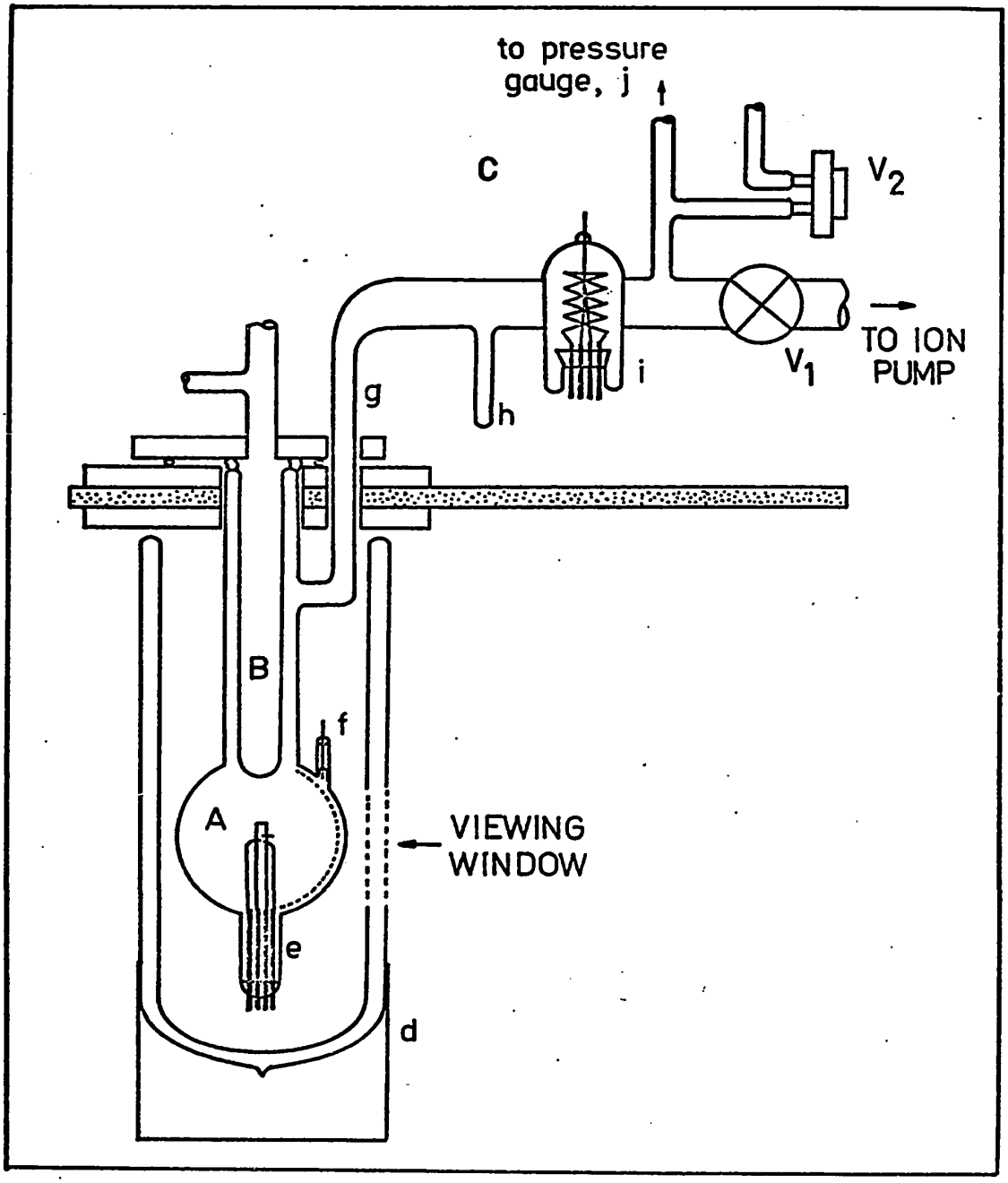

Fig. 10. Ultra-high vacuum system used for field emission studies of ammonia decomposition.

produced by etching in 1N KOH solution a pre-etched 5-mil tungsten wire which had been spot welded to a 10-mil tungsten loop. On the centre portion of the loop two 3-mil tungsten sensing leads were also spot welded for emitter temperature measurement and control. The cold finger B which served as a liquid helium Dewar was designed for trapping gas molecules desorbing from the emitter assembly and maintaining ultra-high vacuum conditions in the microscope during the experiment. To minimize helium consumption a nickel film radiation shield was deposited on the inside walls of the cold finger via vacuum evaporation. The nickel film was also connected to high voltage lead f .

Through 15 mm diameter tubing g, the microscope and cold finger were connected to a small liquid nitrogen cold finger h, ionization gauge i, and an MKS Baratron diaphragm gauge j. The entire system was evacuated by a 20 ℓ sec^{-1} Ultek Differential Ion pump through one-inch metal valve V_1. Purified ammonia could be introduced into the system from a storage bulb via half-inch metal valve V_2.

The electronic arrangement which enables one to control the emitter temperature conveniently and to determine the emission current-applied voltage relation rapidly is shown in Figure 11. Voltages applied across the microscope were supplied by a Fluke 410 B, 0-10 KV dc power supply. Emission currents were measured with a Keithly 610 electrometer with its output displayed on an Analogic digital

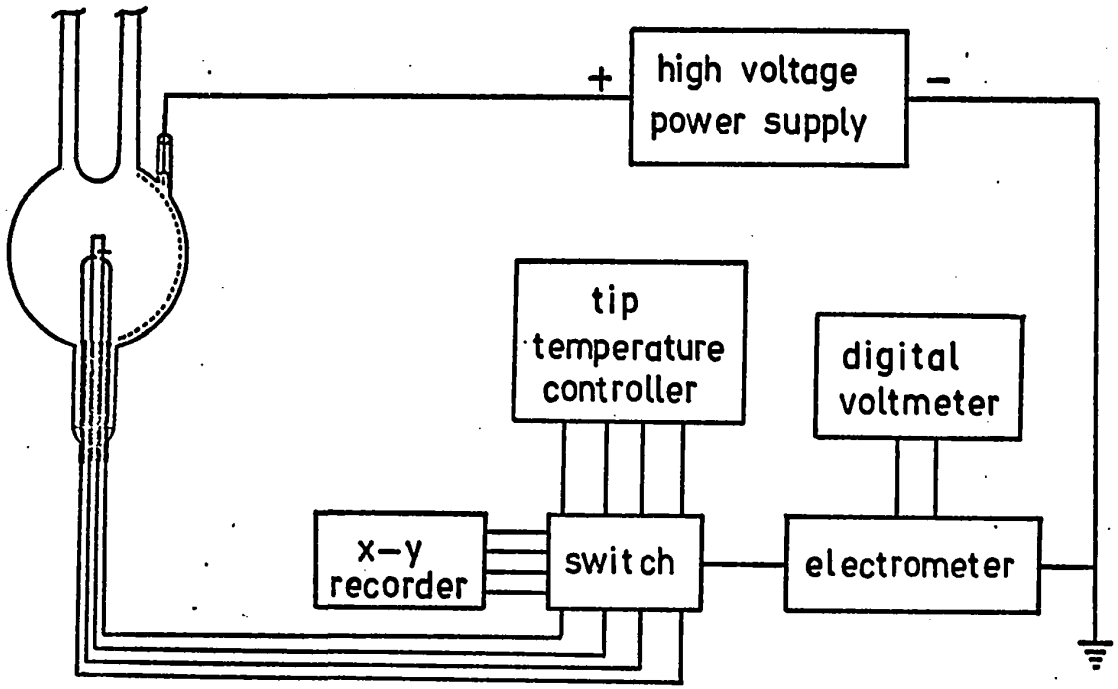

Fig. 11. Electronic arrangement used in the field emission studies.

voltmeter. The emitter temperature was controlled using a Kelvin double-bridge.

Procedure.

The entire system was baked out at 400°C and pumped down to a pressure less than 10^{-9} torr in the usual manner. Before commencing any adsorption experiment, the current-voltage relation and emission pattern of the clean emitter were obtained as follows.

After flash cleaning the emitter the system was isolated from the ion pump by closing the valve V_1. The entire microscope including cold finger B was immersed in liquid nitrogen and liquid helium was continuously transferred into cold finger B. The temperature inside the cold finger was measured during the transfer using a resistance thermometer. After the temperature dropped to a value close to 4°K, the emitter was flashed to 1500°K and its emission pattern was checked for cleanliness. The current-voltage relation was determined rapidly by varying the high voltage across the microscope and measuring the corresponding emission current. The emission pattern was taken on Kodak Tri-X film using a Pentax 35 mm f:1.9 camera. The microscope was allowed to warm up by interrupting the helium transfer and removing the liquid nitrogen Dewar d.

Ammonia was introduced into the microscope by opening valve V_2 slowly until a stable pressure of the required magnitude, as indicated on the diaphragm pressure gauge, was

obtained. The entire microscope was immersed in liquid nitrogen and the permanent gases, i.e. H_2 and N_2, were pumped out through valve V_1. The emitter was flashed and its emission pattern was again checked for cleanliness. A clean pattern was always observed without flashing the emitter to a temperature higher than 1500°K. This observation indicated the high purity of ammonia introduced into the system.

Dosing of the clean emitter with ammonia was carried out by removing the liquid nitrogen Dewar d and allowing the ammonia to evaporate from the walls with valve V_1 closed. When the ambient ammonia pressure reached a steady value, the emitter was heated to the adsorption temperature and maintained at this temperature for varying periods of time. After the adsorption, the emitter was allowed to cool down before ammonia was condensed in the small cold finger h. This procedure of trapping ammonia in the cold finger h was to minimize the adsorption of ammonia on the microscope screen and its subsequent desorption by bombardment with high energy electrons during the work function measurement. The current-voltage relation was measured after the temperature inside the cold finger B had dropped to a value close to 4 °K and the emitter had been pre-flashed to dosing temperature for 20 seconds. All currents and voltages were measured with the emitter at 77°K and all emission patterns were also obtained at this temperature.

Based on equation (17), the work function changes

on adsorption were evaluated from current-voltage relations of clean emitter and the adlayer covered emitter.

CHAPTER 4

RESULTS

4.1 Interaction of ammonia with tungsten.

4.1.1 Interaction of ammonia with tungsten at different temperatures.

After flash cleaning the sample filament and adjusting the filament temperature to that required for adsorption in ultra-high vacuum, ammonia gas at a pressure of 10^{-4} torr was allowed to interact with the filament for 10 minutes. Hydrogen (mass 2) and nitrogen (mass 14) desorption spectra were obtained using Method I and Method II respectively; these spectra are shown in Figure 12 and 13. In order to obtain good resolution in the desorption spectra a slow linear heating rate of 50 deg/sec was employed in all experiments unless otherwise stated. The desorption spectrum obtained from the surface species formed at 200°K is characterized by a low temperature hydrogen peak commencing at 285°K with peak maximum at 450°K, and a high temperature β-nitrogen peak [23], commencing at 1150°K with peak maximum at 1450°K. These observations are in good agreement with the corresponding field emission results obtained by Dawson and Hansen [9].

The hydrogen desorption spectra obtained from interaction at higher temperatures are all characterised by a

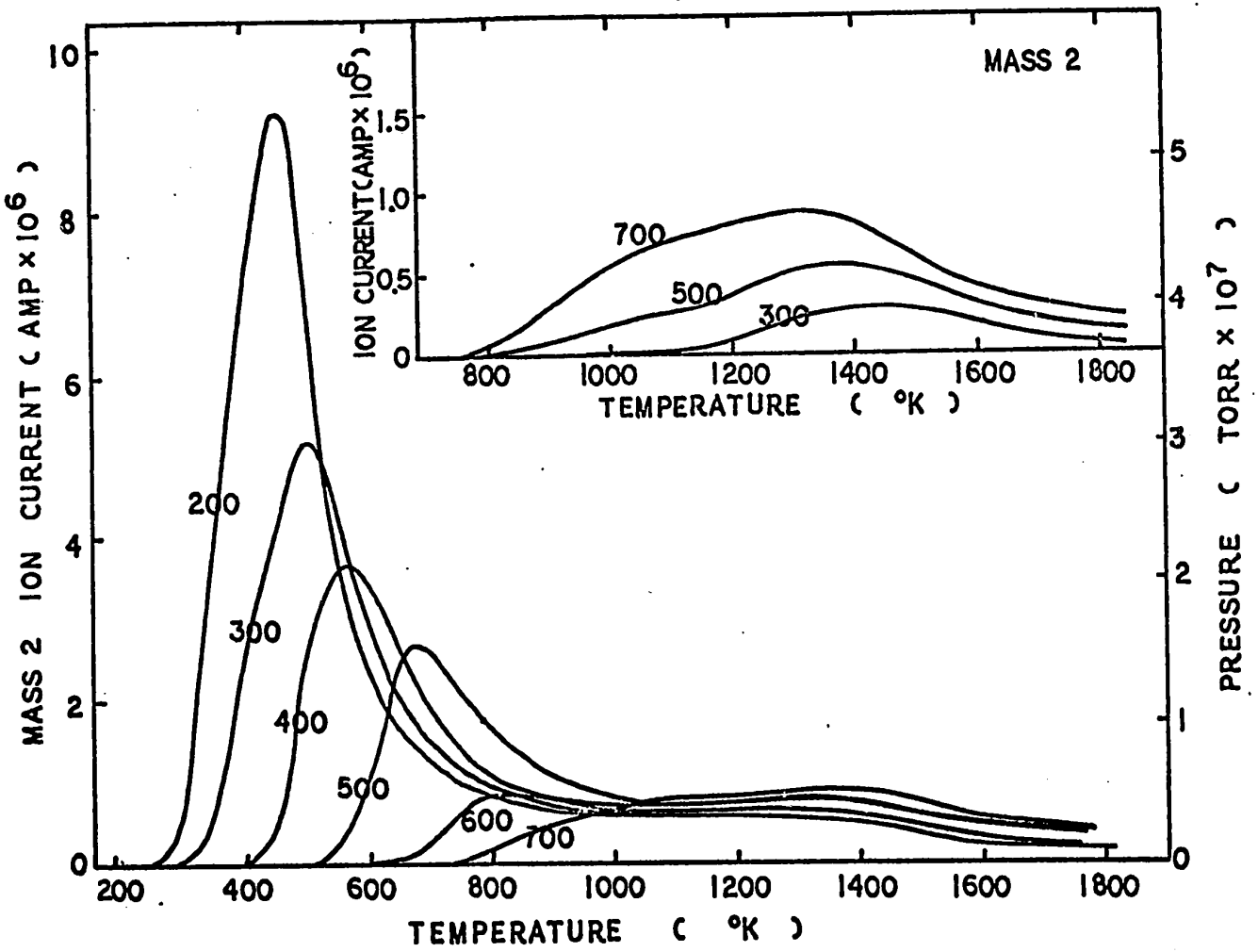

Fig. 12. Hydrogen desorption spectra, obtained using Method I, from adsorption of ammonia at 10^{-4} torr for 10 minutes at temperatures between 200 and 700°K. Inset shows the spectra obtained using the same adsorption conditions but with a preflasn to 700°K before desorption.

low temperature peak and a long high temperature tail which is also observed in the spectrum obtained from interaction at 200°K. This long high temperature tail is partly caused by desorption from the cool ends of the sample filament since the temperature of the filament is non-uniform both during adsorption and thermal desorption with a slow heating rate of 50°K per second. It is unlikely that all of the hydrogen tail originates in this manner since a rapid preflash to 800°K does not eliminate the tail as can be seen in the inset to Figure 12. A small hydrogen desorption centered around 1000°K is apparent for ammonia doses at 500 and 700°K but not for 300°K.

It is significant that the hydrogen desorption spectra for ammonia interaction at successively higher temperatures shown in Figure 12 extend beyond the envelope of the spectra obtained from interaction at lower temperatures. Also, the peak maxima are at progressively higher temperatures. This increased stability of the surface phase towards hydrogen desorption could be caused by a decreased efficiency of hydrogen adatom recombination as the surface coverage of nitrogen increases (Figure 13) or alternatively by an increased stability of the adsorbed NH_x intermediates in the dissociation of adsorbed ammonia. Recently it was shown that on the W{100} crystal plane the presence of nitrogen on the surface causes hydrogen desorption to occur at slightly lower temperature [24]. The former alternative is therefore

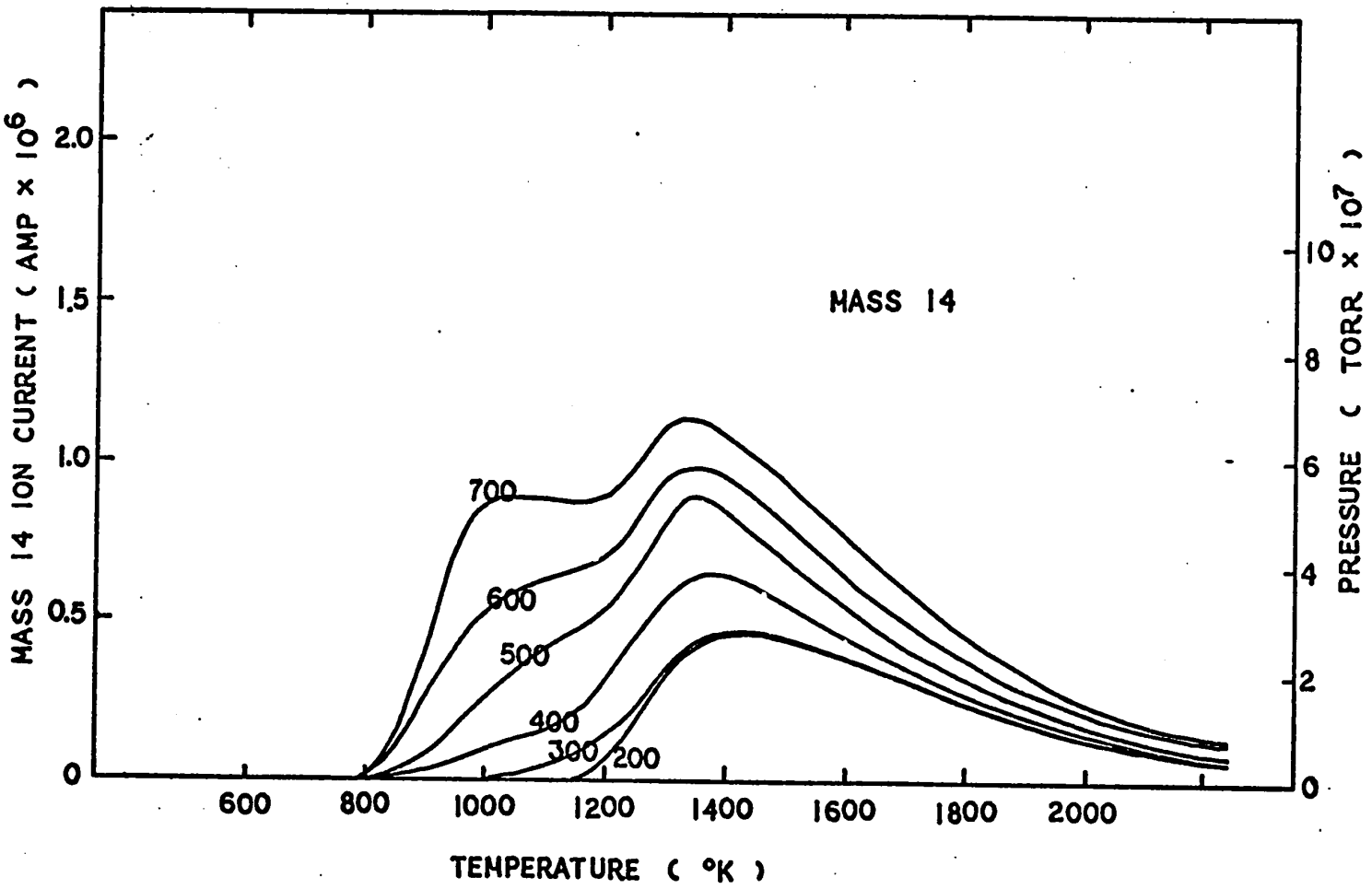

Fig. 13. Nitrogen desorption spectra, obtained using Method II, from adsorption of ammonia at 10^{-4} torr for 10 minutes at temperatures between 200 and 700°K.

believed to be unlikely. The latter alternative can be supported by two observations; first, the total nitrogen and hydrogen adatom concentration exceeds the surface tungsten atom concentration and thus NH_x intermediates can be expected on the surface, and secondly, if the transition state for NH_x dissociation involves adjacent tungsten atoms, occupation of the adjacent sites by adsorbed nitrogen will retard this dissociation.

The nitrogen desorption spectra shown in Figure 13 reveal a steadily increasing surface nitrogen concentration as the temperature of interaction is increased. For interaction at 700°K there is a clearly resolved low temperature state with a peak maximum at approximately 1000°K.

The increase in nitrogen surface concentration, in addition to that shown in Figure 13, has also been observed from adsorption of ammonia on a tungsten surface at 300°K with intermittent preflashing to 800°K. A typical desorption spectrum is shown in Figure 14 where the amount of nitrogen desorbed is approximately twice that of β-nitrogen and any parallel hydrogen desorption is negligible in magnitude. This low temperature desorption feature is designated as δ-nitrogen.

From a comparison of desorption spectrum obtained from δ-nitrogen with that shown in Figure 13 a fundamental question arises; that is whether the low temperature state obtained from ammonia interaction at temperatures higher

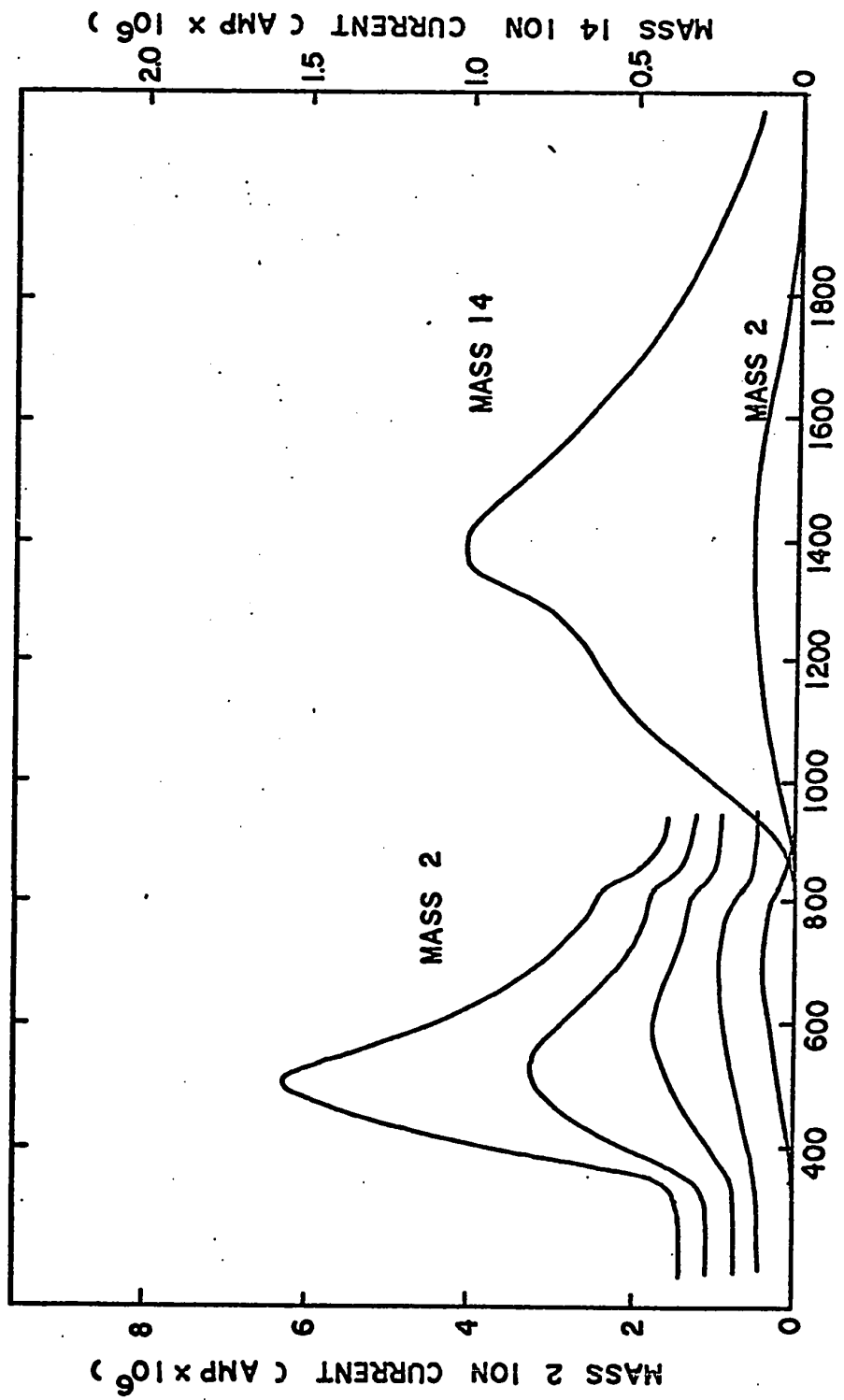

Fig. 14. The formation of δ-nitrogen. Repeated adsorption of ammonia at 10^{-4} torr for 5 minutes at room temperature and heating to 800°K gives the steadily decreasing hydrogen desorption spectra shown on the left-hand side of this figure. After the five adsorption-desorption cycles shown, the nitrogen and hydrogen desorption spectra shown on the right-hand side of the figure were obtained using Method II

than 300°K can be identified with the δ-state, or is, at least in part associated with a new surface state containing hydrogen. In order to answer this question, the interaction of ammonia was carried out with the filament at 700°K using Method II. In this method, the reaction cell walls were covered with an ammonia layer to reduce the residence time for nitrogen on the cell walls at 77°K. This method also produced hydrogen desorption spectra different from those already obtained using Method I. Mass 2 and mass 14 spectra for the adsorption at 700°K of ammonia at pressures of 10^{-4}, 10^{-3} and 10^{-2} torr for 10 minutes are shown in Figure 15. It can be seen that a simultaneous pressure burst of nitrogen and hydrogen is observed, desorption commencing at 700°K with peak maximum at 1000°K. These desorption features are designated as η-nitrogen and η-hydrogen. The dashed curves in Figure 15 were obtained from a 300°K ammonia dose at 10^{-2} torr for 10 minutes and a preflash to 700°K. As expected, no η-nitrogen or η-hydrogen are formed at 300°K and the absence of such features in the 300°K spectra demonstrates that the η-species are not an artefact caused, for example, by desorption of trapped ammonia from the reaction vessel wall. The 1400°K peak in the mass 14 spectra is doubtless β-nitrogen whereas the high temperature shoulder in the mass 2 spectra can be attributed to desorption from the cooler ends of the filament and occurs in all spectra. A slight contribution by interaction with gas phase

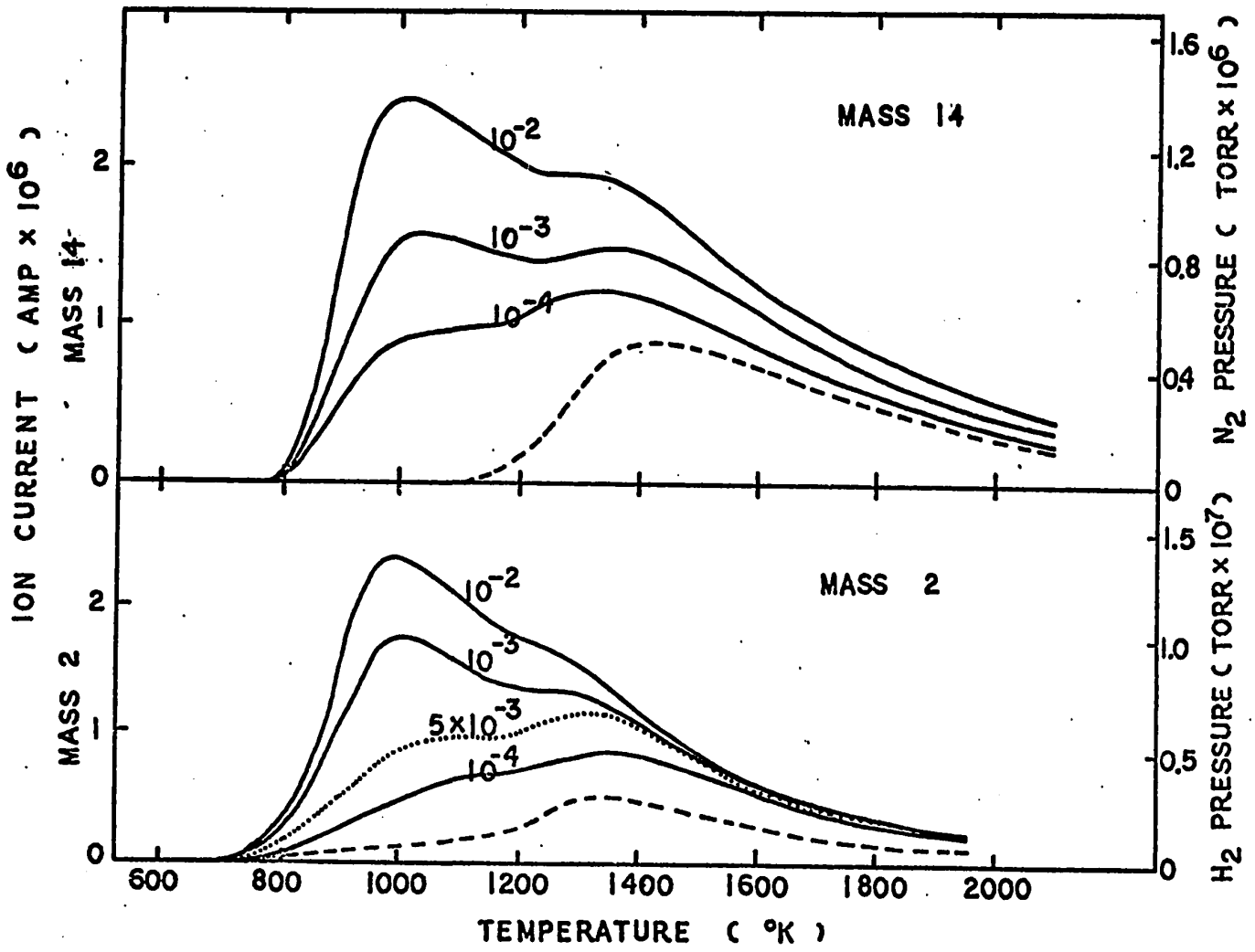

Fig. 15. Hydrogen and nitrogen desorption spectra, obtained using Method II, from the adsorption of ammonia at 10^{-4}, 10^{-3} and 10^{-2} torr for 10 minutes at 700°K. The dashed curves show spectra obtained for adsorption at 10^{-2} torr for 10 minutes at 300°K and preflashing to 700°K. For comparison, the dotted curve shows the hydrogen desorption spectrum, obtained using Method I, from ammonia adsorption at 5×10^{-3} torr for 10 minutes at 700°K.

ammonia is also possible since a line of sight exists between the warm glass of the exit tube of the reaction vessel and the sample filament.

4.1.2 State of hydrogen desorbing from the η-speices.

One conclusion to be drawn from the η-hydrogen desorption results is that the desorbing species is probably atomic and not molecular hydrogen. The results shown in Figure 7 and 12 show that a glass wall at 77°K does not trap molecular hydrogen whether the source be adsorbed hydrogen or chemisorbed ammonia. Yet the η-hydrogen desorption observed using Method I (dotted line in Figure 15) is much less than that observed with Method II. It is well known [25] that atomic hydrogen is effectively trapped by glass at 77°K so apparently a 25 Å thick layer of ammonia on the glass surface at 77°K increases the recombination efficiency of hydrogen atoms. This observation is most significant to an understanding of the ammonia decomposition mechanism and is further confirmed by using Method III to obtain desorption spectra at room temperature.

Hydrogen and nitrogen desorption spectra obtained using Method III are shown in Figure 16 for the same adsorption conditions as used in Figure 15. The simultaneous desorption features of η-nitrogen and η-hydrogen are very clearly resolved with peak maxima of 970 and 985°K respectively. Since the peak maxima do not shift with varying

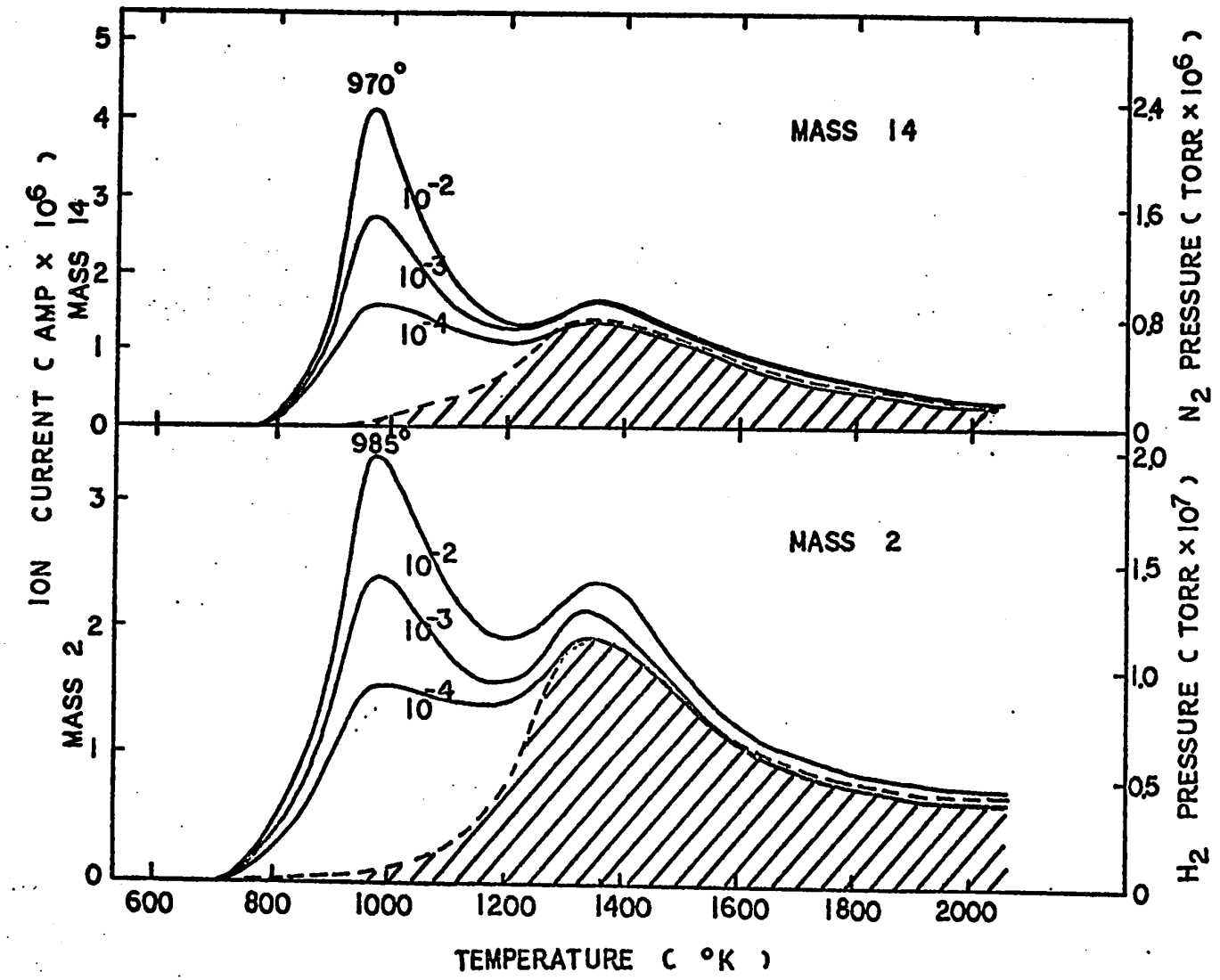

Fig. 16. Hydrogen and nitrogen desorption spectra, obtained using Method III, from the adsorption of ammonia at 10^{-4}, 10^{-3} and 10^{-2} torr for 10 minutes at 700°K. The shaded curves show spectra obtained for adsorption at 10^{-2} torr for 10 minutes at 300°K and preflashing to 700°K.

surface coverage the η-species must desorb by first order kinetics [16]. The shaded nitrogen desorption peak corresponds to β-nitrogen desorption, but the shaded hydrogen peak is sensitive to gas phase ammonia pressure, in this example 5×10^{-7} torr, and must be caused by decomposition of ammonia gas on the hot sample filament. These features appear to have been misinterpreted as new surface features in LEED/thermal desorption studies [10,11]. The η-hydrogen peak is small in a freshly-baked system, but gradually increases in size until fairly constant and reproducible desorption spectra are obtained. A similar behaviour of the hydrogen peak caused by ammonia decomposition during thermal desorption has been reported [11].

The slight delay of peak maximum in hydrogen desorption spectrum with respect to that of nitrogen as shown in Figure 16 can be interpreted in a similar way to the different behaviour between low temperature hydrogen and η-hydrogen on liquid nitrogen cooled glass walls during the desorption; η-hydrogen desorbs atomically with a relatively long residence time on the glass walls in comparison with that of nitrogen molecules. If this is the case a simultaneous desorption of hydrogen and nitrogen would be observed if the rate of desorption of η-species is slow enough so that the long residence time of atomic hydrogen becomes negligible. To test this speculation an experiment using a much slower heating rate, i.e. 10.5 deg/sec instead of 50 deg/sec

as used throughout this experiment, was carried out under the same adsorption conditions as used in Figure 16. Results obtained are shown in Figure 17. The delay between the hydrogen and nitrogen desorption peaks has indeed been reduced from 15^{o} to 5^{o}.

All these observations are in good agreement with those of Hickmott on the interaction of atomic hydrogen with glass surfaces [25]. Atomic hydrogen is pumped by a freshly-baked glass surface at $300^{o}K$ but the surface eventually saturates and will then no longer act as a trap. At $77^{o}K$ the glass acts as an even more efficient trap but again saturates. At first sight this would suggest that eventually after many experiments using Method I an η-hydrogen peak should be obtained equal in magnitude to those obtained using Methods II and III but such an effect was never observed. Again, Hickmott's results explain this effect. A substantial fraction of the atomic hydrogen trapped at $77^{o}K$ is reversibly adsorbed and on warming to room temperature desorbs, creating new trapping sites. Between experiments the reaction vessel must be warmed to room temperature to adsorb ammonia and so the trapping sites effective at $77^{o}K$ are continually regenerated. These observations provide strong, though indirect, evidence that η-hydrogen desorbs atomically.

There are several ways that direct observation could be made : First, if the speculation that η-hydrogen desorbs atomically is correct, an experiment carried out in an

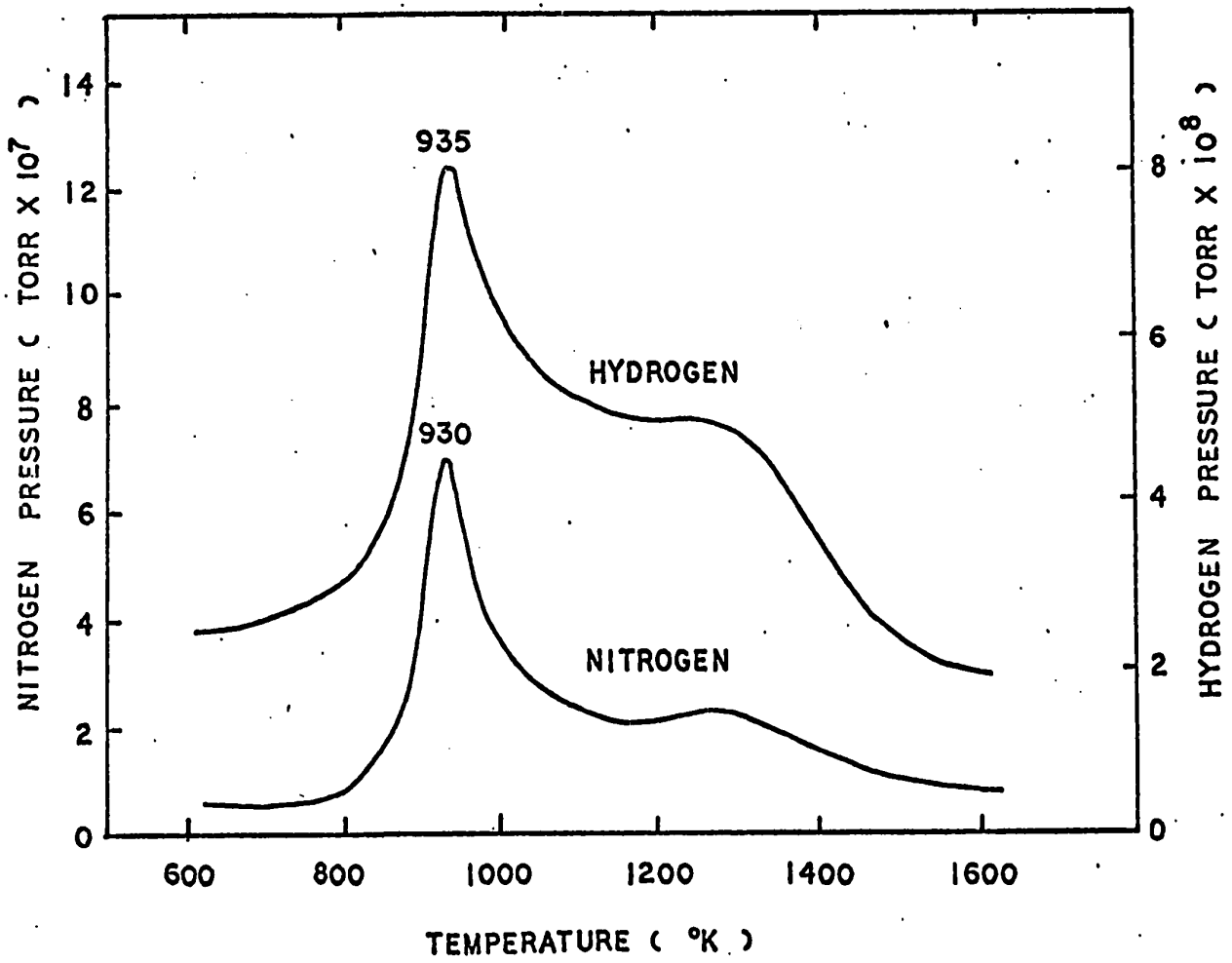

Fig. 17. Hydrogen and nitrogen desorption spectra obtained from the adsorption of ammonia at 10^{-2} torr for 10 minutes at 700°K. Heating rate, 10.5 deg sec.

experimental chamber with line of sight between sample filament and the mass spectrometer would provide a smaller mass 2 to mass 1 ratio than that obtained from the mass spectrometric cracking pattern of molecular hydrogen gas. Second, if η-hydrogen does desorb atomically and recombine with atomic hydrogen trapped on the walls, in a reaction chamber where the walls are saturated with deuterium atoms η-hydrogen would be detected predominently as HD. The following two experiments were attempted using Method III to make these direct observations .

Experiment I: Line of sight experiment.

This experiment was carried out in the experimental set up shown in Figure 8. In order to increase the fraction of desorbing species passing through the mass spectrometer ionization chamber, the sample filament was mounted approximately 0.5 cm under the opening of ionization chamber. After flash cleaning the sample filament ammonia gas at a pressure of 10^{-2} torr was allowed to interact with the filament at $300^{o}K$ and $700^{o}K$ for 10 minutes. The atomic and molecular hydrogen desorption spectra were obtained by monitoring the mass 1 and mass 2 ion currents simultaneously. Typical desorption spectra are shown in Figure 18. The mass 2 to mass 1 ratio was obtained by comparing the peak maximum of these two spectra. This experiment has been repeated for $\sim$30 times at each temperature and the probability of occurrence as a function of mass 2 to mass 1 ratio is shown in

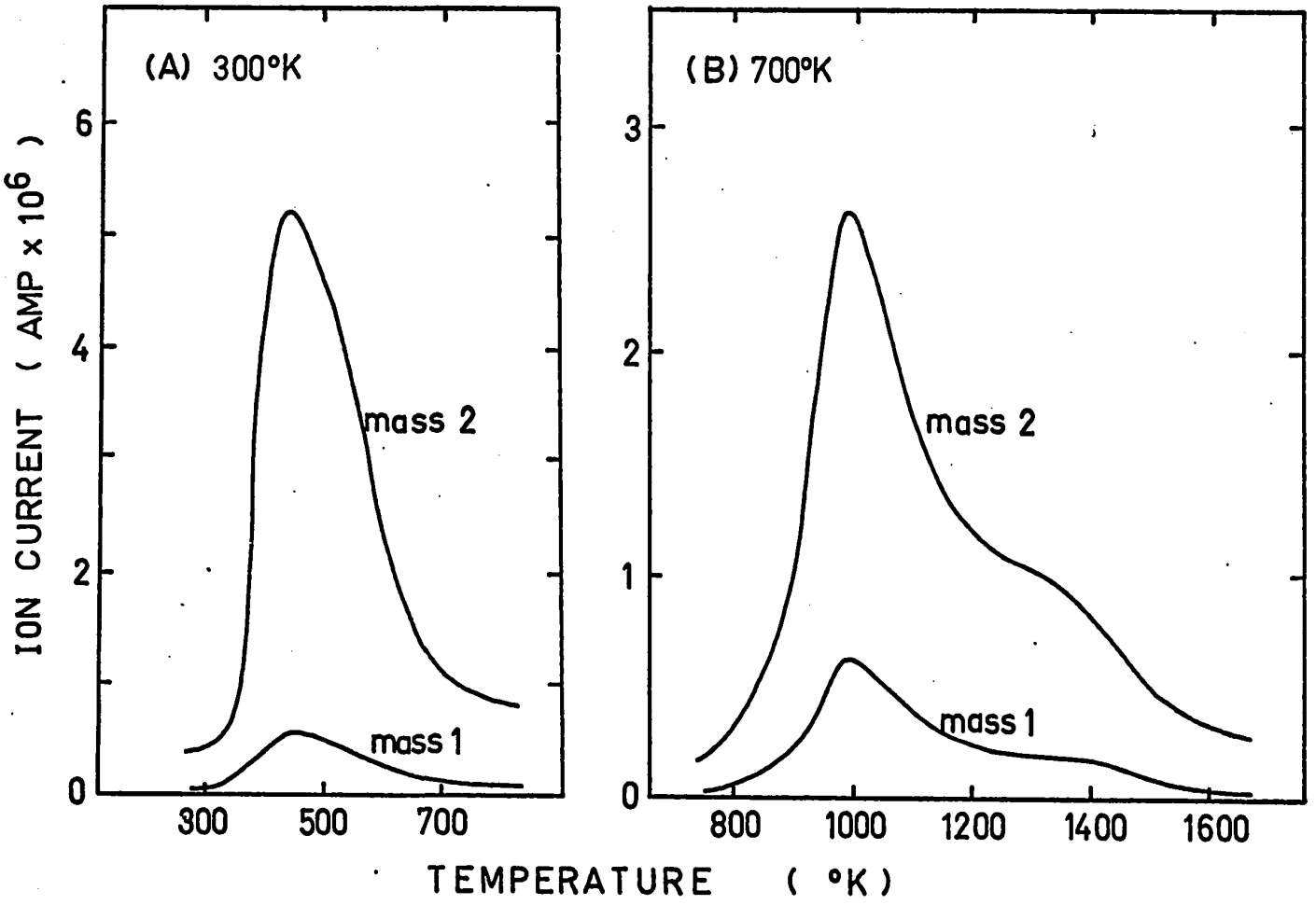

Fig. 18. Atomic hydrogen and molecular hydrogen desorption spectra obtained from adsorption of ammonia at 10^{-2} torr for 10 minutes at 300 and 700°K. A 10 times higher sensitivity was used for recording mass 1 than that used for mass 2.

Figure 19. It is seen that for interaction at 300°K over 80% of the ratios range from 80 to 140. Since the ratio obtained from the cracking pattern of molecular hydrogen gas is ∿110, it can be concluded that hydrogen originated from the surface species formed at 300°K desorbs in the molecular state. For interaction at 700°K, this mass 2 to mass 1 ratio from η-hydrogen as predicted does have a lower value; approximately 80% of these ratios range from 20 to 80. It is thus obvious that a difference exists between these two hydrogen desorption peaks. A simple calculation (see Appendix A) in which it is assumed that all atoms which can enter the ionization chamber directly will be detected as mass 1 and all atoms which collide with walls as mass 2 shows that mass 2 to mass 1 ratio will have a value of ∿33. While in fair agreement with the observed value, ∿56, it seems probable that a fraction of the high temperature η-hydrogen peak desorbs molecularly.

Experiment II: Walls saturated with deuterium.

To carry out this experiment the glass wall was saturated with deuterium atoms by allowing the deuterium gas to flow through the reaction vessel for several hours at a pressure of $\sim 2\times10^{-6}$ torr, with the sample filament at ∿2000°K. After the deuterium gas flow was stopped, the system was evacuated overnight, ammonia gas was allowed to interact with tungsten first at 300° then at 700°K under the same conditions

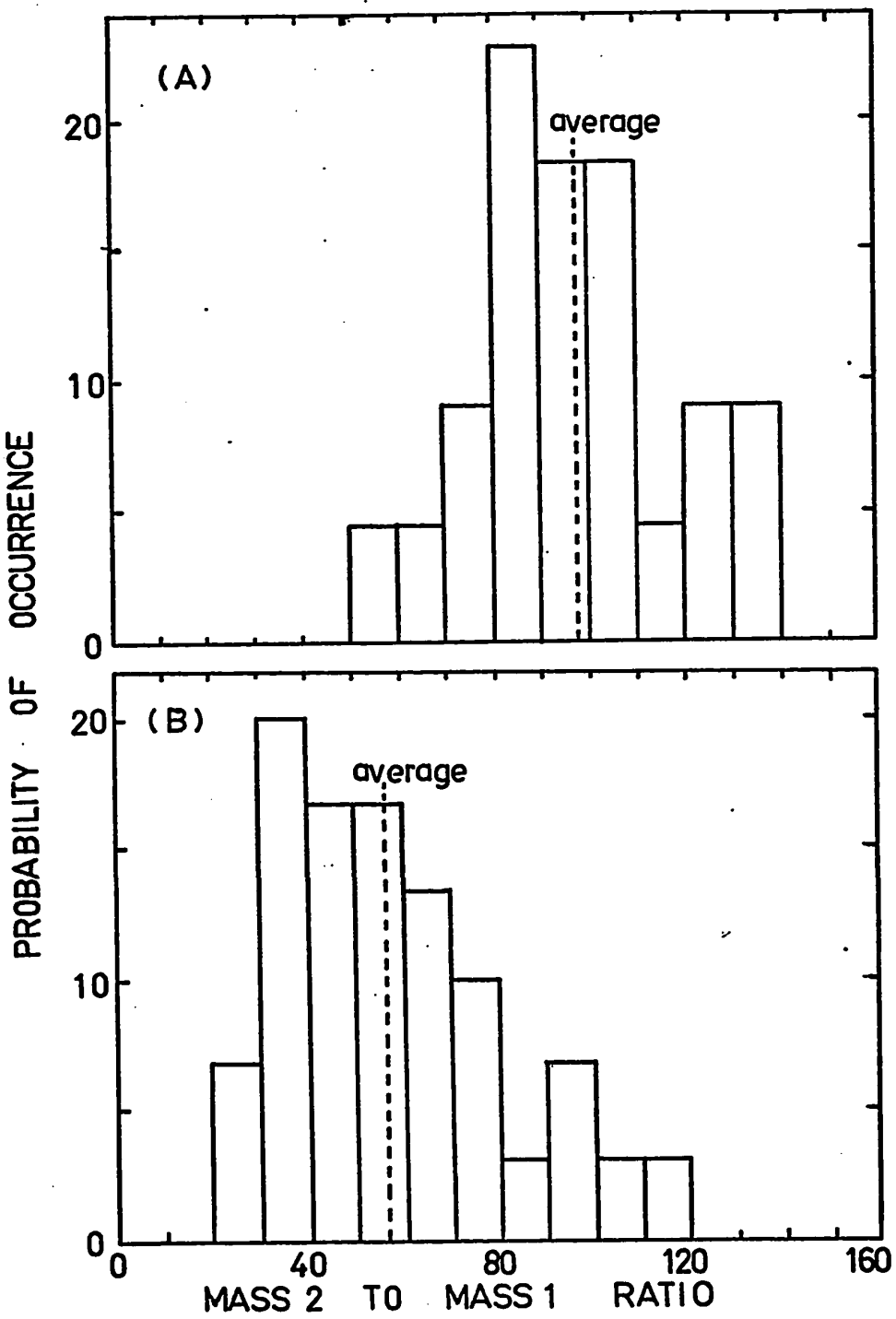

Fig. 19. Probability of occurrence for certain mass 2 to mass 1 ratio obtained by comparing the peak maximum of mass 2 and mass 1 desorption spectra shown in Figure 18. (A) at 300°K and (B) at 700°K

as used in Figure 18. The desorption spectra obtained by monitoring mass 2, 3 and 4 simultaneously are shown in Figure 20. By comparing the peak maxima, mass 3 to mass 2 ratios for interaction at 300 and 700°K are found to be 0.08 and 0.38 respectively. Since adsorbed hydrogen desorbs as atoms appreciably only at temperature higher than 1000°K, this result shows unambiguously that η-hydrogen desorbs, at least in part, atomically, though the hydrogen was not detected predominantly as HD. The discrepancy between speculated and observed values may arise from several effects; (1) The glass wall may not be completely saturated with atomic deuterium. Based on Hickmott's results [25] the method employed in this experiment will generate more than enough atomic deuterium for saturating the glass walls. However, since ammonia can be adsorbed strongly on the walls, the introduction of ammonia into the system could cause an exchange reaction to take place between ammonia and deuterium atoms and reduce the deuterium atom concentration on the walls. It has been reported [26] that a random distribution of hydrogen over ND_3-molecules was observed when ND_3 alone was introduced into the system where the mass spectrometer was operating with such low electron energy that only the peak of the parent ion ND_3^+ was observed in the spectrum. The observed randomization was interpreted as the result of an exchange reaction between ND_3 and hydrogen trapped in the system. (2) Isotopic scrambling presumably by the hot mass spectrometer filament, the

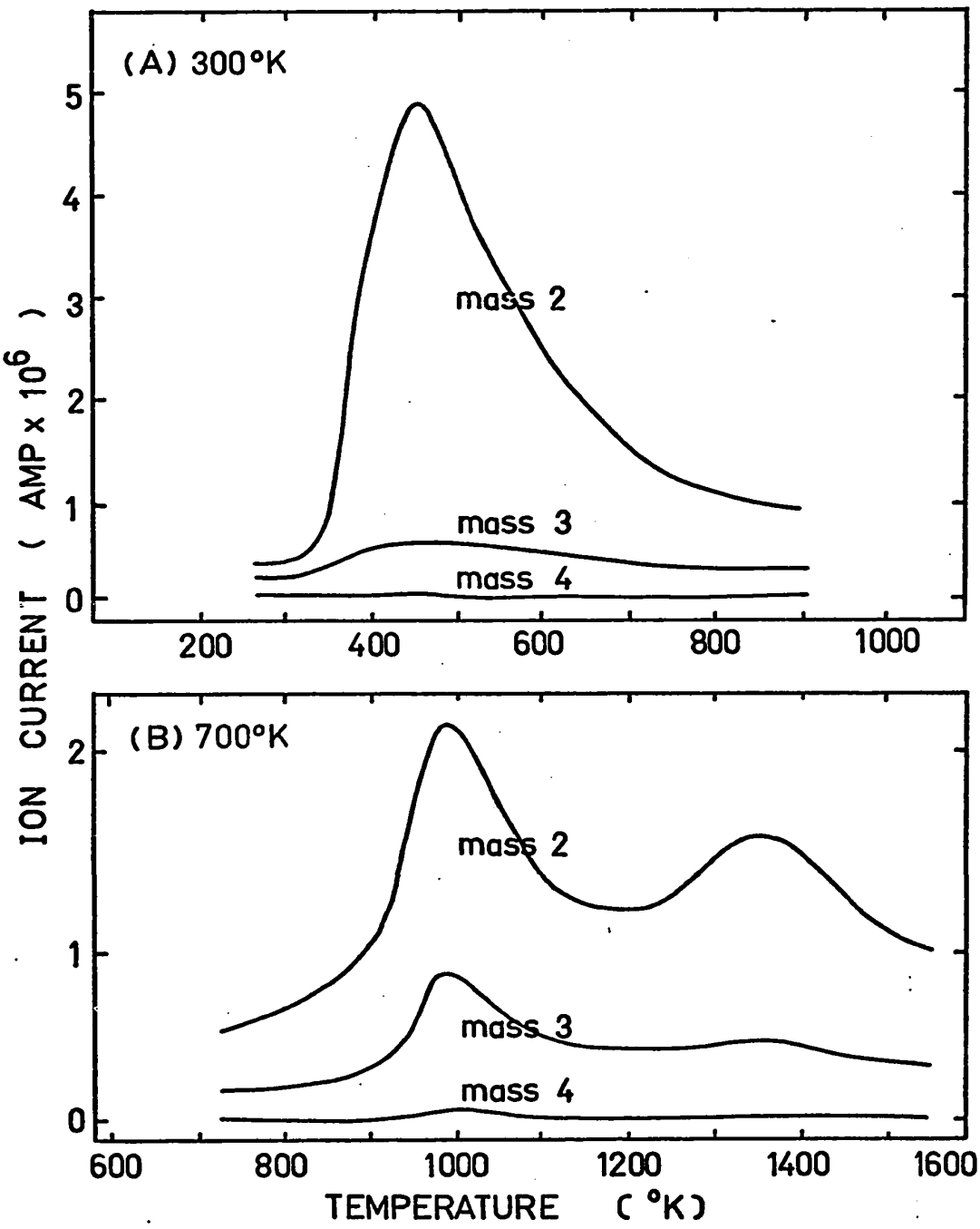

Fig. 20. Desorption spectra of mass 2, 3 and 4 obtained from adsorption of ammonia at 10^{-2} torr for 10 minutes at 300 and 700°K in a reaction vessel where the walls were saturated with deuterium atoms.

tungsten grid of ionization gauge and the metal walls was observed to occur to some extent in the system used in this experiment. As shown in Figure 21 when hydrogen and deuterium were allowed to flow through the system simultaneously from separate reservoirs, mass 3, HD, peak was observed instantaneously. Consequently, any HD resulting from recombination of η-hydrogen and deuterium atoms on the walls would give rise to mass-2 and mass-4 peaks and a reduction in the amount of HD. (3) In addition, it seems also probable that only a fraction of the high temperature η-hydrogen desorbs atomically. Based on the results of these two experiments, the fraction of hydrogen desorbing as atoms can be estimated if these two effects, i.e. the isotopic scrambling and the exchange reaction between ammonia and deuterium atoms on the walls, can be considered as negligible. It is found that in the line of sight experiment about 48% of hydrogen originated from the η-species desorbs as hydrogen atoms whereas the fraction of hydrogen desorbing as atoms calculated from desorption spectra shown in Figure 20 is ∿16%. The large difference between these values could therefore indicate that the isotopic scrambling and the exchange reaction on the walls are considerable.

4.1.3 Quantitative estimates of surface coverage.

4.1.3(a) Low temperature hydrogen, β-nitrogen and δ-nitrogen coverages.

The amount of hydrogen originating from surface

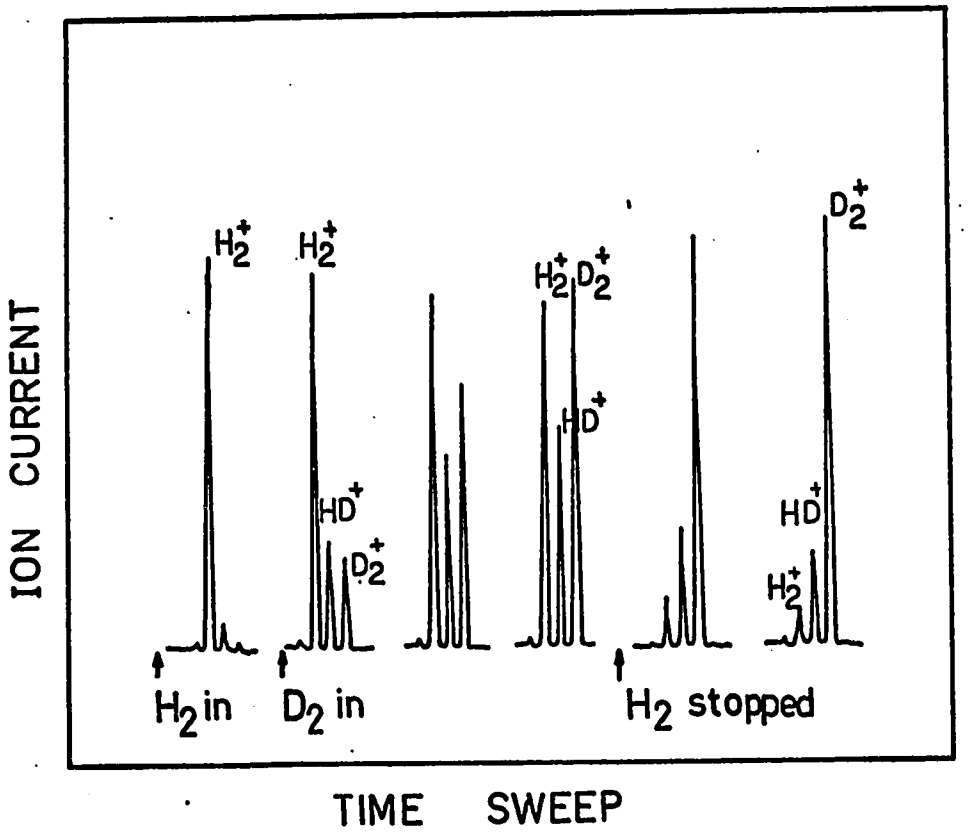

Fig. 21. Relative intensities of mass 2, 3 and 4 when hydrogen and deuterium gases were allowed to flow through the system from separated reservoirs.

species formed from ammonia adsorption at 300°K was determined by using the ionization gauge as a detector operating at very low emission current in a closed system. Since the desorption of low temperature hydrogen was completed at 800°K as shown in Figure 12, the filament was flashed to this temperature after trapping out the ammonia in the gas phase and the instantaneous pressure burst was recorded. The coverage of β-nitrogen and δ-nitrogen which was obtained after five repeated ammonia doses, with intermittent preflashing to 800°K, was determined in similar way by flashing the filament to 2000°K in about one second, but using the mass spectrometer as a detector. Hydrogen and nitrogen coverages calculated using the geometric area of the filament are shown in Figure 22; they are 0.8×10^{15} atoms cm^{-2} for low temperature hydrogen, 0.48×10^{15} atoms cm^{-2} for β-nitrogen and 0.84×10^{15} atoms cm^{-2} for δ-nitrogen regardless of ammonia pressure during adsorption. These observations indicate that on polycrystalline tungsten ammonia was dissociated upon adsorption and about half of the hydrogen desorbed during ammonia adsorption at 300°K.

4.1.3(b) η-hydrogen coverage.

The amount of hydrogen desorbing in the η peak was estimated in the following way using Method III. A hydrogen desorption spectrum for ammonia adsorption at 300°K was obtained before and after each experimental run. Since this hydrogen desorbed molecularly at a low temperature,

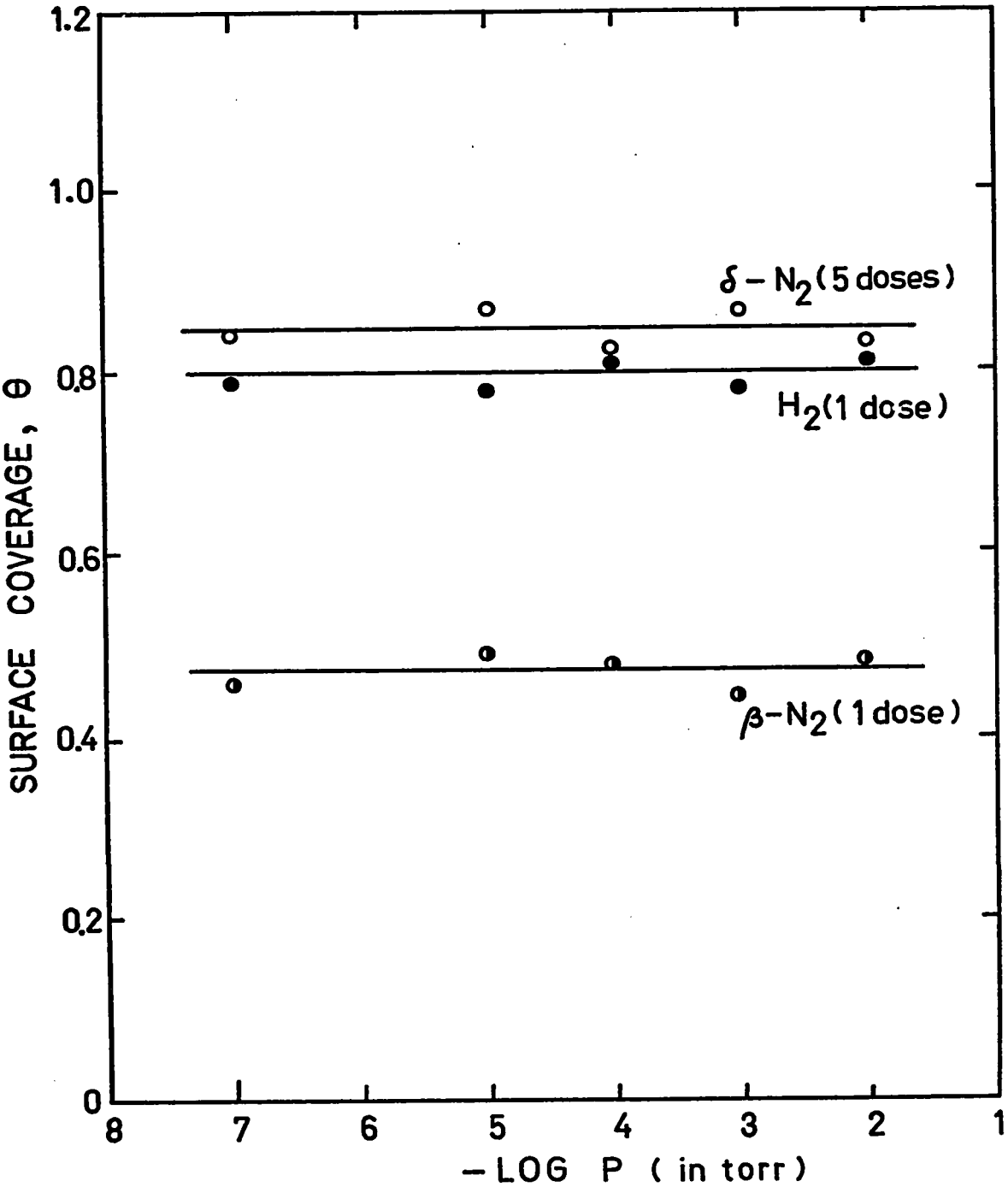

Fig. 22. The variation in hydrogen, β-nitrogen and δ-nitrogen surface coverage with increasing ammonia dosing pressure. Both hydrogen and β-nitrogen were obtained from ammonia adsorption at 300°K for 5 minutes at different pressures, while δ-nitrogen was obtained from 5 repeated doses of ammonia at 300°K with intermittent heating to 800°K.

that is much below the temperature at which the sample filament starts to pump hydrogen (1100°K), the surface coverage for this species could be calculated reasonably accurately. Comparison of the area of the desorption trace from the 700°K adsorption with the average area from the 300°K adsorptions gave the total hydrogen desorbing in the 700°K spectrum. This laborious procedure was necessary because the efficiency of the ion pump decreased steadily between bake-outs. The amount of hydrogen produced by decomposition of gas phase ammonia on the filament was obtained by repeating the experiment at 300°K, with preflash to 700°K, and therefore without the formation of the η-species (dashed curve in Figure 16). Subtraction gave the values for the surface coverage of η-hydrogen shown in row 1 of the Table I. The assumption, implicit in this calculation, that the recombination efficiency for hydrogen atoms is unity on the saturated walls is justified by Hickmott's observations [25]. The reactions leading to the adsorption of atomic hydrogen on the glass wall and its recombination are

$$H(g) + (wall) \rightarrow H\ (wall) \qquad 1$$

$$2H\ (wall) \rightarrow H_2(g) + 2\ (wall) \qquad 2$$

$$H(g) + H\ (wall) \rightarrow H_2(g) + (wall) \qquad 3$$

Hickmott has shown that reaction 2 is very slow and that recombination occurs via reaction 3. This might suggest that

TABLE I

Surface coverage, (atoms cm^{-2})$\times 10^{-15}$, of hydrogen and nitrogen and hydrogen to nitrogen ratios for three different ammonia exposures

Ammonia exposure (torr-sec.)	0.06	0.6	6.0
1. η-hydrogen	0.16	0.27	0.36
2. Total nitrogen	0.81	0.95	1.08
3. η-nitrogen (a)	0.33	0.47	0.60
4. η-nitrogen (b)	0.29	0.50	0.66
5. η-hydrogen/total nitrogen	0.20	0.28	0.33
6. η-hydrogen/η-nitrogen (a)	0.49	0.58	0.60
7. η-hydrogen/η-nitrogen (b)	0.55	0.54	0.55

one-half the detected hydrogen originates on the wall and not from the filament. However, hydrogen atoms desorbing from the filament are lost through reaction 1, reducing the amount detected. In the present experiments we would expect that after repeated experiments, when the desorption had increased to a relatively reproducible magnitude, reactions 1 and 3 occur to an equal extent and the amount of hydrogen detected corresponds to that desorbing from the filament.

4.1.3(c) η-nitrogen coverage.

(i) This was determined by a different procedure using the mass spectrometer as a detector in a closed system. After adsorption and trapping out the ammonia from the gas phase, the filament was flashed to 2000°K in about one second while monitoring the mass 14 ion current. The contribution to the mass 14 ion current from decomposition of gaseous ammonia on the sample is negligible in these experiments. Total nitrogen coverages determined in this way are shown in row 2 of Table I. Subtracting the β-nitrogen contribution to this surface coverage (0.48×10^{15} atoms cm^{-2}) gives the η-nitrogen coverage shown in row 3.

(ii) These values for η-nitrogen coverage were checked by using a method similar to that used to determine the η-hydrogen coverage. Comparing the total area of the mass 14 traces in Figure 16 with that obtained from a β-nitrogen

covered surface gave the values shown in row 4 of Table I for the η-nitrogen coverage. The agreement is quite satisfactory.

4.1.4 Pressure dependence of the η-formation reaction.

The experiments described so far were carried out in the pressure range 10^{-4} to 10^{-2} torr. These pressures, while much below those used in the classical kinetic studies, are higher than those commonly used in ultra-high vacuum studies. It is important to determine whether or not this reaction is peculiar only to these relatively high pressures. The mass 2 and mass 14 spectra for the interaction of ammonia over a wide range of pressure and total exposure with a tungsten filament at 700°K are shown in Figure 23 and 24. Spectra (a) to (f) show that the η-coverage increases with increasing total exposure and that the η-species does indeed form when the ammonia pressure is in the range 10^{-7} to 10^{-4} torr. However, spectrum (g) would suggest that the η-coverage does not vary linearly with exposure since the coverage is greater for an exposure of 0.15 torr-sec at 5×10^{-7} torr (g) than for a larger exposure, 1.2 torr-sec , at the higher pressure of 2×10^{-3} torr (e). Furthermore, the peak maxima in spectra (g) are displaced to higher temperatures than those obtained after much shorter interaction times. Apparently, a long interaction time promotes greater η-formation and also increases its stability. Both these effects could arise from an additional very slow reaction leading to the population

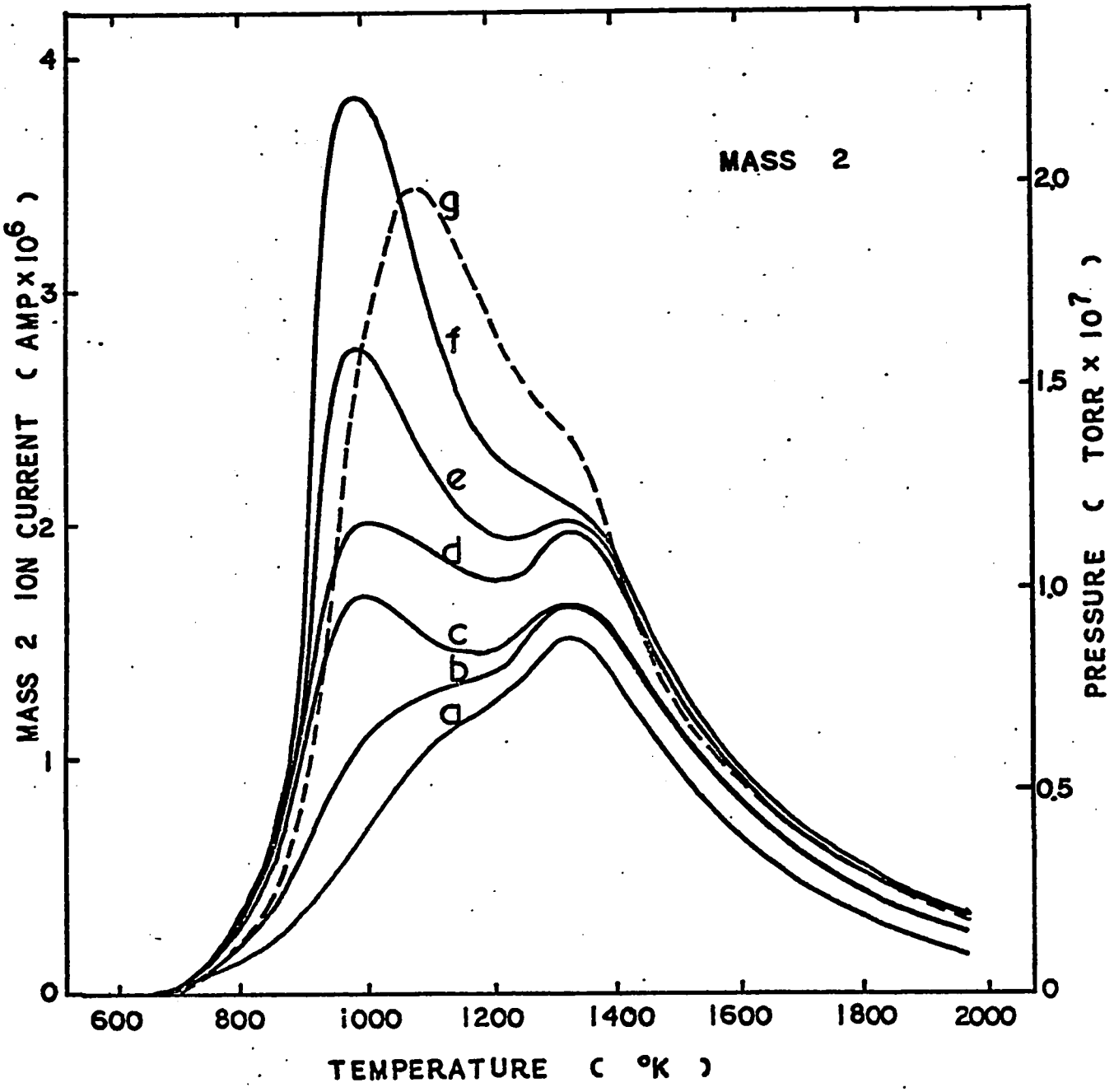

Fig. 23. Hydrogen desorption spectra, obtained using Method IV, from adsorption of ammonia at (a) 5×10^{-7} torr, 3×10^{-4} torr-sec; (b) 2×10^{-6} torr, 1.2×10^{-3} torr-sec; (c) 2×10^{-5} torr, 1.2×10^{-2} torr-sec; (d) 1×10^{-4} torr, 6×10^{-2} torr-sec; (e) 2×10^{-3} torr, 1.2 torr-sec; (f) 1×10^{-2} torr, 6 torr-sec; (g) 5×10^{-7} torr, 1.5×10^{-1} torr-sec.

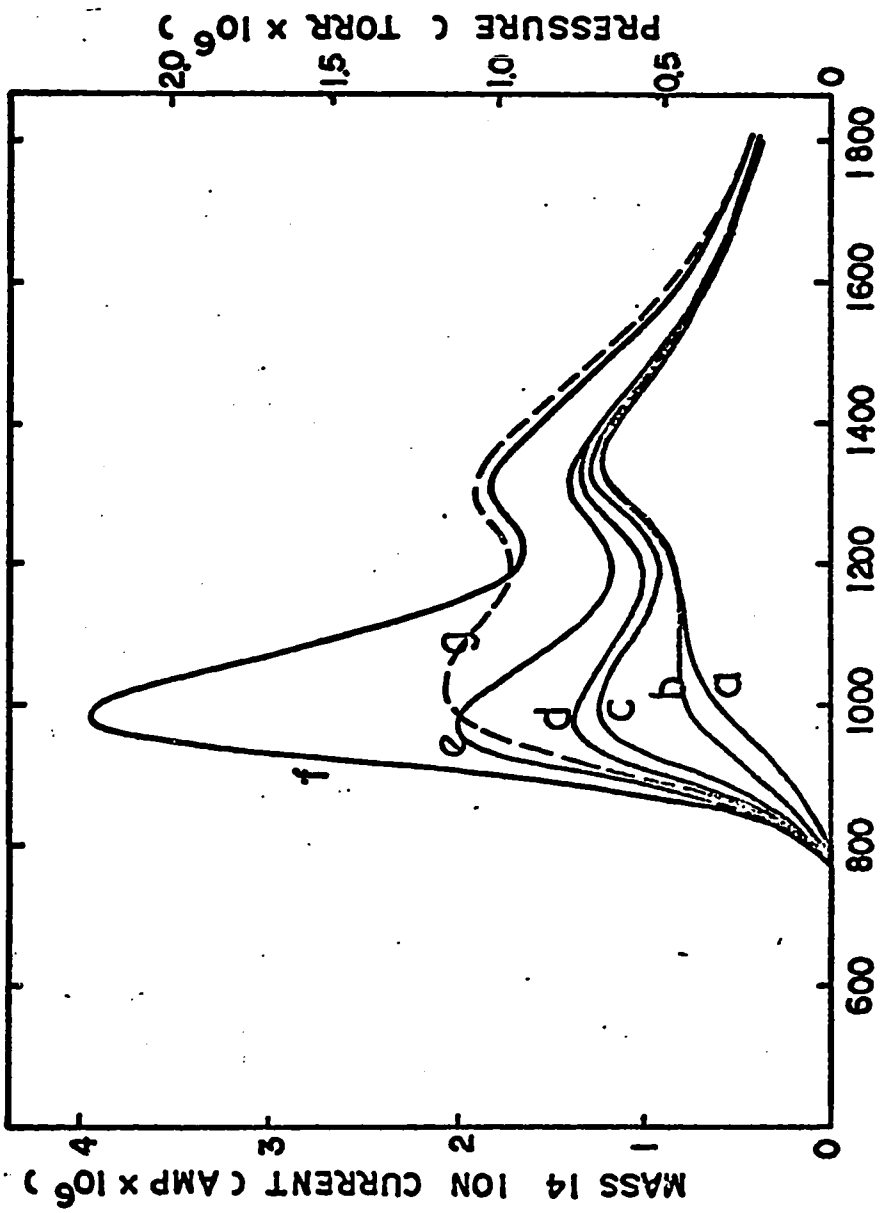

Fig. 24. Nitrogen desorption spectra obtained using Method IV and the same adsorption conditions as described in Fig. 23.

of different states. As will be subsequently discussed in section 4.3.4, nitrogen and hydrogen atoms may penetrate into the surface.

The surface coverage of the η-species is not affected by maintaining the sample at 700°K and condensing the ammonia before desorption. Thus, the η-species is not in equilibrium with gas phase ammonia and is not weakly adsorbed undissociated ammonia.

4.1.5 Hydrogen to nitrogen ratios in the formation and desorption of the η-species.

Formation

As the ammonia exposure increases the ratio η-hydrogen/total nitrogen surface coverage increases until at 6 torr-sec the η-hydrogen is equivalent to one-third of the total nitrogen (row 5, Table I). Figure 25 shows in greater detail the variation in total hydrogen (η-hydrogen) and nitrogen coverage with exposure and it can be seen that an exposure of 6 torr-sec corresponds approximately to a saturated surface. Both β-nitrogen (0.48×10^{15} atoms cm^{-2}) and δ-nitrogen form rapidly, while ammonia interaction to form the η-species is much slower at 700°K. During η-formation the hydrogen and nitrogen surface coverages increase at an equal rate, that is incorporation of each nitrogen atom into the surface layer also incorporates one hydrogen atom. At saturation about 0.35×10^{15} atoms of both hydrogen and nitrogen are incorporated

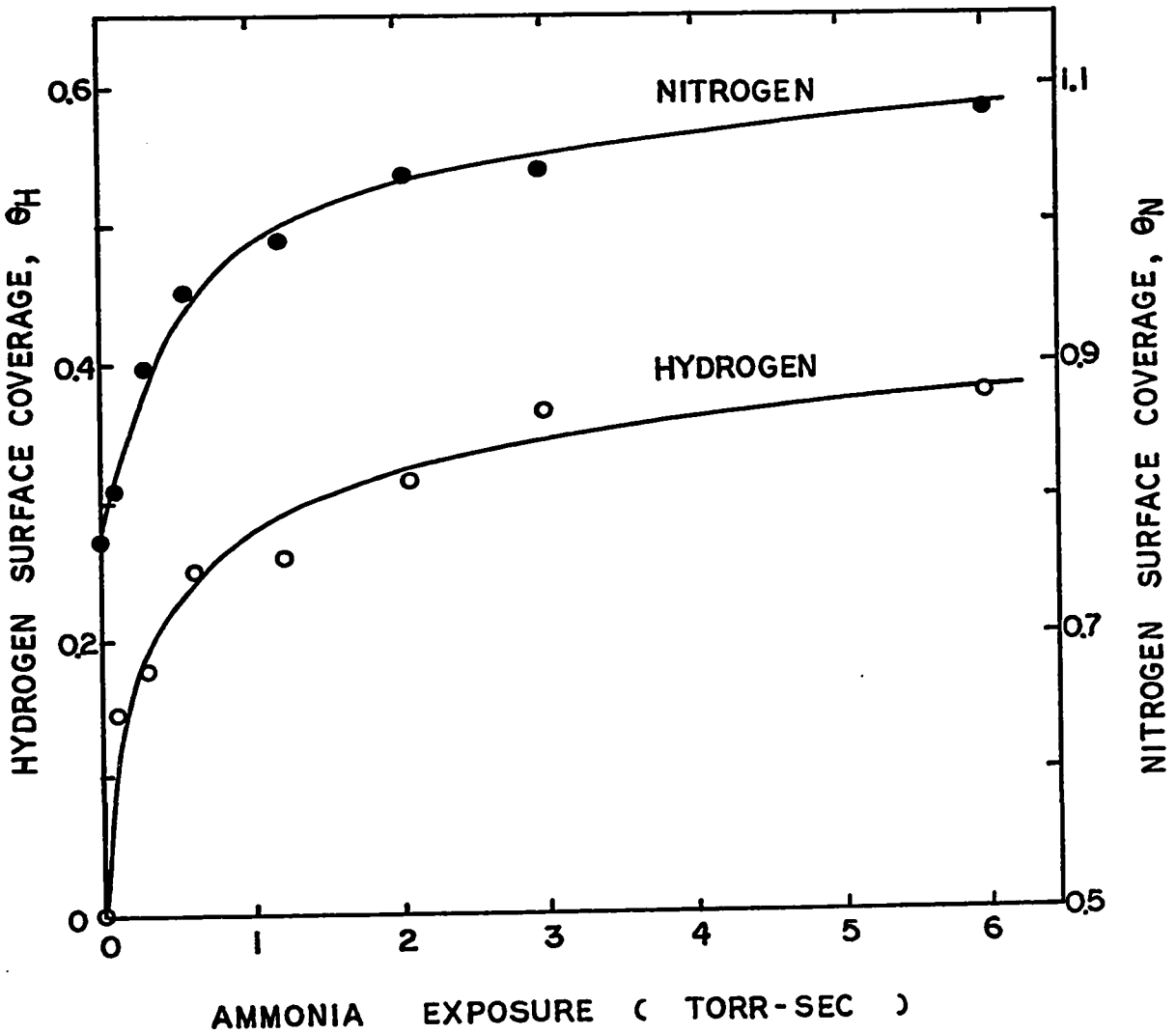

Fig. 25. The variation in total surface coverage of hydrogen and nitrogen with increasing ammonia exposure at 700°K. (θ is the fractional surface coverage calculated by assuming that the surface contains 10^{15} tungsten atoms per cm^2)

per cm^2 of surface in the formation of the η-species from δ-nitrogen.

Desorption.

From the desorption spectra obtained from the η-species (Figure 16) and δ-nitrogen (Figure 14) it appears that the formation of the η-species leads to the incorporation of δ-nitrogen (i.e. excess nitrogen in δ over β) into a single surface species. The results in Figure 25 suggest that this nitrogen is almost quantitatively incorporated into the η-species at saturation. The η-desorption spectra are characterized by exactly concurrent hydrogen and nitrogen desorption (the peak maxima differ by only $5^{o}K$) and no nitrogen desorption feature is resolved corresponding to a consecutive desorption of δ-nitrogen. Consecutive desorption of δ-nitrogen can be observed when adsorption occurs at $600^{o}K$ (Figure 26). It is concluded that the η-hydrogen/η-nitrogen ratio during desorption is in the range 0.5 to 0.6 (rows 6 and 7, Table I) where the η-nitrogen coverage is obtained by subtracting the β-nitrogen coverage from the total nitrogen coverage. The η-species contains nitrogen and hydrogen in the ratio of approximately 2 to 1.

Non-uniform temperature distribution effects.

During adsorption the centre portion of the sample filament was maintained at the specified adsorption temperature of $700^{o}K$. However, towards the ends of the filament the

temperature decreases to 300°K. The calibration experiments were obtained for adsorption at 300°K and thus correspond to a uniform temperature distribution. Consequently the results calculated so far are based on the assumption that the filament surface is uniformly covered with the η-species. This is incorrect, and corrected values for the actual surface coverage of the η-species were obtained in the following way. The continuous temperature distribution of the filament was subdivided into discrete areas with average temperatures 300, 400, 500, 600 and 700°K using the steady-state temperature distribution given by Rowland [27]. The total nitrogen coverage [in (atoms $cm^{-2}) \times 10^{-15}$] determined at each of these adsorption temperatures, using the same method as used in the determination of β- and δ-nitrogen coverages, were 0.48, 0.58, 0.70, 0.86 and 1.10 respectively. Based on these values and the steady-state temperature distribution, the coverage corresponding to each temperature was calculated using the same discontinuous model. For an exposure of 6 torr-sec the corrected value for the total nitrogen coverage at saturation was 1.5×10^{15} atoms cm^{-2} compared to an uncorrected value of 1.1×10^{15} atoms cm^{-2}. Since β-nitrogen accounts for 0.5×10^{15} atoms cm^{-2} the η-species must contain approximately 1.0×10^{15} nitrogen atoms and 0.5×10^{15} hydrogen atoms per cm^2 of surface. The average tungsten atom density can be approximated as 10^{15} atoms cm^{-2} and the present observations can be

concisely represented by the following surface stoichiometries; β-nitrogen ≡ W_2N; δ-nitrogen (+β) ≡ WN; η-species (+β) ≡ W_2N_3H. The formation reaction at 700°K can be represented as,

$$2W + NH_3(g) \longrightarrow W_2N(\beta) + 3/2\ H_2(g)$$

$$W_2N(\beta) + NH_3(g) \longrightarrow 2WN(\delta) + 3/2\ H_2(g)$$

$$2WN + NH_3(g) \longrightarrow W_2N_3H(\eta) + H_2(g)$$

and the desorption spectra of β-nitrogen, δ-nitrogen and the η-species can be represented by the following thermal desorption reactions

$$W_2N(\beta) \xrightarrow{1450^\circ K} 2W + 1/2\ N_2(g)$$

$$2WN(\delta) \xrightarrow{1100^\circ K} W_2N(\beta) + 1/2\ N_2(g)$$

$$W_2N_3H(\eta) \xrightarrow{970^\circ K} W_2N(\beta) + N_2(g) + H(g)$$

where the temperatures correspond approximately to those at which each process occurs at a maximum rate (peak maximum).

4.1.6 Interaction of ammonia with δ-nitrogen at different temperatures.

It was seen in Figure 14 that as the nitrogen surface concentration increases, less and less ammonia can further interact with surface. Consequently at saturation, the surface no longer interacts with ammonia at 300°K. A similar behavior was observed even at higher temperatures. In Figure 26 the interaction of ammonia at different temperatures with

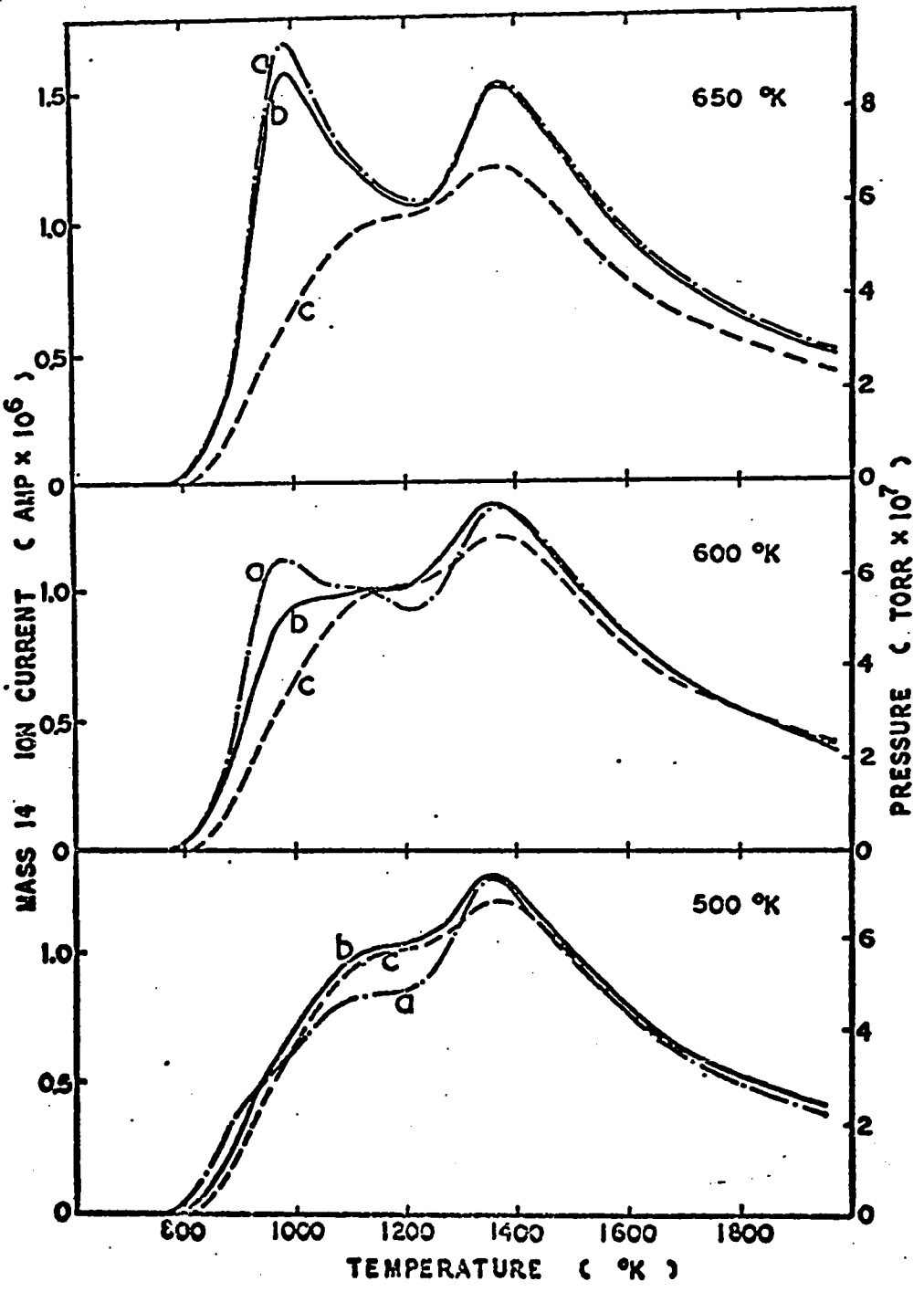

Fig. 26. Nitrogen desorption spectra, obtained using Method III, from adsorption of ammonia at 10^{-3} torr for 10 minutes at 500, 600 and 650°K on (a) a clean tungsten surface, (b) a δ-nitrogen adlayer (Fig. 14), compared with (c) the spectrum obtained for δ-nitrogen.

δ-nitrogen (formed as described in Figure 14) and also with a clean tungsten surface are compared. At 500°K the thermal desorption spectrum for δ-nitrogen is not affected by interaction with ammonia at 10^{-3} torr for 10 minutes. This indicates that even at 500°K the δ-nitrogen covered surface is not active towards ammonia adsorption. Ammonia interaction with clean tungsten at this temperature produces a smaller δ-nitrogen coverage due to the presence of hydrogen in the adsorbed layer at 500°K. At 600°K, some conversion of δ-nitrogen to η-species occurs but surprisingly more η-species is formed by interaction with the clean tungsten surface. At 650°K, extensive formation of the η-species occurs and the δ-nitrogen adlayer no longer retards the reaction. From these observations it is concluded that formation of η-species requires an appreciable activation energy and formation of a complete δ-nitrogen adlayer increases the stability of the δ-nitrogen adlayer.

4.1.7 Kinetics of formation and desorption of the η-species.

Formation.

The rate of formation of η-species can be set to equal the number of ammonia molecules colliding with unit area of surface per second multiplied by the sticking probability, S. That is

$$\text{rate} = \frac{P}{\sqrt{2\pi mkT}} \times S \qquad (20)$$

where P is ambient ammonia pressure, m molecular weight of

ammonia, k Boltzmann's constant, T ammonia gas temperature and in the present example the sticking probability is temperature dependent, $S = S_o \exp(-E^*/RT)$. From the temperature dependence of the sticking probability of η-hydrogen or η-nitrogen the activation energy for the formation of the η-species can be evaluated. The η-nitrogen surface coverages, which can be determined reasonably accurately, were obtained using the same method as used in determining the β-nitrogen coverage. The variation in total surface coverage of η-nitrogen with increasing ammonia exposure at different temperatures is shown in Figure 27. The initial sticking probabilities S evaluated from these curves were 2.6×10^{-7}, 5.1×10^{-7}, 1.1×10^{-6} and 2.2×10^{-6} at 600, 650, 700 and 750°K respectively. From the plot of log S versus 1/T (Figure 28) the activation energy for the formation of η-species was found to be 12 Kcal/mole and the constant $S_o = 6.2\times10^{-3}$. Equation 19, which describes the initial rate of formation of η-species, can therefore be written as

$$\text{rate} = 3.10^{18}.P_{NH_3}.\exp(-12{,}000/RT) \qquad (21)$$

with P_{NH_3} in torr.

Desorption

The desorption kinetics for the η-species will be deduced directly from that of η-nitrogen. To investigate the desorption process of η-nitrogen, ammonia gas at a

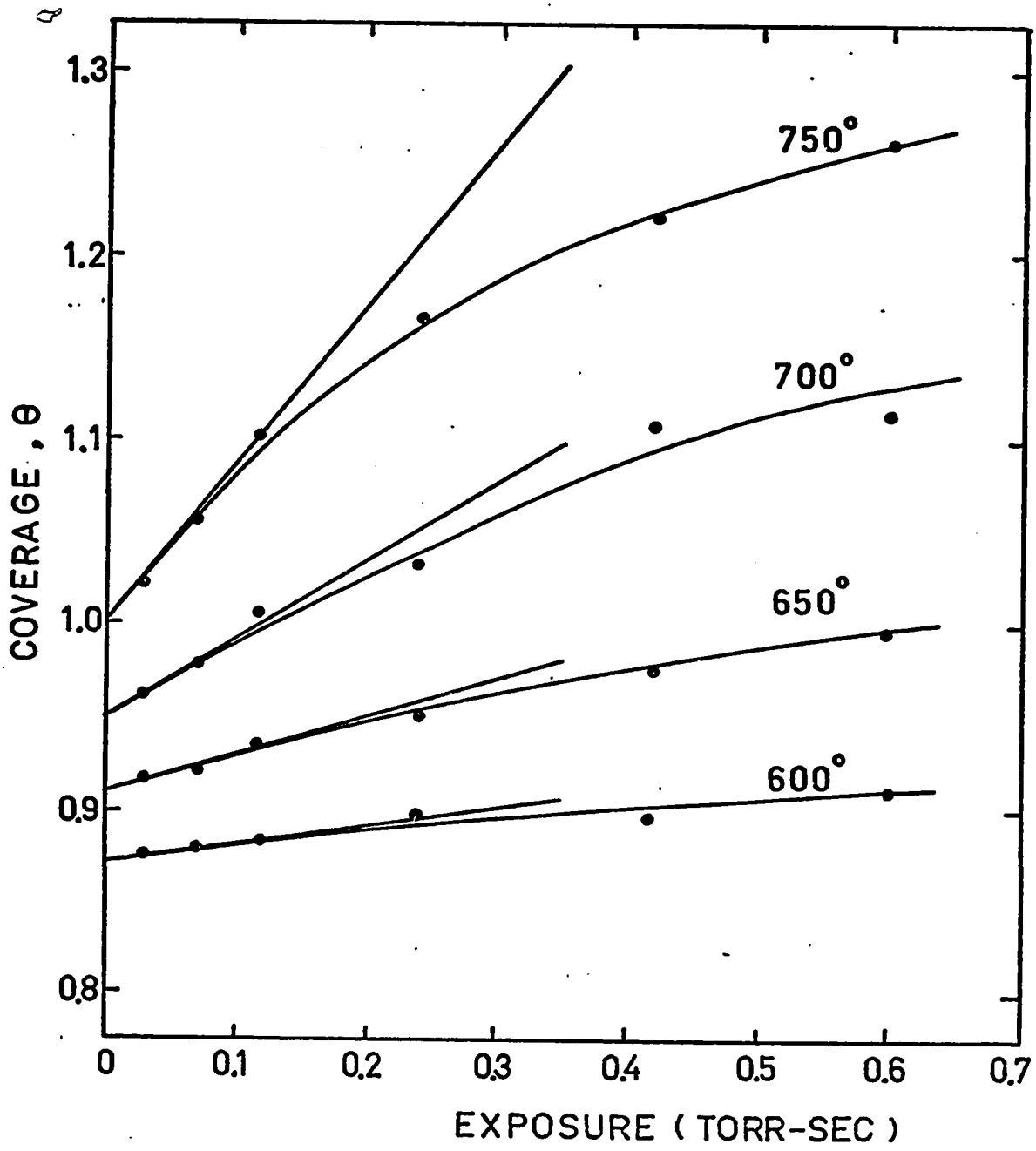

Fig. 27. The variation in total surface coverage (corrected) of nitrogen with increasing ammonia exposure at 600, 650, 700 and 750°K. (θ is the fractional surface coverage calculated by assuming that the surface contains 10^{15} tungsten atoms per cm^2)

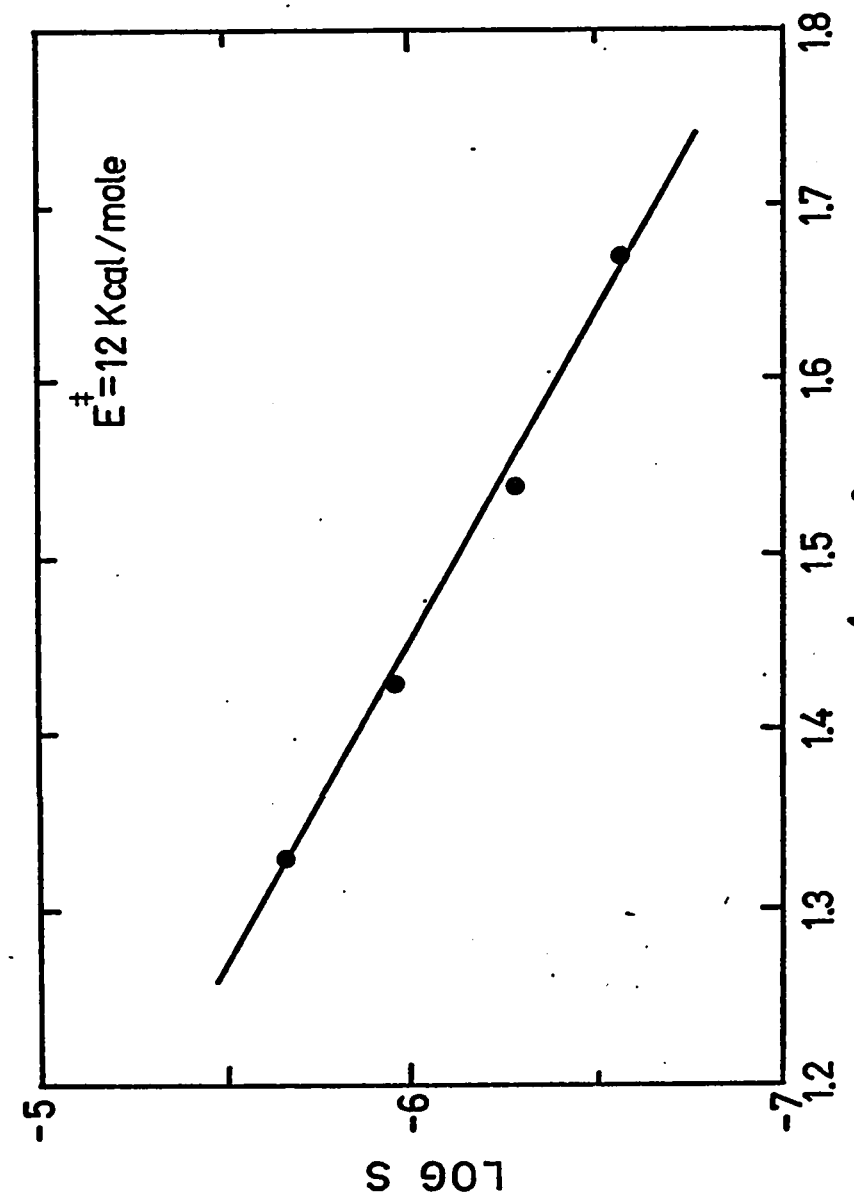

Fig. 28. The evaluation of the activation energy for the formation of the η-species from a plot of log S versus 1/T.

pressure of 10^{-2} torr was allowed to interact with the filament for 10 minutes at 700°K and nitrogen desorption spectra were obtained using Method IV and various heating rates. The temperature, T_m, at which the desorption rate was a maximum was obtained directly from the desorption spectrum [16]. From the variation of T_m with heating rate, b, the activation energy of desorption was determined by using equation (8). The plot of $\ell n(T_m^2/b)$ versus $1/T_m$ as shown in Figure 29 gave an activation energy equal to 35 Kcal $mole^{-1}$. By substituting this activation energy into equation (5), the frequency factor, ν, was found to be 4×10^7 sec^{-1}. It was concluded in section 4.1.2 that the η-species desorbs by first order kinetics, the rate of desorption of η-nitrogen, hence the η-species, can be represented by

$$\text{rate} = 4.10^7 \exp(-35{,}000/RT).n \qquad (22)$$

where n is the surface coverage of η-species.

4.1.8 Attempts to form the η-species from nitrogen and hydrogen.

In order to determine if the η-species is a mixed hydrogen and nitrogen adlayer, the formation of the η-species was attempted using hydrogen and nitrogen gas rather than ammonia. However, no desorption features characteristic of the η-species were observed under any of the following conditions;

(a) adsorption of pure hydrogen or nitrogen at pressures up to 5×10^{-3} torr at 300, 700 and 800°K.

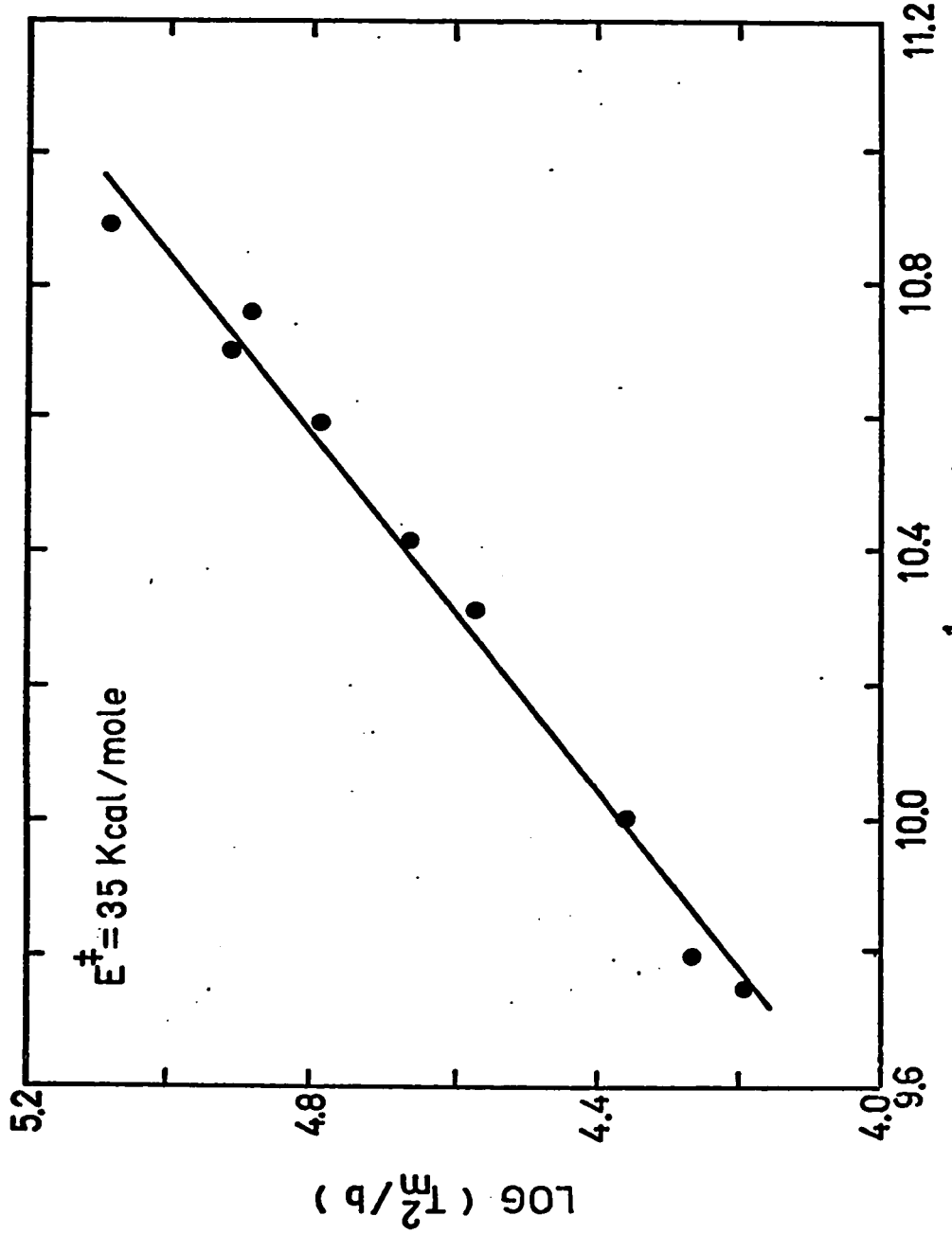

Fig. 29. The evaluation of the activation energy for the desorption of the η-species from a plot of log (T_m^2/b) versus $1/T_m$.

(b) adsorption of mixtures of hydrogen and nitrogen in the ratio 4 to 1 at pressures up to 5×10^{-3} torr at 300, 700 and 800°K.

(c) interaction of hydrogen at 5×10^{-3} torr with δ-nitrogen at 700°K.

These results clearly indicate that the η-species is not a mixed hydrogen and nitrogen adlayer, and, within the limitations of the present experimental conditions, the η-species can be formed only by interaction with ammonia.

4.2 λ-state of nitrogen on tungsten surfaces.

In the previous section describing the interaction of ammonia with tungsten surfaces it was shown that competing pathways for the decomposition reaction are possible. One path involves the hydrogen containing η-species and the second proceeds via the desorption of δ-nitrogen. A detailed understanding of the mechanism of ammonia decomposition requires kinetic data for both paths. While the kinetic parameters for the formation and desorption of η-species have been evaluated, many difficulties have been encountered in the attempt to evaluate kinetic parameters for the desorption of δ-nitrogen. First, the δ-nitrogen desorption feature overlaps considerably with that of β-nitrogen and second, the complications arising from the difficulties of handling the ammonia gas in an ultra-high vacuum system severely restrict the type of experiments which can be performed. The

latter problems have been avoided by studying the λ-state of nitrogen [28] which can be prepared from nitrogen gas, has desorption features strongly resembling those of δ-nitrogen and the same stoichiometry, WN. As will be discussed in section 5.1, it is very probable that δ-nitrogen is identical with λ-nitrogen.

4.2.1 Thermal desorption spectra obtained after adsorption of activated nitrogen.

Electron bombardment of molecular nitrogen produces activated nitrogen which consists of atoms, ions and metastable states. The thermal desorption spectra obtained from the tungsten filament after exposure to activated nitrogen for periods of time varying from 2 to 30 minutes are shown in Figure 30, curves (a) to (e). These spectra obtained by employing the ultra-high vacuum system shown in Figure 9 can be compared with those obtained from the adsorption of non-activated nitrogen, the dashed curves in Figure 30, showing the characteristic and well-known β_1- and β_2-states. Several important features should be noted in the activated adsorption spectra. First, the surface coverage is increased greatly over that for the β-state and the excess nitrogen desorbs at lower temperatures. This excess nitrogen has been assigned to a λ-state [28] and in spectrum (e), the total nitrogen adatom coverage is 0.86×10^{15} atoms cm^{-2} or approximately double that observed for the β-state. Second, the desorption spectra have a very characteristic shape in

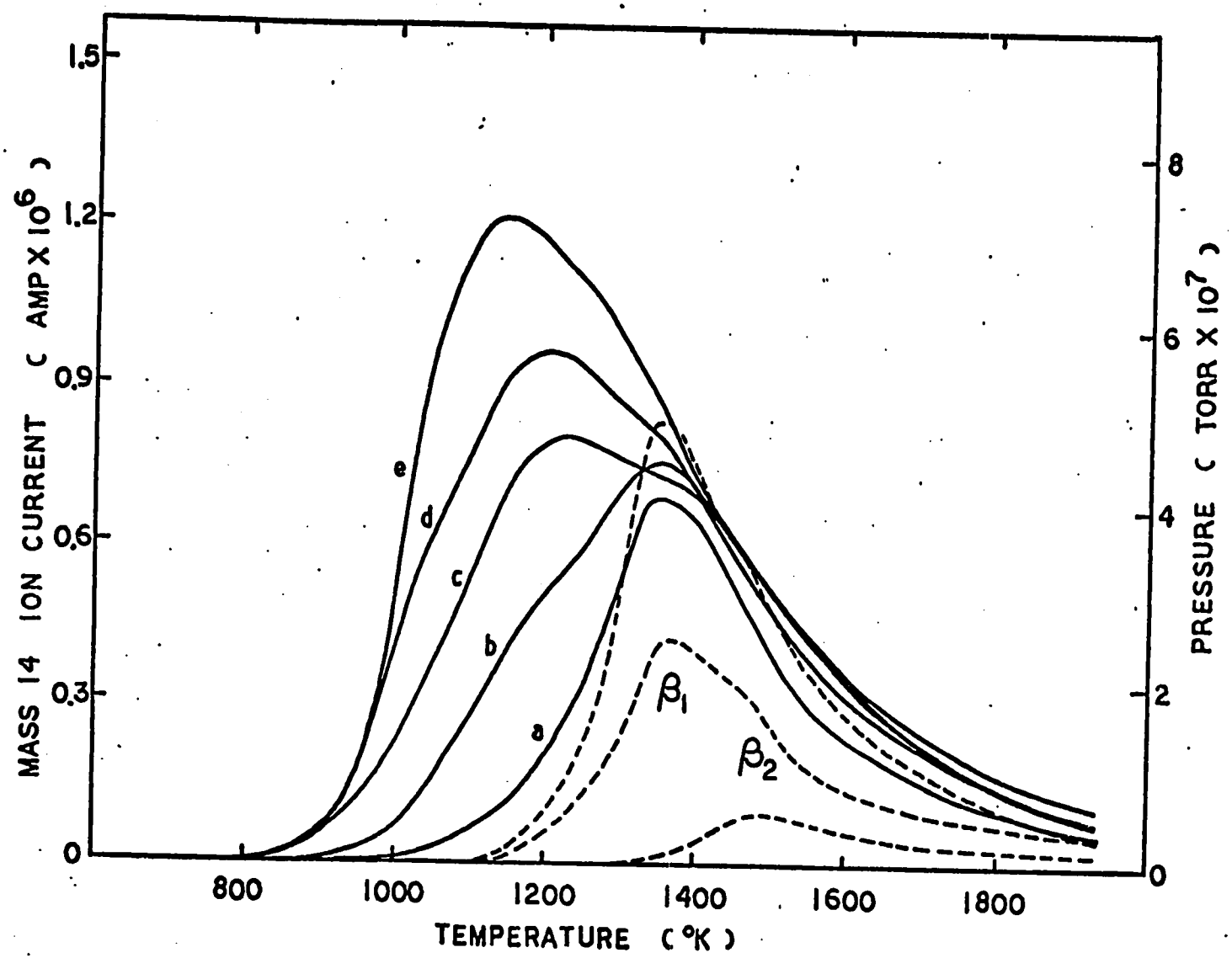

Fig. 30. Thermal desorption spectra obtained from activated nitrogen adsorption at 300°K for 2, 5, 10, 15 and 30 minutes, curves (a) to (e) respectively. Adsorption of non-activated nitrogen for 6×10^{-7}, 5×10^{-6} and 6×10^{-4} torr-sec produced the spectra indicated by the dashed curves. Heating rate, $\beta = 18$ deg sec^{-1}.

that the resolution of different binding states is extremely poor even with a heating rate of only 18 deg sec^{-1}. Several minor features can be detected but it would not be unreasonable to approximate the desorption spectrum as a single desorption peak. It is impossible to assign the excess nitrogen over the maximum observed for the β-state as being in a single additional desorption peak superimposed on the β-desorption peak. The high-temperature tail of such a desorption peak would certainly enhance the amount desorbing at the peak maximum of the β-desorption peak. The presence of a large number of binding states, or the same state on a large number of different crystal faces, is one possibility. However, curve fitting with a DuPont 310 curve resolver shows that each such state would be required to have an unusually small half width. Finally, it should be noted that the β-nitrogen peak is actually depleted somewhat as the coverage increases. No superposition model can account for this observation.

4.2.2 Desorption kinetics.

The total lack of resolution in the spectra shown in Figure 30 makes it impossible to determine the desorption kinetics for states additional to β by an analysis of the type described in section 2.2.1, i.e. determining the activation energy for desorption, $E^{\ddagger}$, from the variation of peak maximum temperature, T_m, with heating rate, b. Consequently, experiments were carried out in a closed system with fast

heating of the sample filament. The desorption spectra obtained were analyzed according to equation (13) by computer fitting. These experiments do not suffer from additional complications caused by the non-uniform temperature of the filament during desorption with slow heating.

4.2.2(a) Desorption in a closed system with fast heating.

The experimental nitrogen desorption spectra obtained in a closed system with average heating rates varying from 503 to 1080 deg sec^{-1} are shown in Figure 31. Fast linear heating rates were not accessible using the linear temperature sweep generator and so a constant current heating source was used for these experiments. A constant current source can usually be assumed to produce an approximately hyperbolic heating programme, however, in the present application, because the temperature range of desorption is so large (1000 to 1750^{o}K), the temperature does not vary in a hyperbolic fashion and in fitting the desorption curves to various possible models the rate equations have been integrated numerically.

The desorption spectra are featureless and provide no obvious clues as to their interpretation. In choosing trial models, the following principles have been adopted; first, at the low coverage limit the desorption kinetics are assumed to equal those for the β-state and second, a "two-state" model is assumed. Thus,

$$\text{Desorption rate} = \text{Rate}(\lambda) + \text{Rate}(\beta)$$

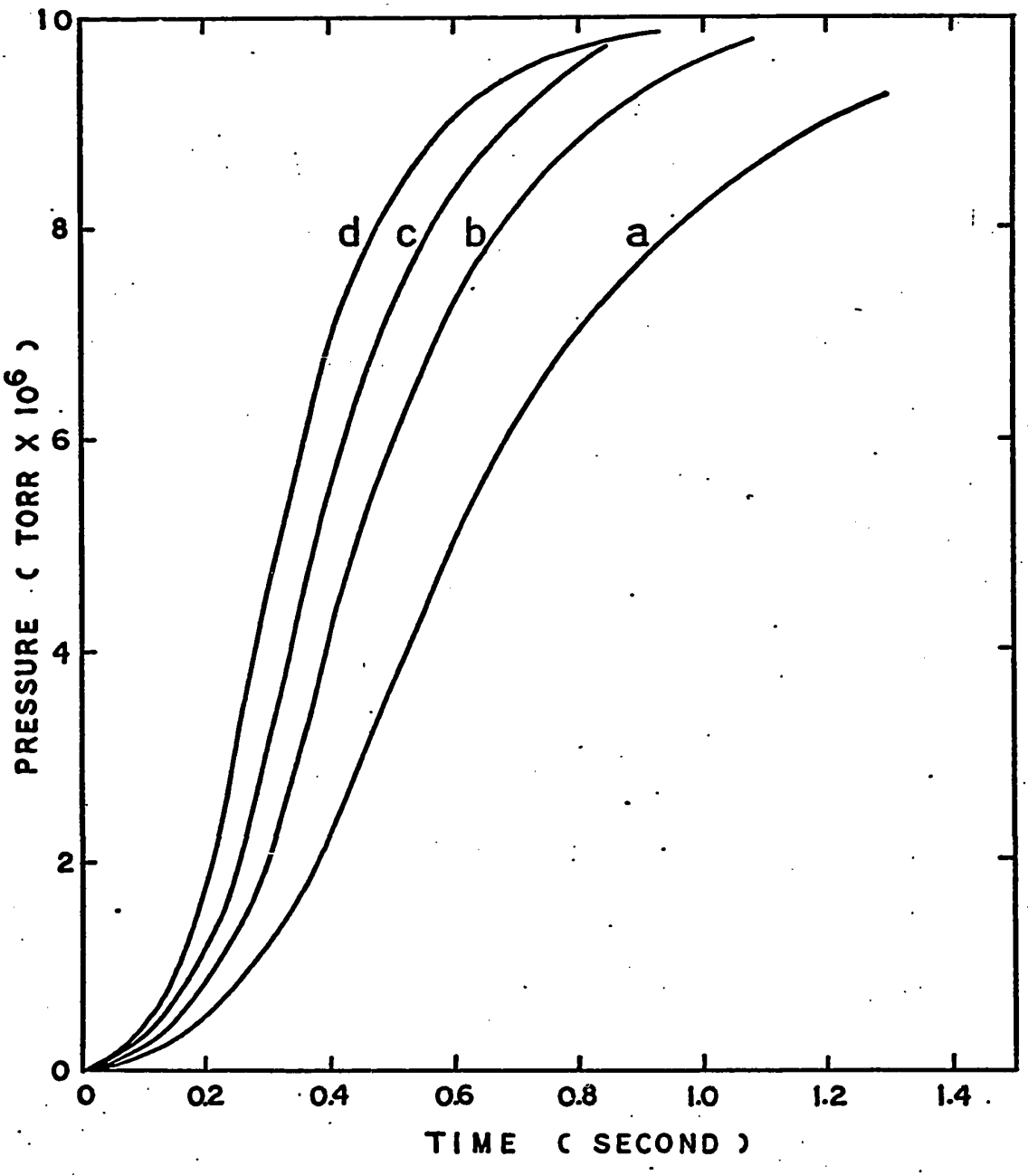

Fig. 31. Thermal desorption traces obtained from activated nitrogen adsorption at 300°K for 30 minutes. Desorption was carried out in a closed system with average heating rates of (a)503, (b)670, (c)886 and (d)1080 deg sec^{-1}. The filament temperature was 1000°K at t = 0 sec.

The first assumption is very reasonable whereas the second is open to question. The slow heating experiments show little evidence for multiple "binding states" and thus it would unnecessarily complicate the analysis to introduce additional, unjustifiable, adjustable parameters associated with their existence, even though this might produce a better fit to the data. Extensive experiments on various different single crystal planes and a determination of the distribution of these planes on polycrystalline filaments will be required to give a final answer to this question.

For the β contribution, Ehrlich's rate equation which was determined from desorption measurements on polycrystalline filaments [29] was used.

$$\text{Rate}(\beta) = 1.4\times10^{-2} \exp[-81{,}000/RT]\cdot N_\beta^2 \text{ molecules cm}^{-2} \text{ sec}^{-1} \quad (23)$$

where N_β is the number of nitrogen molecules cm^{-2} in the β-state. This rate law was observed to be valid up to a surface coverage of 2.5×10^{14} molecules cm^{-2}.

Four trial models were used for the λ-state; (1a) first order with constant activation energy, (1b) first order with activation energy varying linearly with coverage; (2a) second order with constant activation energy, and (2b) second order with activation energy varying linearly with coverage,

$$\text{(1a)} \quad \text{Rate}(\lambda) = \nu_{1a} \exp[-E^{\ddagger}_{1a}/RT] \cdot N_{\lambda}$$

$$\text{(1b)} \quad \text{Rate}(\lambda) = \nu_{1b} \exp[-(E^{\ddagger}_{1b}-\alpha\theta)/RT] \cdot N_{\lambda}$$

$$\text{(2a)} \quad \text{Rate}(\lambda) = \nu_{2a} \exp[-E^{\ddagger}_{2a}/RT] \cdot N^2_{\lambda}$$

$$\text{(2b)} \quad \text{Rate}(\lambda) = \nu_{2b} \exp[-(E^{\ddagger}_{2b}-\alpha\theta)/RT] \cdot N^2_{\lambda}$$

The various models were tested by using a CDC 6400 computer to integrate the rate equations and determining the best fit possible by scanning all the rate parameters.

The first trials were carried out with variable frequency factors, ν, activation energies, $E^{\ddagger}$, and, where applicable its variation with coverage, α, but keeping the surface coverage of the β-state fixed and equal to the maximum observed in these experiments, $N_{\beta} = 2.2\times10^{14}$ molecules cm^{-2}. The best fit parameters and standard deviations are shown in Table II. For the 886 deg sec^{-1} heating rate, the curve generated by using these parameters for each model is compared with the experimental curve in Figure 32. (filled circles). Clearly the fit is unsatisfactory.

The slow heating desorption spectra shown in Figure 30 suggested that with increasing nitrogen coverage the amount of desorption in the β-state actually decreased somewhat. It seemed reasonable therefore to allow the computer to sweep the amount desorbing in the β-state, N_{β}, in

Table II

Computer analysis of nitrogen desorption spectra with β-nitrogen surface coverage fixed at a value equal to 4.4 atoms cm^{-2} (initial total nitrogen surface coverage No : 8×10^{14} atoms cm^{-2})

Model	b (deg sec^{-1})	α (Kcal $mole^{-1}$)	N_β (atoms cm^{-2}) 10^{15}	ν	$E_o^\ddagger$ (Kcal $mole^{-1}$)	Δ ($\times10^2$)
1(a)	503	0	0.44	10^4	18.6	9.7
	670	0	0.44	10^3	12.7	10.6
	886	0	0.44	10^5	22.9	12.2
	1080	0	0.44	10^4	17.0	15.0
1(b)	503	6	0.44	10^5	25.3	10.2
	670	8	0.44	10^4	20.3	12.2
	886	6	0.44	10^6	29.7	12.5
	1080	10	0.44	10^5	24.2	15.6
2(a)	503	0	0.44	10^{-4}	49.4	9.4
	670	0	0.44	10^{-4}	49.0	10.1
	886	0	0.44	10^{-4}	48.7	12.4
	1080	0	0.44	10^{-4}	47.5	14.7
2(b)	503	0	0.44	10^{-6}	38.7	10.1
	670	0	0.44	10^{-6}	38.4	10.6
	886	2	0.44	10^{-6}	38.1	13.3
	1080	0	0.44	10^{-6}	32.	20.5

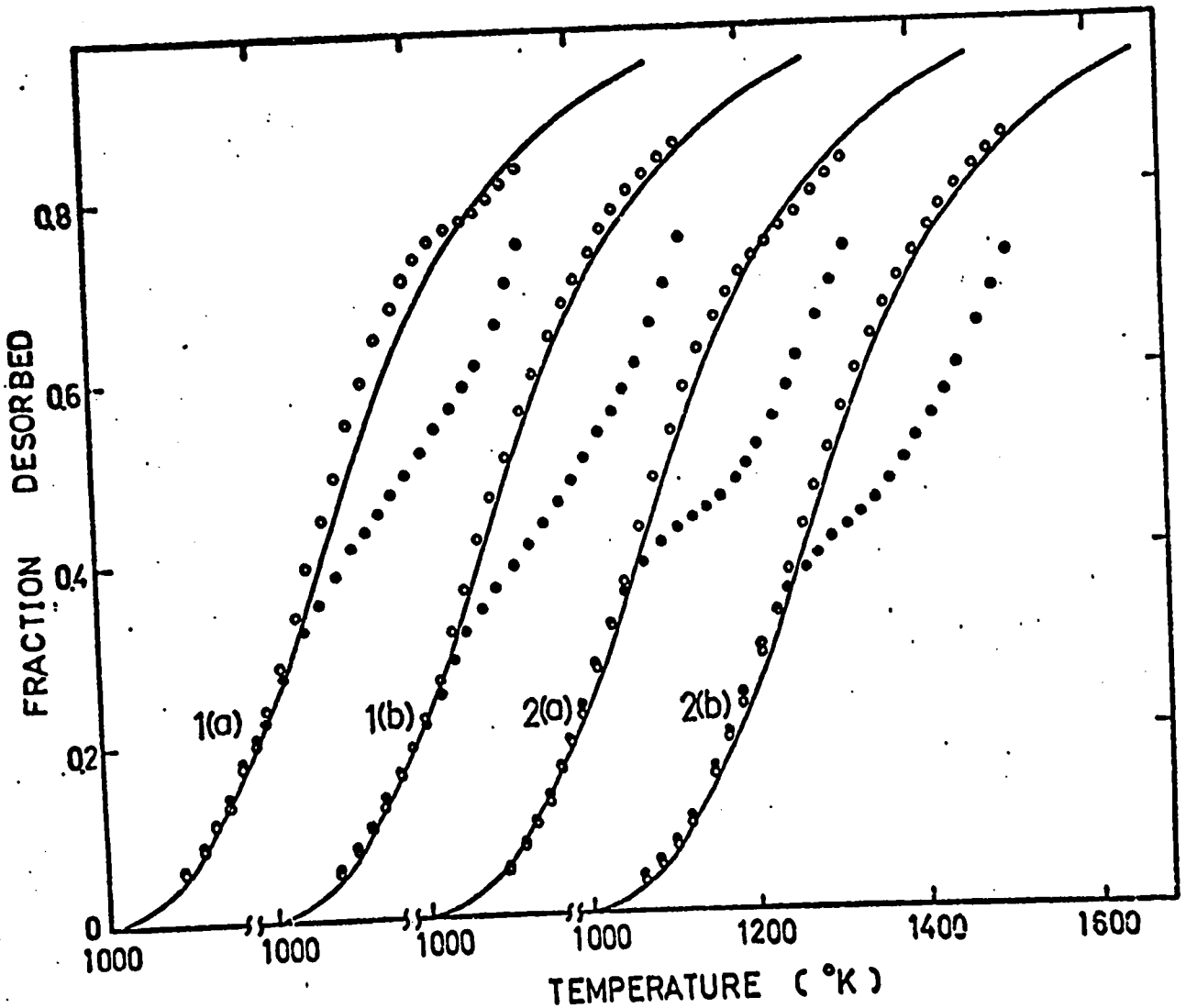

Fig. 32. Computer fitting of the 886 deg sec^{-1} trace of Figure 31 to models 1(a), 1(b), 2(a) and 2(b) using (i) $N_\beta = 2.2 \times 10^{14}$ molecules cm^{-2} (filled circles), and (ii) N_β variable (open circles).

addition to the other parameters. The fit obtained, again for the 886 deg sec^{-1} spectrum, is also shown in Figure 32 (open circles). The fit is improved tremendously for all models and each could be considered satisfactory in view of the limitations of these models. The best fit parameters and standard deviations obtained for each model are shown in Table III. It should be noted that the best-fit parameters for each model are very similar for all four heating rates. In <u>each</u> case the β-coverage has to be <u>reduced</u> from 0.44×10^{15} atoms cm^{-2} to the vicinity of 0.14×10^{15} atoms cm^{-2} in order to obtain this fit. Also included in Table III is the analysis for model (S) which assumes the existence of only a single species desorbing via second order kinetics with an activation energy varying linearly with coverage. Again, the low coverage limit has been assumed to be the observed kinetics for β-nitrogen desorption, i.e.

$$\text{(S)} \qquad \text{Rate} = 1.4\times10^{-2} \exp[-(81{,}000-\alpha\theta)/RT]\cdot N^2 \tag{24}$$

The spectra recorded in Figure 31 and analyzed in Table III were obtained using the ionization gauge G_1 to monitor the pressure burst. An identical set of experiments was carried out using the mass spectrometer as the detector. Analysis of this data gave best fit parameters as shown in Table IV corresponding extremely closely to those displayed in Table III. The standard deviation was

Table III

Computer analysis of nitrogen desorption spectra with β-nitrogen coverage being allowed to vary

(No : 8×10^{14} atoms cm^{-2})

Model	b (deg sec^{-1})	α (Kcal $mole^{-1}$)	N_β (atoms cm^{-2}) 10^{15}	ν	$E_o^{\ddagger}$ (Kcal $mole^{-1}$)	Δ ($\times10^2$)
1(a)	503	0	0.20	10^5	25.3	2.0
	670	0	0.08	10^4	20.3	4.2
	886	0	0.20	10^6	29.6	2.5
	1080	0	0.16	10^5	24.2	2.0
1(b)	503	10	0.16	10^8	46.4	2.8
	670	10	0.08	10^7	43.6	8.6
	886	8	0.16	10^8	44.7	1.2
	1080	10	0.08	10^8	46.3	1.9
2(a)	503	0	0.20	10^{-6}	42.8	2.0
	670	0	0.20	10^{-6}	42.5	3.4
	886	0	0.16	10^{-6}	42.8	1.7
	1080	0	0.12	10^{-6}	41.8	2.7
2(b)	503	8	0.08	10^{-6}	48.4	1.7
	670	7	0.10	10^{-6}	47.5	2.0
	886	8	0.08	10^{-6}	48.4	1.7
	1080	7	0.08	10^{-6}	46.9	1.7

Table III (continued)

Model	b (deg sec^{-1})	α (Kcal $mole^{-1}$)	N_β (atoms cm^{-2}) 10^{15}	ν	$E_o^{\ddagger}$ (Kcal $mole^{-1}$)	Δ ($\times 10^2$)
S	503	23,4	-	1.4×10^{-2}	81.0	3.5
	670	23.4	-	1.4×10^{-2}	81.0	3.7
	886	24.0	-	1.4×10^{-2}	81.0	3.8
	1080	27.1	-	1.4×10^{-2}	81.0	4.7
P*	503	23.4	0.04	10^{12}	81.0	2.3
	670	23.4	0.0	10^{12}	81.0	3.5
	886	24.2	0.08	10^{12}	81.0	3.5
	1080	26.9	0.08	10^{12}	81.0	4.7

* see section 5.2.1

Table IV

Computer analysis of nitrogen desorption spectra (mass spectrometer as detector)
(No : 8 10^{14} atoms cm^{-2})

Model	b (deg sec^{-1})	α (Kcal $mole^{-1}$)	N_β (atoms cm^{-2}) 10^{15}	ν	$E_o^{\ddagger}$ (Kcal $mole^{-1}$)	Δ ($\times 10^2$)
1(a)	503	0	0.20	10^5	25.6	2.3
	670	0	0.12	10^4	20.5	6.7
	886	0	0.16	10^5	25.0	1.7
	1080	0	0.12	10^5	24.7	2.6
1(b)	503	10	0.12	10^8	46.7	2.2
	670	12	0.08	10^7	44.1	6.2
	886	8	0.16	10^8	45.3	1.4
	1080	10	0.08	10^8	46.3	1.9
2(a)	503	0	0.20	10^{-5}	47.8	2.1
	670	0	0.20	10^{-6}	43.4	5.8
	886	0	0.16	10^{-5}	49.4	2.2
	1080	0	0.16	10^{-5}	47.2	3.1
2(b)	503	4	0.12	10^{-6}	45.9	1.9
	670	6	0.12	10^{-6}	45.3	2.1
	886	4	0.16	10^{-6}	45.0	2.0
	1080	4	0.08	10^{-6}	44.7	1.9

Table IV (continued)

Model	b (deg sec^{-1})	α (Kcal $mole^{-1}$)	N_β (atoms cm^{-2}) 10^{15}	ν	$E_o^\ddagger$ (Kcal $mole^{-1}$)	Δ ($\times 10^2$)
S	503	24.1	-	1.4×10^{-2}	81.0	2.4
	670	19.7	-	1.4×10^{-2}	81.0	5.8
	886	21.3	-	1.4×10^{-2}	81.0	2.7
	1080	25.6	-	1.4×10^{-2}	81.0	3.8

larger for a heating rate of 670 deg sec^{-1} in all experiments. This can be simply understood as arising from a compressed time scale on the oscilloscope trace for this heating rate, leading to a reduced precision in the data.

The first comment to be made on the data recorded in Table III (or Table IV) is that the standard deviations are comparable for all models and therefore no choice of model can be made on the basis of a fit to the data. The number of adjustable parameters, either one, three, or four, is sufficient to ensure a satisfactory fit. It must be stressed that this analysis is not presented to justify one or other of the trial models; the important point to be made is that, in <u>each</u> case, in order to achieve an acceptable fit to the data the amount of nitrogen desorbing in the β-state must be considerably reduced from 0.44×10^{15} to values varying between 0.08 and 0.20×10^{15} atoms cm^{-2}. Additional, more complex, trial models with additional adjustable parameters may remove this requirement to reduce the β-nitrogen coverage. However, since the thrust of all two-state models tried is in this direction and there is direct evidence for β-depletion (Figure 30) it is felt that this interpretation has considerable merit.

The success of a single-state model (S) with one adjustable parameter, α, suggests another experimental method for the determination of the kinetic parameters. This success is presumably a result of the reduced contribution from the

β-state to the desorption peak. If the contribution from the depleted β-state at peak maximum is negligible, then the analysis of desorption spectra obtained under conditions of slow heating and fast pumping ($\tau \rightarrow \infty$) becomes possible.

4.2.2(b) Kinetic analysis for pumped system with slow heating.

The temperature at which the desorption rate becomes a maximum, T_m, was determined for a constant surface coverage of 0.65×10^{15} atoms cm^{-2}, and heating rates varying from 8 to 97 deg sec^{-1}. The peak maximum temperature shifts from 1170 to 1335°K.

If the activation energy for desorption is independent of surface coverage then according to equation (8) a plot of $\ell n(T_m^2/b)$ versus $(1/T_m)$ should be linear with a slope of $E^{\ddagger}/R$. This plot is shown in Figure 33 and can be reasonably well fitted to a straight line corresponding to an activation energy, $E^{\ddagger}$, of 43 Kcal $mole^{-1}$. This is in good agreement with the value obtained from computer fitting the fast flash data to a second order constant activation energy trial model, 2(a) (Table III). There is no agreement with the first order constant activation energy value of 25 Kcals $mole^{-1}$, 1(a) (Table III). This is to be expected since the desorption peaks shift to lower temperatures with increasing surface coverage (equations 5, 7, Figure 30).

For a desorption with an activation energy varying linearly with surface coverage, according to equation (12)

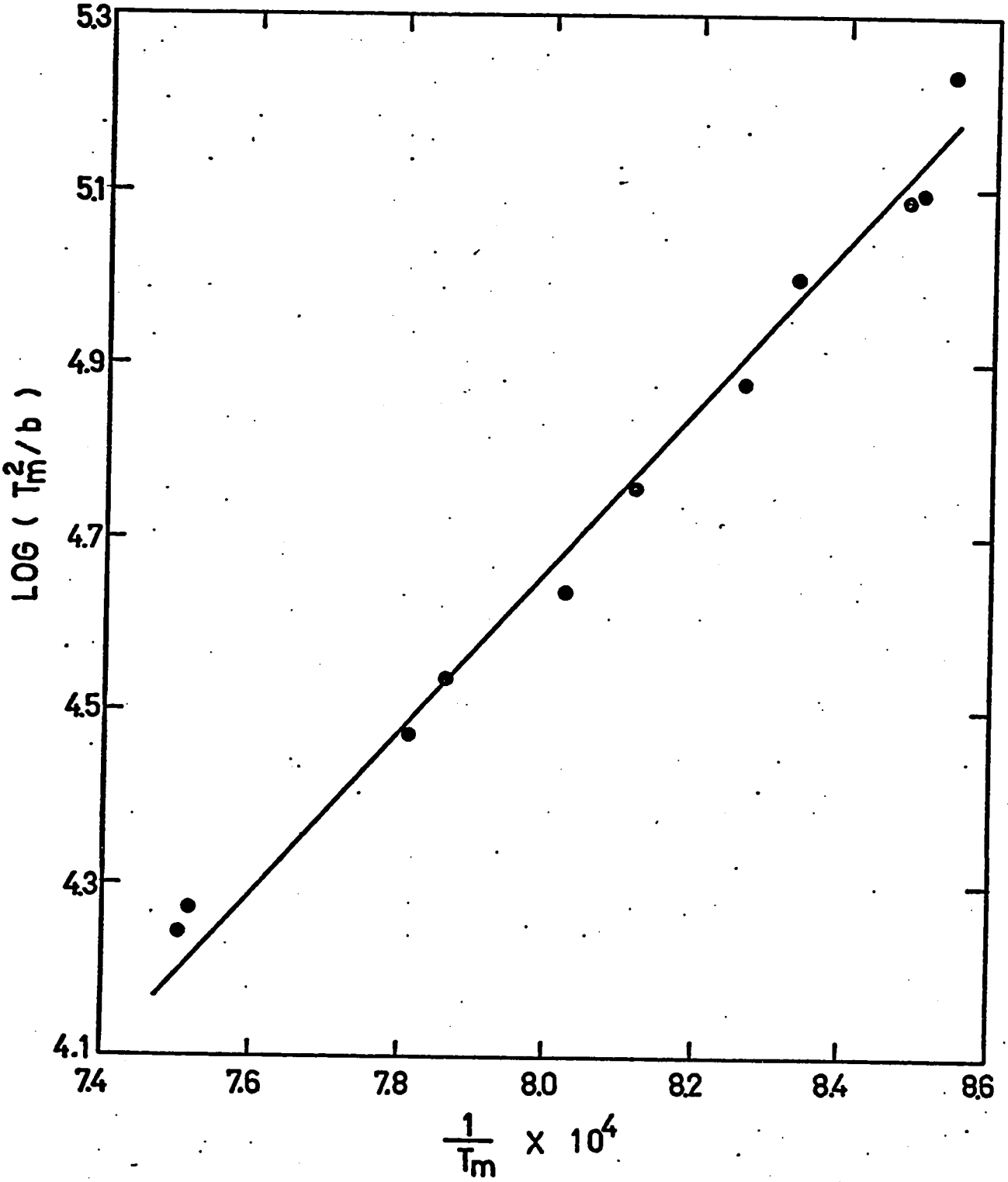

Fig. 33. The evaluation of the activation energy for desorption of λ-nitrogen from a plot of log (T_m^2/b) versus ($1/T_m$).

the slope in Figure 33 can be interpreted as $(E_o^{\ddagger}-\alpha\theta_m)/R$, and $E_o^{\ddagger}-\alpha\theta = 43$ Kcal mole^{-1} as long as the last term of this equation makes negligible contribution to the slope. This is consistent with trial models 1(b) and 2(b), Table III, and using a value of $\alpha = 10$ Kcals mole^{-1} it is found that the last term of equation (12) does contribute only 3% to the slope.

Thus, this analysis of the slow heating spectra, neglecting the contribution of the β-desorption in the vicinity of the peak maximum, yields kinetic parameters consistent with the fitting of the fast flash data to models 1(b), 2(a), and 2(b).

4.2.3 Isotope exchange experiments.

Isotope exchange experiments are potentially extremely useful in discriminating between different models for desorption processes. Thus experiments in which the β-state is occupied by one nitrogen isotope and then the adlayer is completed using the other might be expected to produce complete isotope scrambling if desorption occurred via bimolecular recombination of freely mobile adatoms. However, a desorption of immobile adjacent atom pairs would yield only N_2^{29} on desorption (assuming that in the β-state the nitrogen atoms occupy next nearest neighbours, {100}C(2×2) structure[30]).

A β-N^{15} adlayer was prepared by allowing the filament to interact with N_2^{30} gas at a pressure of 2×10^{-6} torr for 10

minutes in a freshly baked system with all ionization gauge and mass spectrometer filaments cold. The N_2^{30} was then replaced with N_2^{28} and electron bombardment of this gas produced additional activated adsorption as described earlier. Simultaneous mass 28, 29 and 30 desorption spectra were obtained and these are shown for two different surface coverages in Figure 34. Also recorded in this figure is the mole fraction of N_2^{29} in the desorbing gas, X^{29}, over the whole desorption spectrum.

The desorption spectra for the three isotopic species have identical shapes with constant X^{29}. The theoretical values for X^{29} determined from the integrated magnitudes of the desorption peaks are 0.49 for 0.86×10^{15} atoms cm^{-2}, and 0.44 for 0.57×10^{15} atoms cm^{-2} adsorbed; this agrees with the experimental observations. Thus complete statistical mixing occurs between the β- and λ-states, even at high surface coverage, which suggests that the nitrogen is bound atomically and that the β- and λ-states do not exist on different crystal planes. Although the weak fine structure in the desorption spectra indicates some account should be taken of surface heterogeneity this cannot be the origin of the different "binding states".

Similar experiments carried out with fast heating also showed complete isotope mixing.

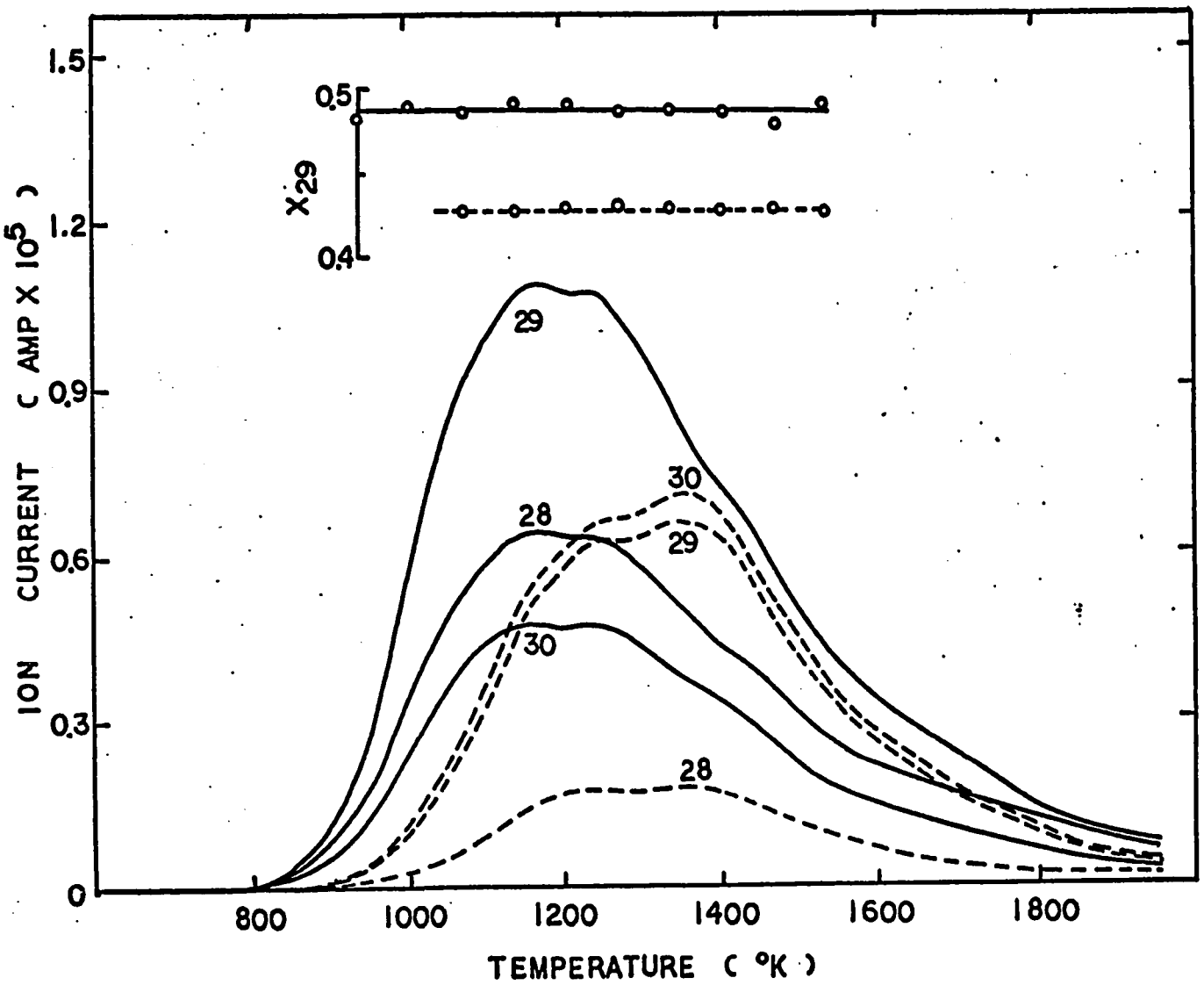

Fig. 34. Mass 28, 29 and 30 desorption spectra for surface coverages of 5.7×10^{14} (dashed curves) and 8.6×10^{14} atoms cm^{-2}. X^{29} is the mole fraction of N_2^{29} in the desorption gas.

4.2.4 The adsorption of non-activated nitrogen.

In order to understand the nature of the high density nitrogen adlayer formed by adsorption of activated nitrogen gas, it is important to determine whether adsorption of non-activated nitrogen gas can produce the same result. In particular, the energy of the high density adlayer relative to that of non-activated nitrogen gas needs to be established. Possible activation of the nitrogen gas was avoided by carrying out this experiment in a freshly-baked system with all detector filaments cold during the adsorption. The sample filament was maintained at 300°K and exposed to nitrogen gas at a pressure of 2×10^{-3} torr for exposures up to 140 torr-sec. The desorption spectra obtained are shown in Figure 35 and are very similar to those obtained with activated nitrogen. The sticking coefficient is extremely small, of the order of 10^{-7}, compared with that for the formation of β-nitrogen, 10^{-1}. An isotope exchange experiment carried out in the same manner as that described earlier also showed complete statistical mixing between the new state and the β-state providing further evidence that the new state is identical with the λ-state formed by activated nitrogen gas adsorption.

Winters and Horne have suggested [31] that in the λ-state of nitrogen the adatoms occupy endothermic sites, i.e. thermodynamically unstable relative to gas phase nitrogen but preserved by a high activation barrier to desorption. The

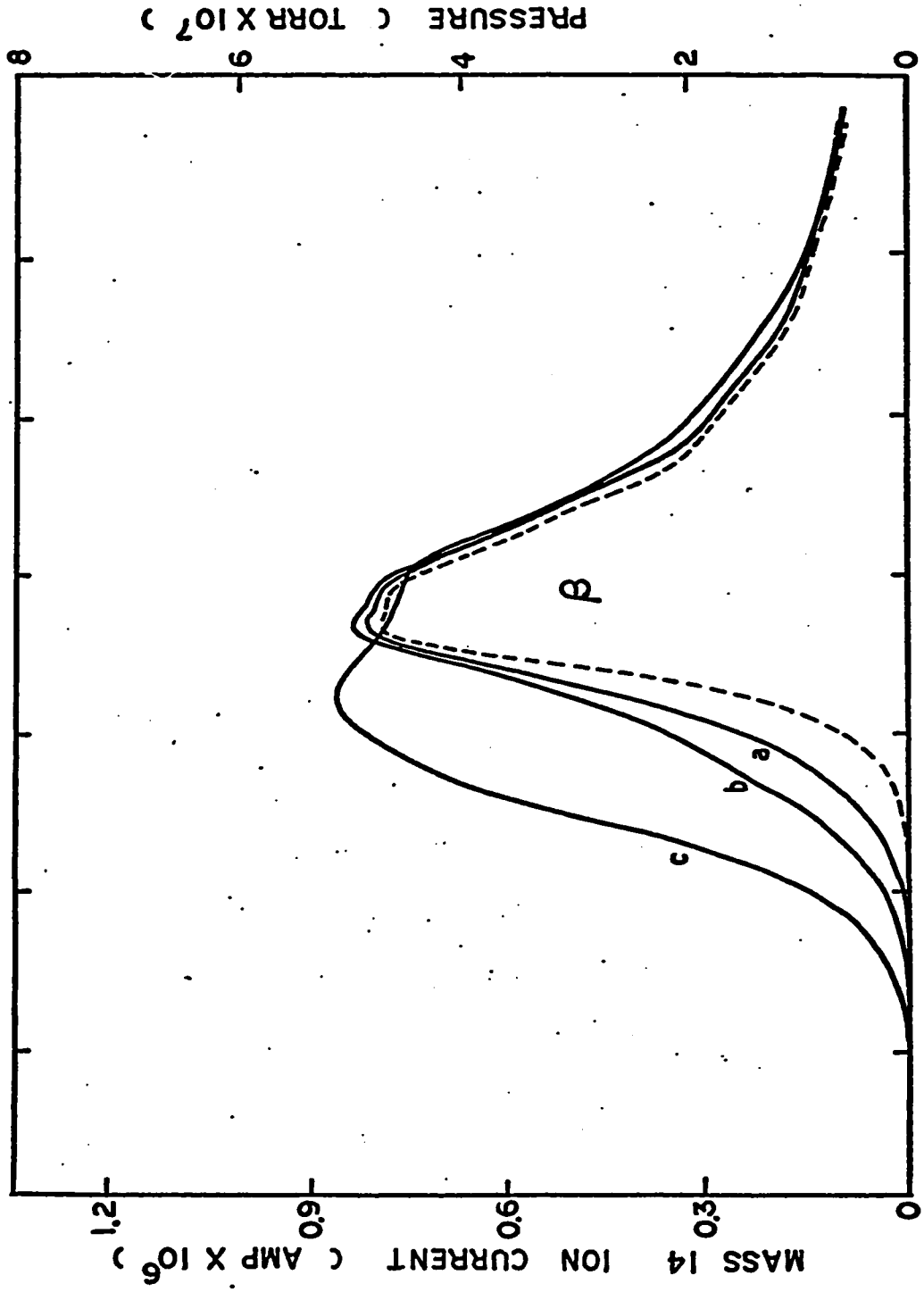

Fig. 35. Thermal desorption spectra obtained from adsorption of non-activated nitrogen gas at 2×10^{-3} torr for exposures of (a)1, (b)10 and (c)140 torr sec. The β-nitrogen desorption spectrum (dashed curve) was obtained from an exposure of 6×10^{-4} torr-sec.

only evidence for this interpretation seems to be the inability to form the λ-state from non-activated nitrogen gas. Since this has now been observed we must conclude that in the λ-state the adatoms occupy exothermic sites.

With such long exposures as used in these experiments even a minute trace of an impurity, carbon monoxide in particular, could become a serious surface contaminant. Monitoring the mass-12 ion current showed negligible carbon monoxide contribution to the desorption spectra. Another possible complication is a catalytic role for CO in producing the λ-state. In nitrogen and carbon monoxide replacement experiments on tungsten, Rigby showed [32] that as nitrogen replaced carbon monoxide a new nitrogen state of lower binding energy was formed and that a total of 0.32×10^{15} atoms cm^{-2} of nitrogen was added beyond the β-nitrogen coverage. It is possible that in the present experiments a background CO partial pressure of about 10^{-10} torr could also induce further nitrogen adsorption. However, Winters and Horne were not able to repeat Rigby's results [31]. The conclusions concerning the exothermic nature of the λ-state adatom sites are not affected by such a catalytic mechanism for the adsorption of non-activated nitrogen gas.

4.2.5 Desorption in a closed system with varying heating rate.

The strong implication that occupation of the λ-state causes depletion of the β-state suggests a prominent role for

surface diffusion, or the lack of it, in determining the desorption mechanism. Thus, if surface diffusion is extremely rapid compared to the rate of desorption then once the surface coverage is reduced to that of the β-state (0.44×10^{15} atom cm^{-2}) rearrangement to the lower energy β-configuration should precede desorption and there should be no β-depletion. Consequently the extent of β-depletion should be a function of heating rate and should become zero at a slow enough heating rate.

In Figure 36 the desorption spectra for β-nitrogen and (λ + β) nitrogen adlayers are recorded at three different heating rates. Also recorded on this figure is the difference in magnitude between these two spectra. Clearly if no β-depletion occurred then the difference plot should represent the λ-desorption and be featureless, and asymptotic with the total amount in the λ-state. This would appear to be the case only for the slowest heating rate used of 18 deg sec^{-1}. For heating rates of 200 and 886 deg sec^{-1} the difference plot passes through a maximum indicating β-depletion and also suggesting that this is a function of heating rate.

In order to eliminate the hump in the difference plot, calculation indicates that the amount of nitrogen desorbing in the β-state must be reduced to 0.12×10^{15} atoms cm^{-2}. This calculation was carried out for the 886 deg sec^{-1} experiment using Ehrlich's rate equation [17].

There is one obvious complication to the interpretation

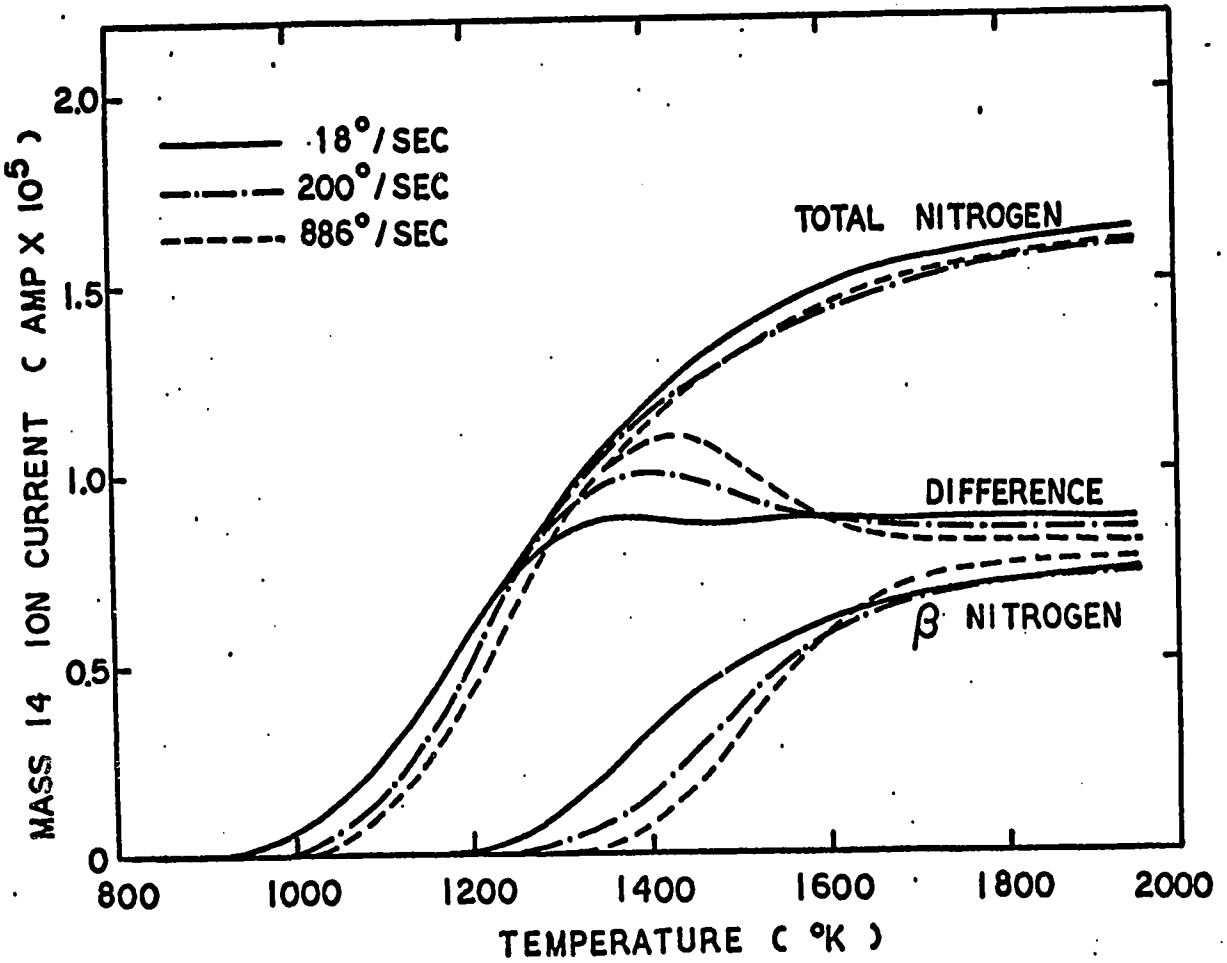

Fig. 36. Thermal desorption traces for β-nitrogen and (λ+β)-nitrogen in a closed system with heating rates of 18,200 and 886 deg sec^{-1}. Also shown is the difference between these traces for each heating rate.

of these results and this concerns the possibility of re-adsorption of nitrogen gas desorbed from the λ-state into the β-state, since this experiment was conducted in a closed system. This does not affect the interpretation of the hump in the difference plot as due to β-depletion but the reverse, i.e. the decrease in magnitude and ultimate elimination of the hump as being due to readsorption, rather than surface rearrangement to form the β-state at its maximum average. The magnitude of this effect can be estimated. At the temperature at which the difference curves show a maximum the ambient pressure is about 10^{-6} torr and the surface coverage is about 0.3×10^{15} atoms cm^{-2}. Taking as the sticking coefficient for nitrogen at this coverage Becker and Hartman's value of 0.008 at 1100°K,[33] the amount of nitrogen adsorbed in one second is only about one hundredth of a monolayer. Thus readsorption is expected to be negligible except in the case of the slowest heating rate of 18 deg sec^{-1}. The implication that β-depletion is not negligible for a heating rate of 18 deg sec^{-1} is satisfying since the experiments carried out in a pumped system using this heating rate (Figure 30) do suggest some β-depletion. The change in the difference plots for heating rates of 200 and 886 deg sec^{-1} does indicate that the extent of β-depletion is a function of heating rate, confirming the role of surface mobility in the desorption mechanism. This introduces some uncertainty as to the validity of the assumption used in the kinetic analysis for

the slow heating rate experiments (Section 4.2.2(b)). However, the contribution from readsorption during desorption with pumping will be only about 1/10th of that observed in these closed system experiments.

An additional complication associated with the slow heating rate experiment is the non-uniform temperature of the sample during desorption. There will be a concentration gradient along the filament with the minimum at the centre. There is therefore an additional driving force for diffusion over that present with a uniform temperature using rapid heating. It is expected that local rearrangement would occur more rapidly than such long range diffusion and that this complication is much less serious than readsorption.

4.3 Field emission results.

4.3.1 Formation of δ-nitrogen.

Thermal desorption observations indicate that repeated ammonia adsorption at 300°K with intermittent heating to 800°K (Figure 14) and ammonia interaction at a temperature high enough to dissociate adsorbed ammonia (Figure 13) lead to the formation of δ-nitrogen which is not well resolved from β-nitrogen. Field emission microscopy can distinguish species with similar kinetic parameters but with different surface potentials by comparing the work function changes and emission properties. It is of interest therefore to repeat these experiments on a field emitter tip.

4.3.1(a) Repeated dosing at 300°K.

The work function, i.e. the average work function unless otherwise stated, versus temperature plot obtained for a deposit generated from repeated dosing at 300°K is shown in Figure 37. The first work function measurement was carried out after five successive doses of ammonia at a pressure of 10^{-2} torr for 5 minutes with the emitter tip at 300°K. Between each dose the tip was heated to 700°K for 20 seconds to desorb the hydrogen from the surface. The deposit generated in this manner produces a rather low work function, 2.75 eV, suggesting the presence of undissociated ammonia on the surface [9]. The observed large work function shift is not unexpected since the ammonia molecule has a large dipole moment. The negative sign of this work function shift indicates that ammonia is adsorbed with the positive end of the dipole pointing away from the surface. Heating the deposit for 10 second intervals to the temperature indicated causes the work function first to increase steadily and eventually at 600°K to exceed that of the clean emitter. Between 700 and 900°K it stays fairly constant at a value of 4.65 eV and above 900°K it starts to decrease and reaches a value of 4.32 eV at 1200°K, which is a value typical for β-nitrogen covered surfaces in the environs of the {100} planes [23]. A value nearly equal to that of the clean emitter, 4.5 eV, is observed at 1500°K.

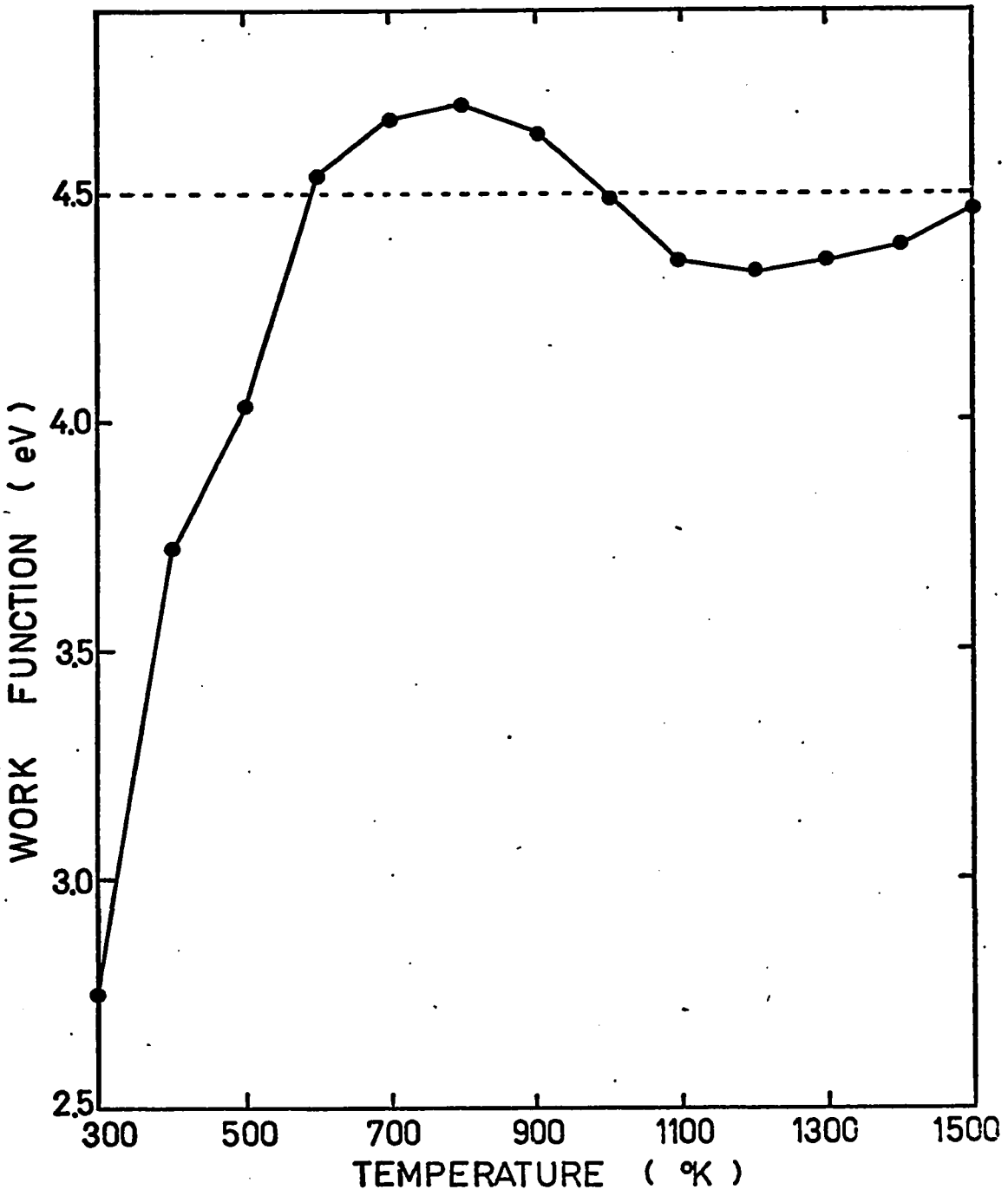

Fig. 37. The variation in work function with temperature of a tungsten emitter which had been repeatedly dosed with ammonia at 300°K with intermittent heating to 700°K. The emitter was held at the temperatures indicated for 10 seconds.

These observations are consistent with thermal desorption results; the initial increase in work function between 300 and 650°K corresponds to ammonia dissociation and hydrogen desorption, while the work function decrease at temperature above 900°K corresponds to the desorption of δ-nitrogen.

The field emission patterns corresponding to this heating sequence are shown in Figure 38. The patterns obtained after each dose at 300°K and subsequent heating to 700°K are also included. The voltage recorded under each pattern is the voltage required for 1×10^{-8} amps emission current. The average work function is also recorded under each pattern. At 300°K, the pattern observed (Figure 38.1) is identical to that observed in earlier field emission experiments [9]. The bright area, where electrons are emitting with greatest intensity, corresponds to the surface where the work function is the lowest after ammonia adsorption. Since the average work function decreases after ammonia adsorption, it is certain that ammonia is adsorbed on the planes corresponding to the bright areas of the emission pattern. In the dark areas ammonia may also be present on the surface, however, due to their higher clean work function, these areas are emitting with negligible intensity under the voltage applied. On heating the deposit to 700°K, adsorbed ammonia undergoes dissociation with hydrogen desorption, and therefore the pattern observed (Figure 38.2)

(1) NH_3 dose at 300°K
2580V

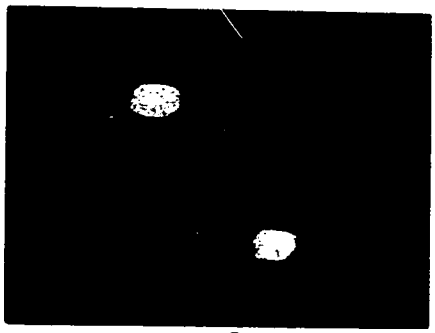

(2) 700°K
3750V

(3) Second dose at 300°K
2300V

(4) 700°K
3800V

(5) Third dose at 300°K
2100V

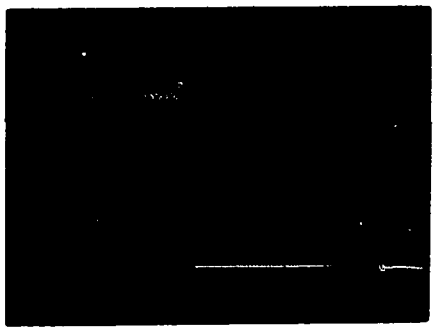

(6) 700°K
3930V

Fig. 38. Field emission patterns obtained for the repeated adsorption of ammonia as described in Figure 37 and its subsequent decomposition.

(1) NH_3 dose at [illegible] °K
[illegible] V

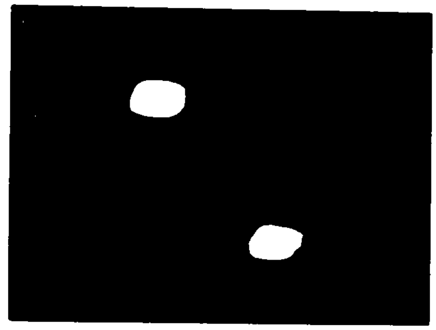

(2) 700°K
3750V

[illegible] second dose at [illegible] °K
[illegible] V

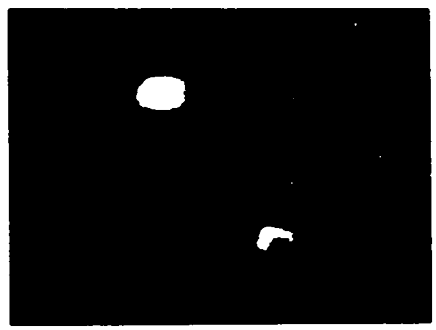

(4) 700°K
3800V

[illegible]

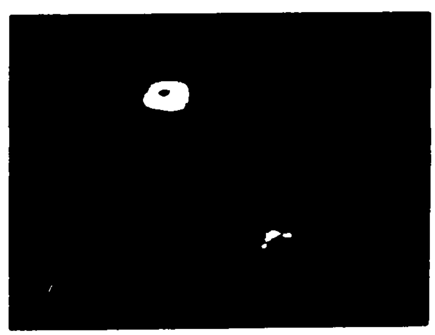

[illegible] 700°K
[illegible] V

[illegible] pattern [illegible] for the repeated [illegible] described in Figure 37 [illegible]

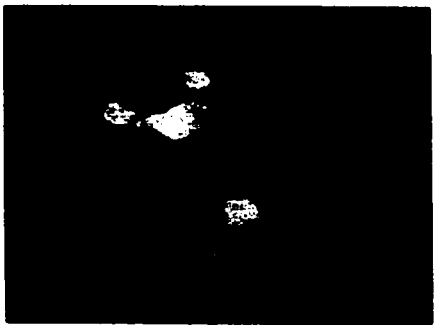

(7) Fourth dose at 300°K
2110V

(8) 700°K
3880V

(9) Fifth dose at 300°K
$\overline{\varphi}$ = 2.74 eV

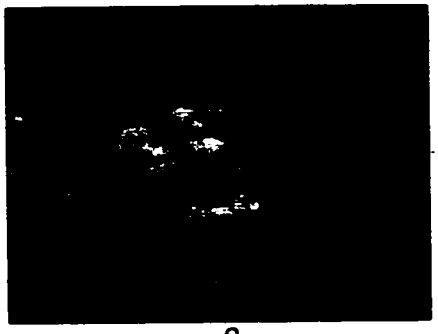

(10) 400°K
3.73 eV

(11) 500°K
4.03 eV

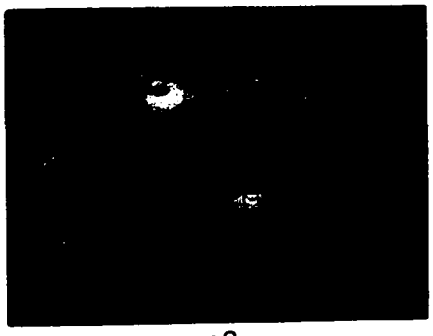

(12) 600°K
4.53 eV

Figure 38 (continued)

[illegible] Fourth [illegible] at 3[illegible] °K

[illegible]

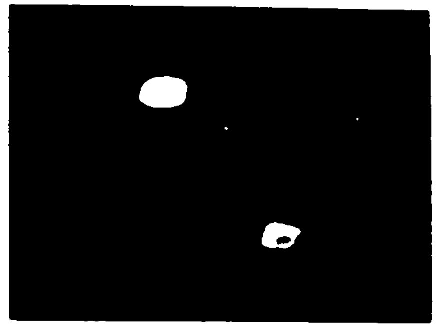

(9) 7[illegible] °K

[illegible]

([illegible] Fifth [illegible] at 3[illegible] °K

[illegible]

(10) 400°K

3.73 eV

[illegible]

[illegible] °K

4.[illegible] eV

[illegible])

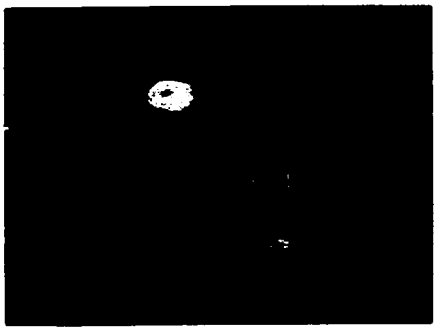

(13) 650°K
4.63 eV

(14) 700°K
4.66 eV

(15) 900°K
4.62 eV

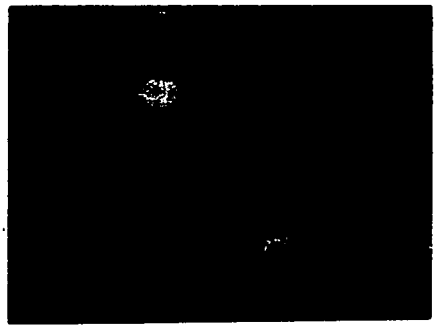

(16) 1000°K
4.48 eV

(17) 1300°K
4.30 eV

(18) 1500°K
4.47 eV

Figure 38 (continued)

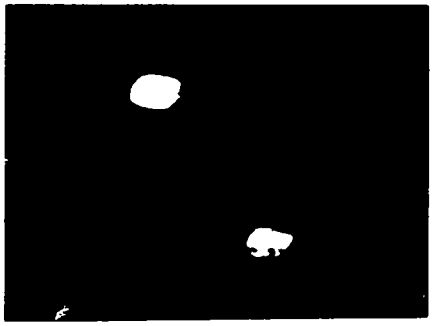

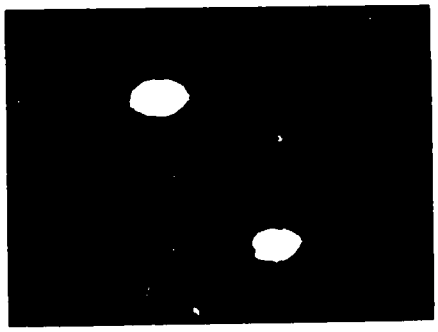

corresponds to a β-nitrogen covered surface with lower work function in the environs of the {100} planes. Upon further dosing at 300°K and heating to 700°K, the surface nitrogen adatom concentration increases and the pattern produced (Figure 38.4, 38.6 and 38.8), which differs from the β-nitrogen pattern (Figure 38.2) by lack of emission from the {100} planes, corresponds therefore to the δ-nitrogen adlayer. The patterns obtained upon each repeated dosing have the same bright areas (Figure 38.3, 38.5, 38.7 and 38.9), the large negative work function shift again indicating the presence of undissociated ammonia on the {210} and {310} planes. It was deduced from thermal desorption observations that a surface which is saturated with nitrogen adatoms is not active towards further ammonia interaction, therefore this bright area would correspond to the surface where tungsten atoms were available for ammonia adsorption at 300°K. In the dark areas, it is not necessary that all the surfaces are saturated with nitrogen, since the emitter tip consists of many different crystal planes, only those planes which have the lowest work function after ammonia adsorption will become visible. The ammonia covered surfaces in the dark areas may eventually become visible upon heating the deposit, if ammonia dissociation on the bright areas is completed before that on the dark areas takes place. The emitting properties of the {321} plane and the low work function observed at 400°K (Figure 38.10) would therefore indicate that

ammonia is present on this plane though it was not visible at 300°K. The pattern changes observed between 400 and 700°K (Figure 38.10 - 38.14), which are accompanied by a work function increase, correspond to the dissociation of ammonia and desorption of hydrogen. At 700°K the pattern observed (Figure 38.14) again corresponds to a δ-nitrogen covered surface in the environs of the {100} planes. Though it is difficult to draw any conclusion about δ-formation on other planes, it is obvious that the species present on the {111} plane (Figure 38.14) can not be β-nitrogen since formation of β-nitrogen adlayer on this plane causes the work function of this plane to increase to 4.67 eV [34]; the {111} plane would emit with a comparable intensity to the environs of the {100} planes if β-nitrogen was present on this plane. The complete lack of emission from this plane therefore indicates that δ-nitrogen is also formed on the {111} plane and the formation of δ-nitrogen raises the work function on this plane. Upon further heating, a typical β-nitrogen pattern is observed at 1000°K (Figure 38.16), and above 1100°K the pattern changes again correspond to the desorption of β-nitrogen.

4.3.1(b) Ammonia interaction under low pressure at 500°K.

The work function versus temperature plot and the field emission patterns obtained from interaction under a pressure of 2×10^{-6} torr and at 500°K for an exposure of 10^{-5} torr-sec are shown in Figure 39 and 40 respectively. A

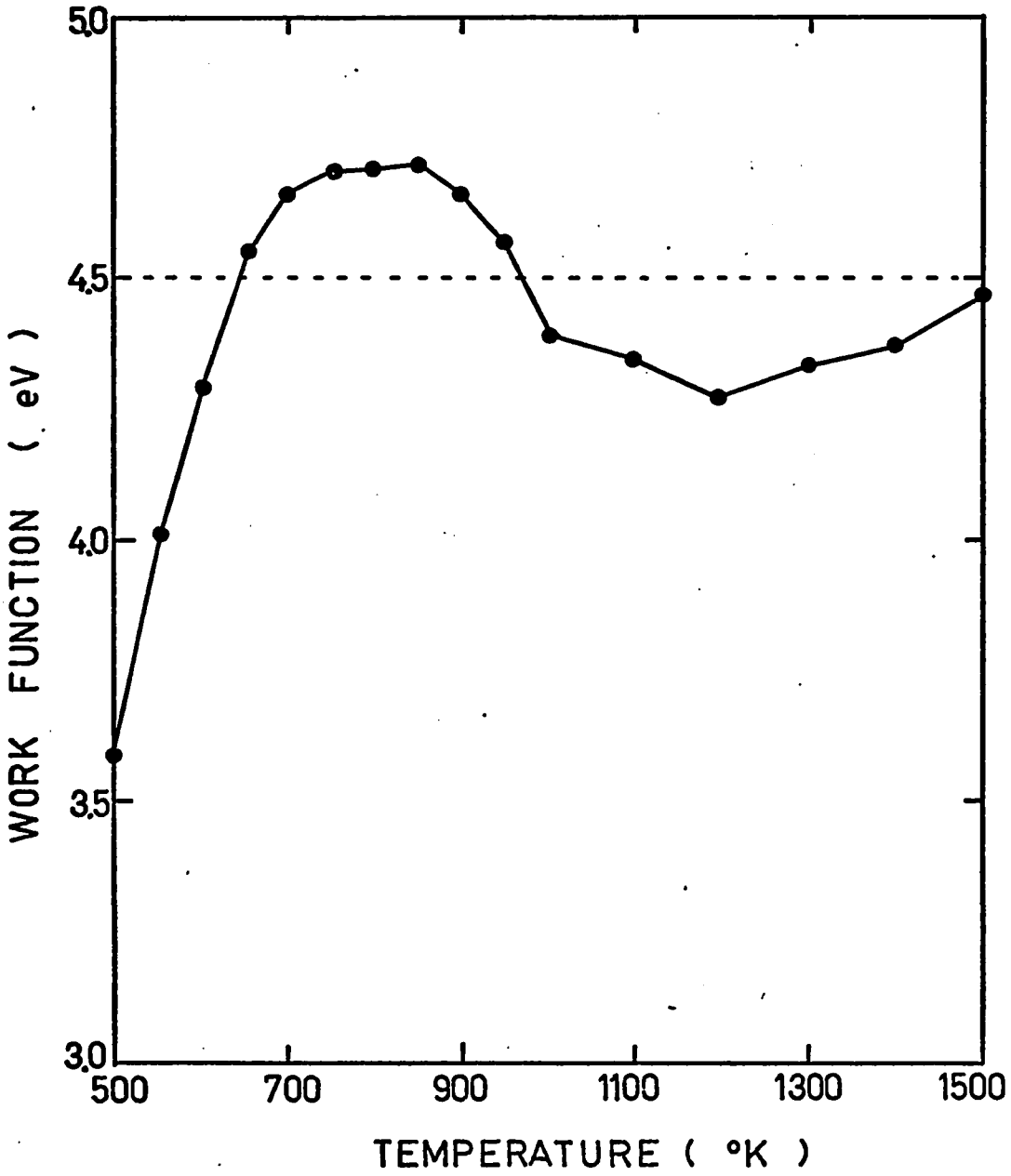

Fig. 39. The variation in work function with temperature of a tungsten emitter which had been dosed at 2×10^{-6} torr for 10^{-5} torr-sec at 500°K.

comparison of these results with those shown in Figure 37 and 38 indicates that above 650°K the emission patterns and work functions observed in both cases, i.e. low pressure interaction at 500°K and repeated dosing at 300°K, change in an identical manner, in agreement with thermal desorption observations: both dosing conditions produce identical species, δ-nitrogen.

The large negative work function shift observed on formation of the deposit shown in Figure 40.2 again indicates that ammonia is present on the surface. The presence of undissociated* ammonia on the surface at temperatures as high as 500°K may be unexpected, since at 200°K interaction of ammonia with clean tungsten surfaces takes place on all crystal planes with the possible exception of the {110} plane and adsorbed ammonia dissociates readily at 400°K [9]. It was concluded from thermal desorption observations that the intermediates, NH_x, formed upon ammonia dissociation become more and more stable with increasing nitrogen surface concentration. Thus, the present observation that undissociated ammonia remains on the surface at 500°K is consistent with this result and appears to be the result of the high nitrogen surface concentration, since the interaction of ammonia with tungsten at this temperature is shown to produce a densely populated nitrogen adlayer (Figure 13). The dissociation of ammonia presumably

* The adsorption of completely undissociated ammonia, NH_3, is implied by the large lowering of the work function. However there is no unambiguous evidence that partially dissociated ammonia, NH_x, could not produce the same effect.

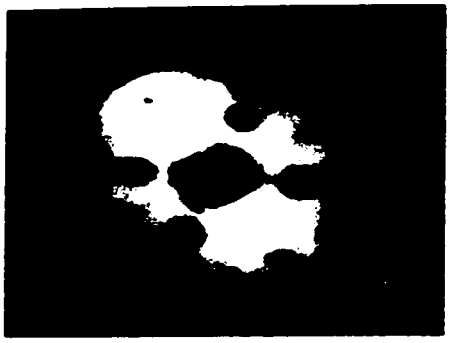

(1) Clean W
$\bar{\varphi}_0$ = 4.5 eV

(2) NH_3 dose at 500°K
$\bar{\phi}$ = 3.57 eV

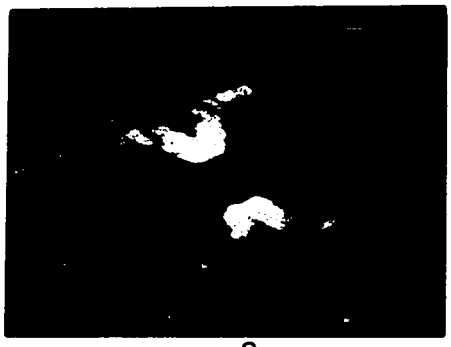

(3) 550°K
4.01 eV

(4) 600°K
4.28 eV

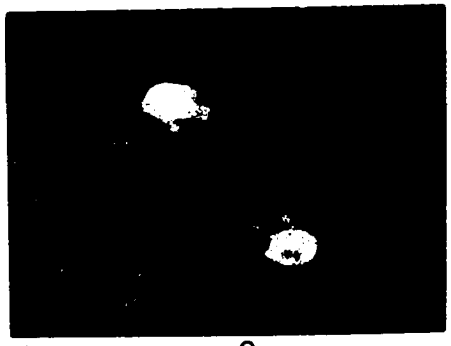

(5) 650°K
4.57 eV

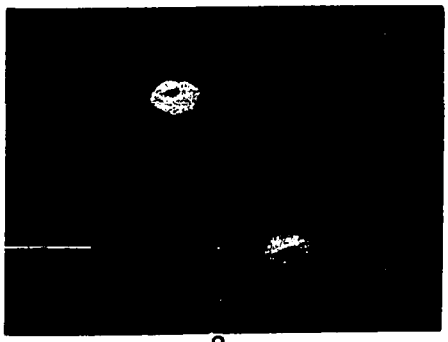

(6) 700°K
4.67 eV

Fig. 40. Field emission patterns obtained for the adsorption of ammonia on tungsten as described in Figure 39 and its subsequent decomposition.

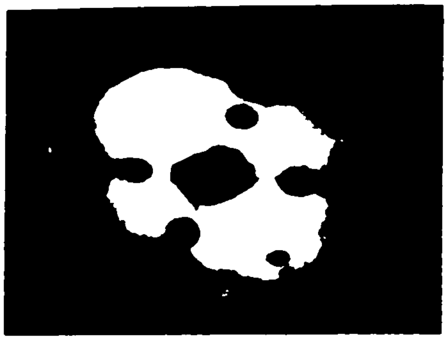

(1) [illegible] W

$\bar{\phi}$ = 4.[illegible] eV

(2) NH_3 dose at 500°K

$\bar{\phi}$ = 3.57 eV

(3) 550°K

4.[illegible] eV

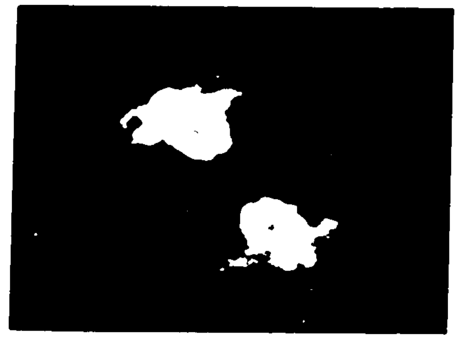

(4) 600°K

4.28 eV

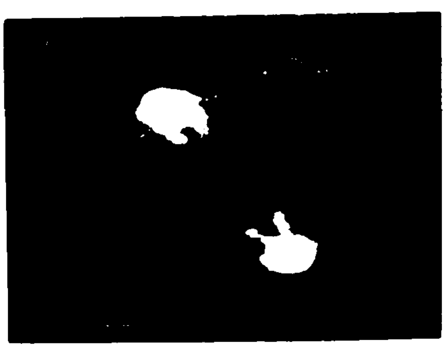

(5) [illegible]°K

4.[illegible] eV

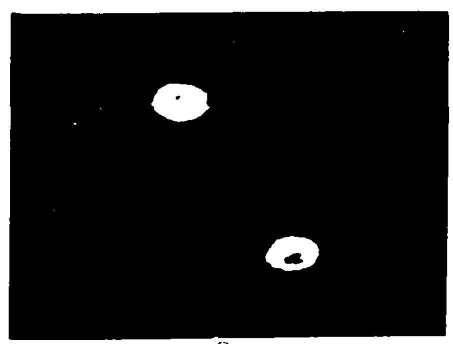

(6) 700°K

4.67 eV

[illegible] patterns obtained for the adsorption of ammonia on tungsten as described in Figure [illegible] decomposition.

(7) 800°K
4.71 eV

(8) 900°K
4.66 eV

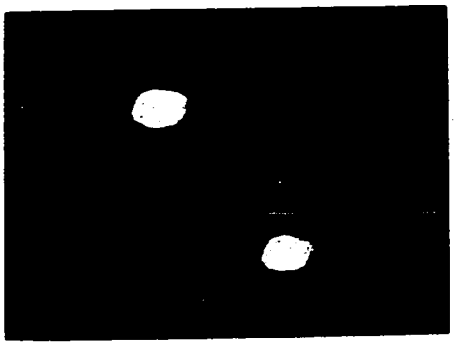

(9) 1000°K
4.38 eV

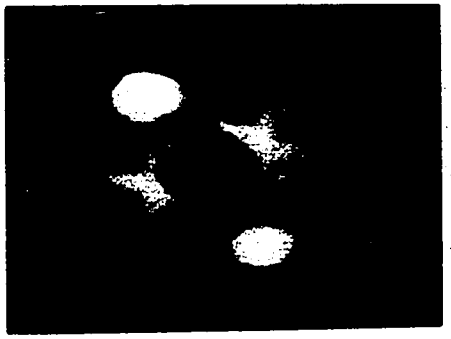

(10) 1200°K
4.26 eV

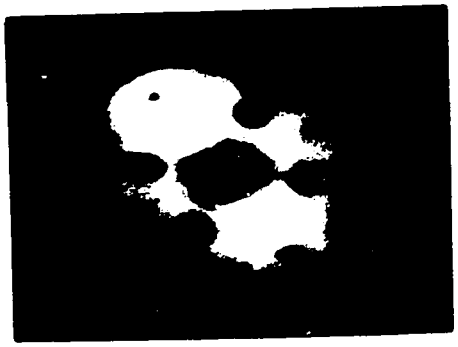

(11) 1500°K
4.48 eV

Figure 40 (continued)

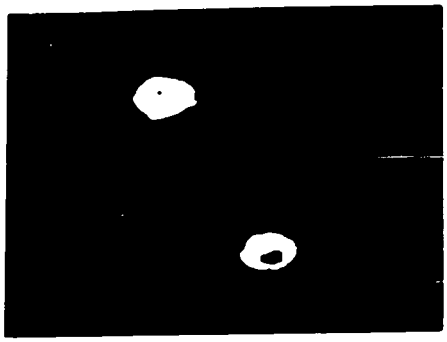

(a) 900°K
4.66 eV

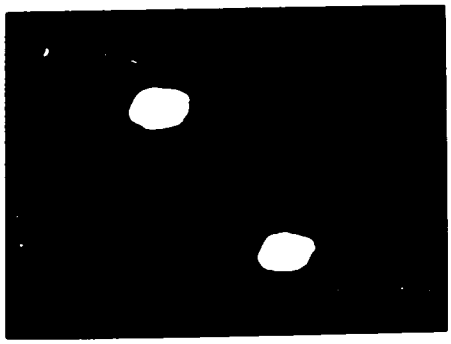

(c) 1200°K
4.26 eV

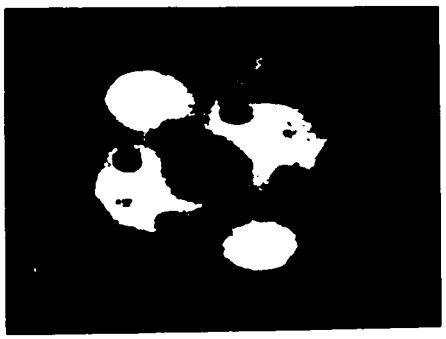

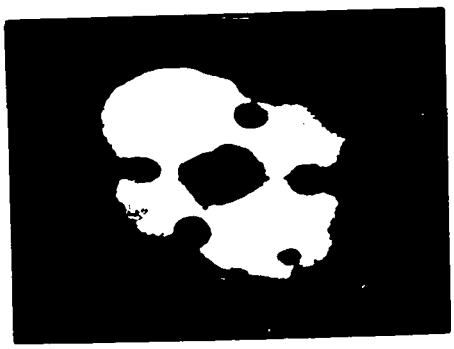

requires participation of adjacent tungsten atoms in the transition state.

4.3.2 Ammonia interaction at 500°K under higher pressure.

Dosing the emitter tip with ammonia at 4×10^{-4} torr for an exposure of 0.1 torr-sec at 500°K produces a different emission pattern (Figure 41.2) from that shown in Figure 40.2. The complete lack of emission from the {210} and {311} planes would appear to indicate that these planes are now saturated with nitrogen adatoms. For the bright area, i.e. the {321} planes, the observed large work function decrease again indicates that undissociated ammonia is present on this surface. Heating this deposit to 600°K causes the work function to increase and the {320} planes, which have a higher clean work function than that of the {321} planes, to emit indicating that ammonia is also present on these planes. At 700°K the entire emitter becomes visible and the work function increases to 4.9 eV which is $\sim$ 0.2 eV higher than that of the δ-nitrogen covered environs of the {100} planes. The species present in these areas, i.e. the environs of the {100} planes, therefore can not be the δ-nitrogen, otherwise an emission pattern similar to that in Figure 40.6 should be observed. It is very likely that this species present on the surface in the environs of the {100} planes is the η-species since thermal desorption observations indicate that a small amount of the

(1) Clean W
$\bar{\phi}_0$ = 4.5 eV

(2) NH_3 dose at 500°K
$\bar{\phi}$ = 3.81 eV

(3) 600°K
4.25 eV

(4) 700°K
4.90 eV

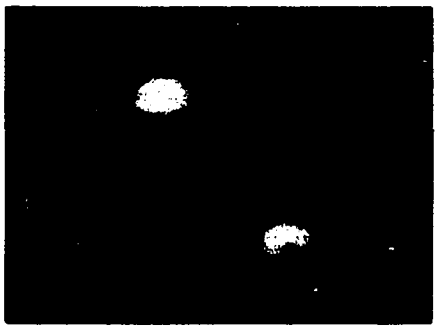

(5) 800°K
4.85 eV

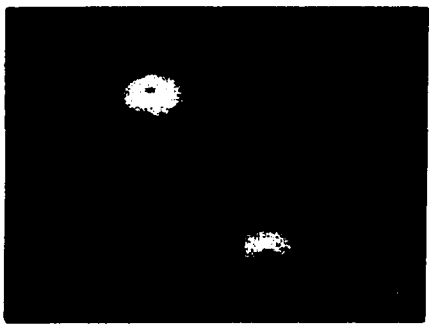

(6) 900°K
4.75 eV

Fig. 41. Field emission patterns obtained for the adsorption of ammonia on tungsten at 4×10^{-4} torr for an exposure of 0.1 torr-sec at 500°K and its subsequent decomposition.

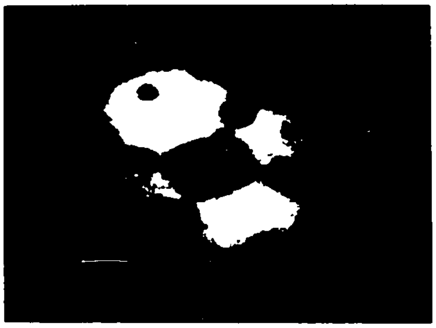

(1) Clean W
$\bar{\phi}$ = [illegible] eV

(2) NH_3 dose at [illegible] °K
$\bar{\phi}$ = 3.81 eV

(3) [illegible] °K
4.25 eV

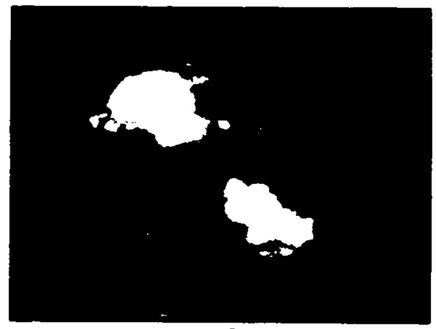

(4) 700 °K
4.90 eV

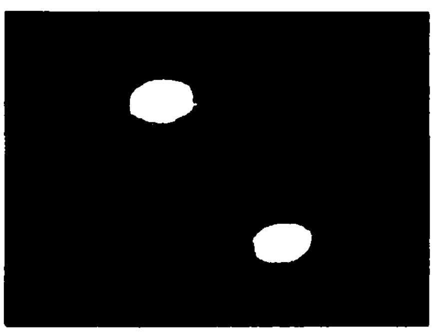

(5) [illegible] °K
[illegible] eV

(6) [illegible] °K
4.75 eV

Fig. [illegible] Field emission patterns obtained for the adsorption of ammonia on tungsten at 4×10^{-4} torr for an exposure [illegible] °K and its subsequent [illegible].

η-species can be formed at 500°K and at slightly higher ammonia pressure (Figure 26). At 700°K desorption of hydrogen from the surface is complete, so on the other planes such as the {111},{210} and {310}, δ-nitrogen could be the species present on the surface. Further heating to 800°K causes the work function to decrease and produces an emission pattern similar to that of δ-nitrogen (Figure 40.6).

The interaction of ammonia with tungsten at 500°K with even higher exposure such as 1.0 torr-sec produces similar work function changes and emission patterns (Figure 42). However, the bright ring around the {110} plane as shown in Figure 42.2, which is not present in the emission pattern obtained under lower exposure, indicates that more ammonia is adsorbed on the surface around this plane.

Based on field emission observations [9], it has been concluded that the rate of ammonia decomposition is slower on crystal planes of higher work function. Though the present results are obtained from successive ammonia interaction with a surface covered with dissociation intermediates, they appear to add some support to this conclusion. By comparing the emission patterns shown in Figure 40.2, 41.2 and 42.2 it can be seen that:

(1) dosing ammonia for 10^{-5} torr-sec, the {210} and the {311} planes both with ϕ_o:4.5 eV are the main emitting area,

(2) for 0.1 torr-sec the {321} plane with ϕ_o:4.6 eV

(1) Clean W

$\bar{\phi}_0$ = 4.5 eV

(2) NH_3 dose at 500°K

$\bar{\phi}$ = 3.46 eV

(3) 600°K

4.10 eV

(4) 700°K

4.92 eV

(5) 800°K

4.81 eV

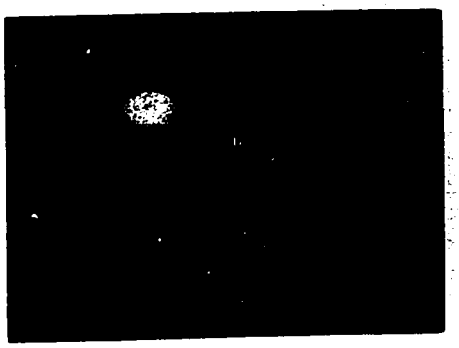

(6) 900°K

4.75 eV

Fig. 42. Field emission patterns obtained for the adsorption of ammonia on tungsten at 4×10^{-3} torr for 1 torr-sec at 500°K and its subsequent decomposition.

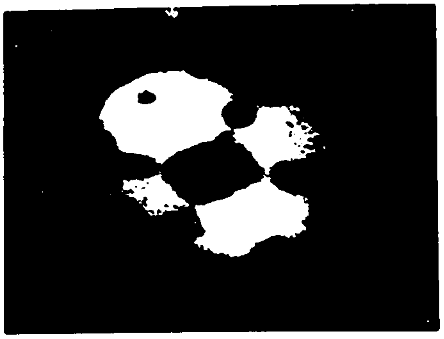

[illegible] W

$\bar{\phi}$ = 4.[illegible] eV

(2) NH_3 dose at 500°K

$\bar{\phi}$ = 3.46 eV

[illegible] °K

4.10 eV

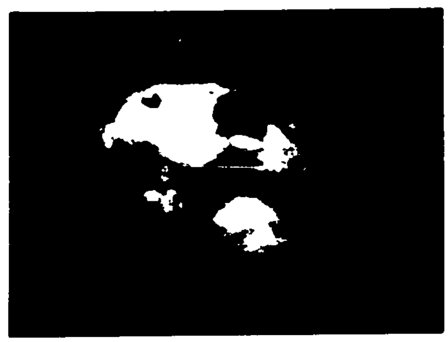

(4) 700°K

4.92 eV

[illegible]

[illegible]

(6) [illegible]°K

4.75 eV

[illegible] field emission patterns obtained for the adsorption [illegible] ammonia on tungsten at 4×10^{-3} torr for 1 torr-[illegible] at [illegible]°K and its subsequent decomposition.

is the only emitting area and

(3) for 1.0 torr-sec in addition to the {321} plane, the {320} plane with ϕ_o:5.3 eV is also visible.

All these emission patterns are associated with a large negative work function shift with respect to the clean values, thus, undissociated ammonia is the species which gives rise to the observed emission. The increased stability of ammonia on the surface at 500°K, as previously mentioned, can be attributed to the formation of a densely populated nitrogen adlayer, δ-nitrogen. This suggests that the dissociation of ammonia will become slower and slower as the interaction proceeds. However, at 500°K the surface would eventually be saturated with nitrogen and possibly a small amount of hydrogen if ammonia dissociation proceeded with an appreciable rate. The observed change from an emitting (Figure 40.2) to a non -emitting (Figure 41.2) property on the {210} and {311} planes upon increasing the exposure probably corresponds to the formation of a nitrogen adatom saturated surface, while the change from a non-emitting to an emitting property on the {321} planes corresponds to the formation of densely populated nitrogen adlayer and the stabilization of adsorbed ammonia. Since the faster ammonia dissociates, the earlier the surface will be saturated, the present observations would appear to indicate that the rate of dissociation would have the following order

$$\{210\}, \{311\} > \{321\} > \{320\}$$

which is consistent with the order of increasing clean work function.

4.3.3. Formation and desorption of η-species.

The field emission patterns obtained from the interaction of ammonia at a pressure of 4×10^{-4} torr with tungsten at 700°K for an exposure of 0.05 torr-sec are shown in Figure 43. It can be seen that ammonia interaction under these conditions produces a deposit (Figure 43.2) which causes the work function to increase by 0.46 eV from that of the clean emitter. Heating the deposit to 750°K causes a slight decrease in work function but the emission pattern remains almost unchanged. Further heating to 800°K causes a large decrease in work function and a slight change in emission pattern (Figure 43.4) is observed, to one which is similar to that of δ-nitrogen. Between 800 and 950°K no further significant change either in work function or emission pattern is observed. By comparing the work function and emission pattern (Figure 43.2) with that shown in Figure 40.6 it is certain that δ-nitrogen is not the species present on the emitting area, otherwise a pattern and work function similar to that shown in Figure 40.6 should be observed. It was noted from thermal desorption observations that the η-species can be formed to some extent under these dosing conditions, but the η-species is not stable and starts to desorb at temperature above 780°K.

(1) Clean W

$\bar{\phi}_0$ = 4.5 eV

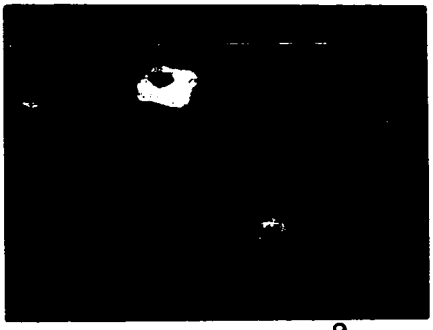

(2) NH_3 dose at 700°K

$\bar{\phi}$ = 4.96 eV

(3) 750°K

4.89 eV

(4) 800°K

4.68 eV

(5) 850°K

4.74 eV

(6) 900°K

4.68 eV

Fig. 43. Field emission patterns obtained for ammonia interaction for 5×10^{-2} torr-sec at 700°K to form the η-species and its subsequent decomposition.

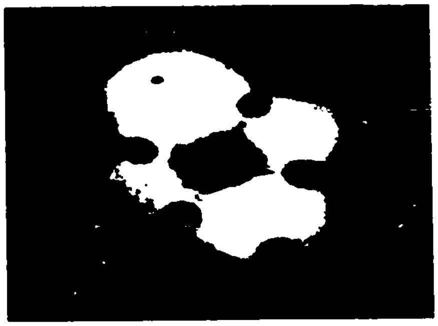

(1) [illegible] W

[illegible] eV

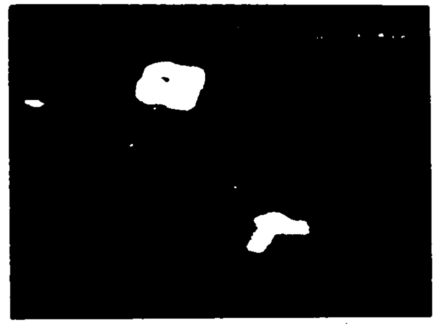

(2) [illegible] °K

[illegible] eV

(3) 750°K

4.39 eV

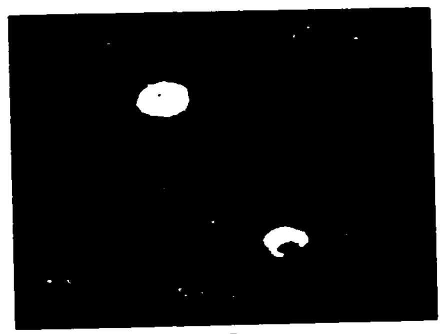

(4) [illegible]0°K

4.6[illegible] eV

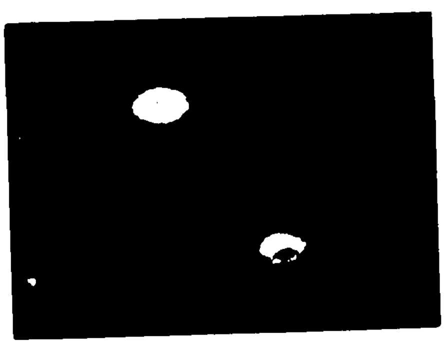

(5) [illegible]50°K

4.74 eV

(6) [illegible]00°K

4.68 eV

Fig. 43. Field emission patterns obtained for ammonia interaction for 5x10[illegible] torr-sec at 7[illegible]°K to form the [illegible]-species and its subsequent decomposition.

The observed decrease in work function and change in emission pattern at 800°K therefore parallels this observation and one can conclude that the species present in the environs of the {100} planes (Figure 43.2) is the η-species. It is difficult to draw any conclusion about the η-formation on other planes, however, a comparison of Figure 42.4 and 43.2 appears to provide some information about η-formation on the {111} plane. In Figure 42.4 where the η-species is present in the environs of the {100} planes, the {111} planes emit with a comparable intensity to the environs of the {100} planes, while in Figure 43.2 these planes are almost invisible. Since both deposits produce a comparable work function shift, these different emission properties may indicate that the η-species is also present on the {111} planes in Figure 43.2. This argument assumes that formation of the η-species further increases the work function on this plane from that of δ-nitrogen covered surface. The distinction between the emission properties of the δ-nitrogen and the η-species as shown in Figure 43.2 and Figure 40.6 is not large but detectable. However, it becomes clearer when ammonia interaction takes place at higher exposures. In Figure 44 the field emission patterns obtained from ammonia interaction at 700°K under an exposure of 0.2 torr-sec are shown. The interesting pattern shown in Figure 44.2 is completely different from that of δ-nitrogen (Figure 40.6); in addition to the environs of the {100} planes the entire emitter with the exception

(1) Clean W

$\bar{\phi}_0$ = 4.5 eV

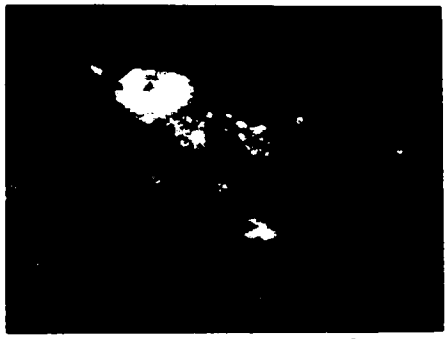

(2) NH_3 dose at 700°K

$\bar{\phi}$ = 5.01 eV

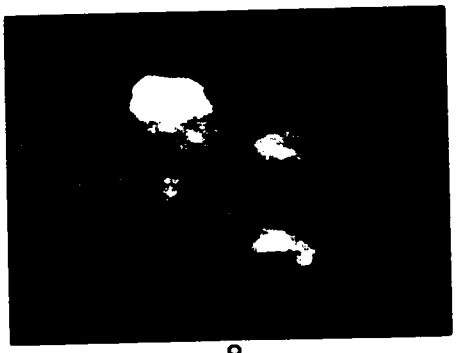

(3) 750°K

5.09 eV

(4) 800°K

4.98 eV

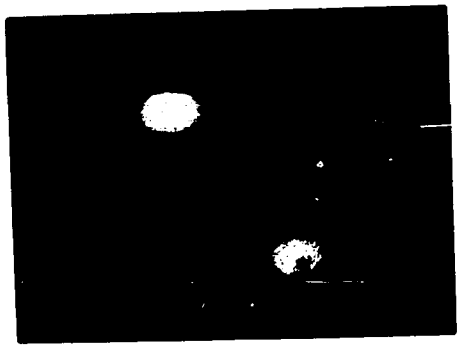

(5) 850°K

4.76 eV

(6) 900°K

4.72 eV

Fig. 44. Field emission patterns obtained for ammonia interaction for 0.2 torr-sec at 700°K to form the n-species and its subsequent decomposition.

(1) Clean W

$\bar{\phi}$ = 4.5 eV

(2) NH_3 dose at 700°K

$\bar{\phi}$ = 5.01 eV

(3) 750°K

5.09 eV

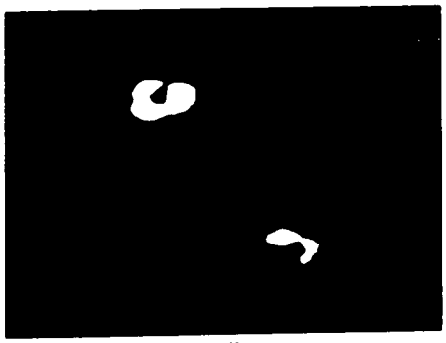

(4) 800°K

4.98 eV

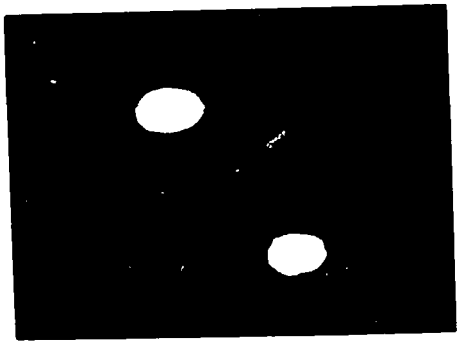

(5) 850°K

4.76 eV

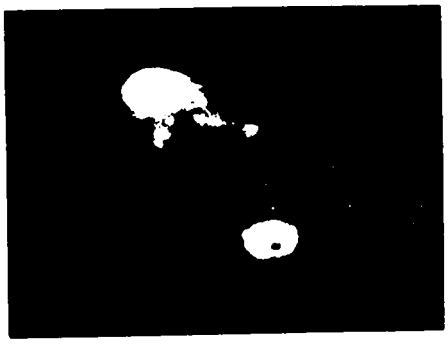

(6) 900°K

4.72 eV

Fig. 44. Field emission patterns obtained for ammonia interaction for 0.2 torr-sec at 700°K to form the γ-species and its subsequent decomposition.

of the low index planes, i.e. {100},{110} and {211}, becomes visible. By comparing the work function and emission pattern (Figure 44.3) with that shown in Figure 42.4 where on the {111} plane the surface is covered with δ-nitrogen, it can be concluded that formation of the η-species also increases the work function on the {111} plane from that of the δ-nitrogen covered surface. Heating the deposit causes the work function to increase and to reach its maximum value at 750°K. This increase in work function is accompanied by the increase in emission anisotropy as shown in Figure 44.3. Heating to 800°K leads to a decrease of work function and a change in emission pattern (Figure 44.4). On further heating to 850°K (Figure 44.5), where η-desorption is considerable, a pattern similar to that of δ-nitrogen is observed and a work function of 4.76 eV, corresponding to the work function of the δ-nitrogen covered emitter, is observed.

Under an even higher exposure, 1.0 torr-sec, where the formation of the η-species is almost complete (Figure 25), the emission pattern observed in Figure 45.2 has a rather uniform intensity. Upon heating, the work function changes with temperature in a similar manner to that observed after an 0.2 torr-sec exposure; it increases steadily with increasing temperature until its maximum value is reached at 800°K. In this temperature range, between 700 and 800°K, the emission patterns do not show significant change (Figure 45.2, 45.3 and 45.4). Further heating causes the work function to

(1) Clean W

$\bar{\phi}_0$ = 4.5 eV

(2) NH_3 dose at 700°K

$\bar{\phi}$ = 4.98 eV

(3) 750 °K

5.13 eV

(4) 800°K

5.18 eV

(5) 850°K

4.87 eV

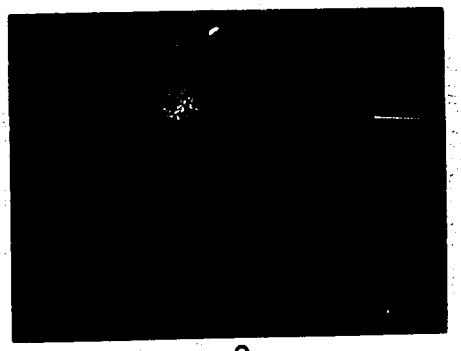

(6) 900°K

4.82 eV

Fig. 45. Field emission patterns obtained for ammonia interaction for 1 torr-sec at 700°K to form the η-species and its subsequent decomposition.

(1) Clean W

$\bar{\phi}$ = 4.5 eV

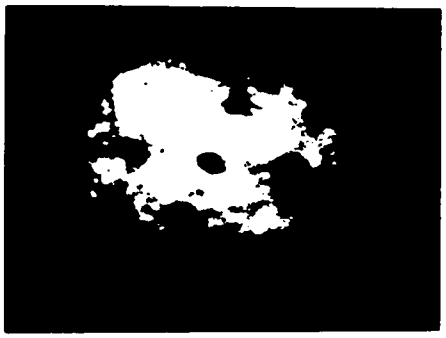

(2) NH_3 dose at 700°K

$\bar{\phi}$ = 4.98 eV

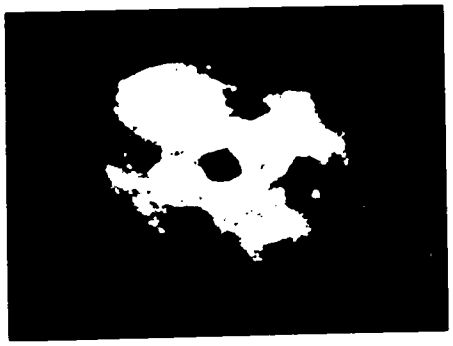

(3) 750 °K

5.13 eV

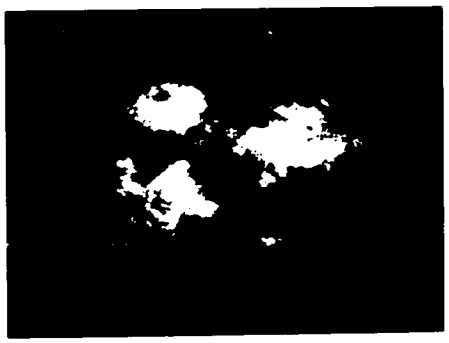

(4) 800°K

5.18 eV

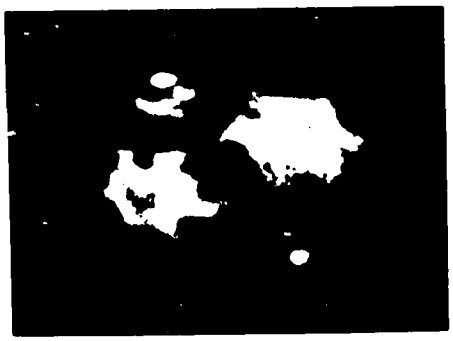

(5) 850°K

4.87 eV

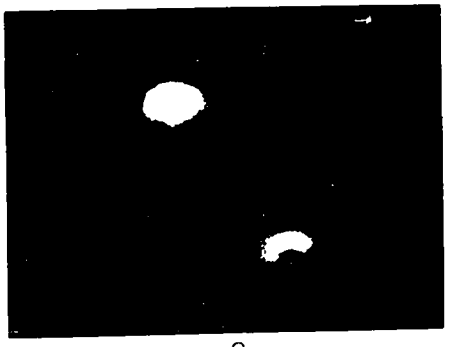

(6) 900°K

4.82 eV

Fig. 4. Field emission patterns obtained for ammonia interaction for 1 torr-sec at 700°K to form the intermediate and its subsequent decomposition.

decrease and at 900°K a pattern similar to that of δ-nitrogen around the {100} planes is again observed with slightly higher work function than that corresponding to the value for the δ-nitrogen covered emitter (Figure 40.6). In Figure 46 the work function versus temperature plots obtained under these three different exposures at 700°K are summarized. These observations are all in good agreement with the thermal desorption results. The interesting emission patterns (Figure 44.2 and 45.2), which are obtained only under an exposure where η-formation is considerable, undoubtedly represent the η-species. The pronounced decrease in work function and change of emission patterns are observed at temperatures higher than 780°K where the η-desorption starts to set in (Figure 16).

From Figure 43, 44, 45 and 46 the observations obtained for η-formation from ammonia interaction at 700°K under exposures of 0.05, 0.2 and 1.0 torr-sec can be summarized:

(1) Formation of the η-species at 700°K leads to an increase in work function above that observed for δ-nitrogen which then remains almost unchanged upon further increase of coverage.

(2) A maximum work function is observed upon heating the deposit obtained at 700°K and the temperature at which this maximum is observed is higher the higher the exposure.

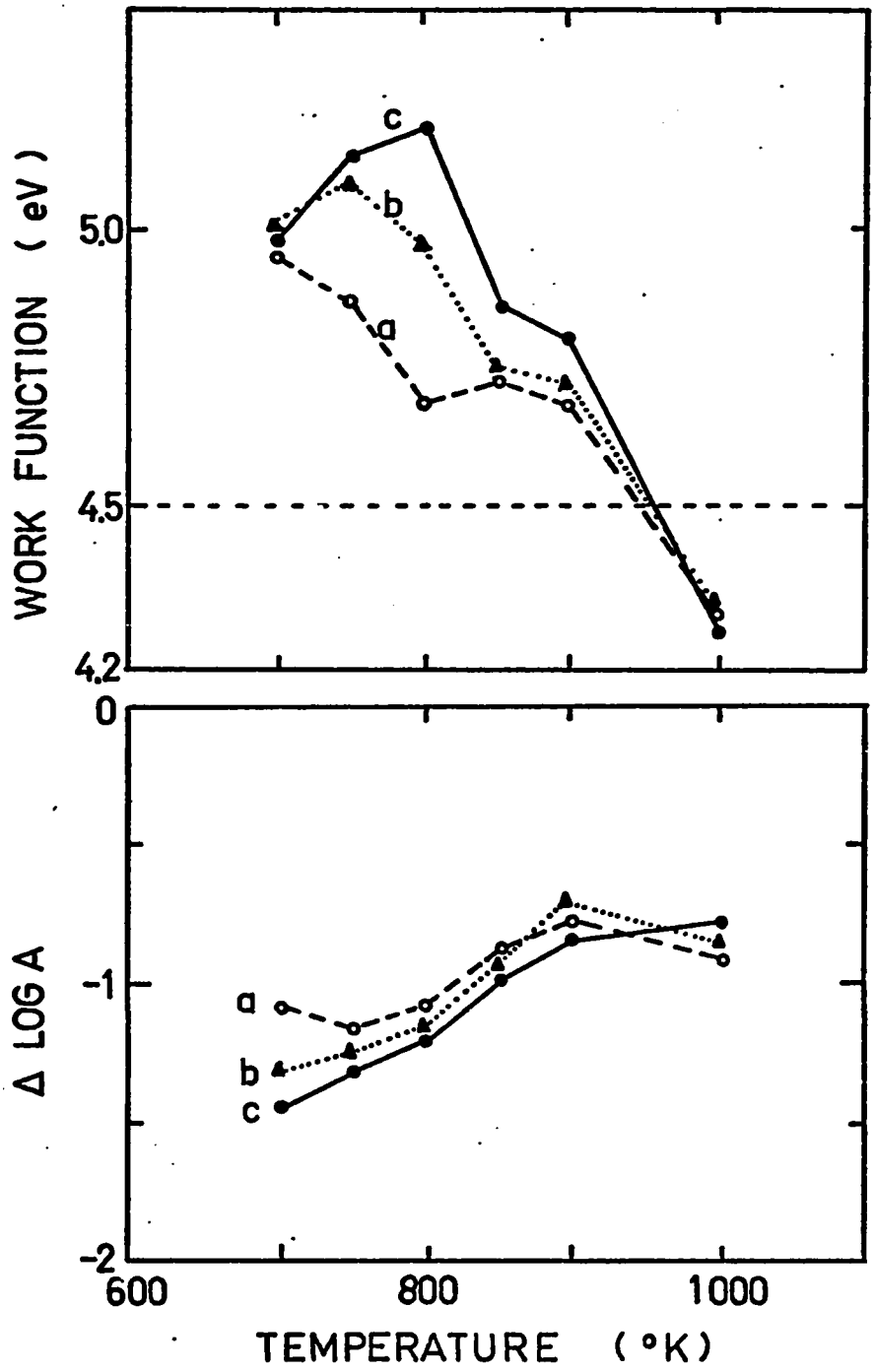

Fig. 46. The variation in work function and Δ log A, A being the pre-exponential term of equation (16), with temperature of a tungsten emitter which had been dosed with ammonia for 0.05 torr-sec (curve a), 0.2 torr-sec (curve b) and 1 torr-sec (curve c) at 700°K.

(3) A pattern similar to that of δ-nitrogen appears upon heating the deposit to a temperature higher than 800°K. The temperature at which this pattern is observed also varies with exposure.

These observations suggest that η-formation is a complicated process. The observed increase in work function in the temperature range between 700 and 800°K, where decomposition of the η-species is negligible, would indicate that the surface underwent some change during the heating of the deposit obtained at 700 °K. It is very probable that at a temperature where η-formation is considerable, i.e. 700°K, the surface could undergo reconstruction as a consequence of η-formation, since this temperature is higher than that required for migration of a tungsten atom over its own substrate [35]. If this is the case the observed increase in work function upon annealing would appear to indicate that the surface rearrangement occurred on η-formation in such a way that the surface roughened on an atomic scale. The formation of such a surface would give rise to a work function decrease by modifying the surface double layer (see section 2.3.2), and heating the surface in the absence of ammonia gas between 700 and 800°K, where η-desorption is negligible, could smooth out the surface and cause the work function to increase as observed. A pattern similar to that shown in Figure 45.2 has been obtained by bombarding a tungsten emitter tip with argon ions at a temperature where argon could

not be adsorbed and a diminution of 0.4 eV in work function was observed after prolonged bombardment [36].

On further heating to temperatures above 800°K where the η-species desorbs, all the changes in emission pattern are accompanied by a large work function decrease. The high emission current from the {111} planes in Figure 45.5 can therefore be taken to indicate that desorption of η-species from this plane proceeds faster than that on the environs of the {100} planes. The observation of a pattern similar to that of δ-nitrogen in the heating sequence would suggest that η-desorption leaves behind a δ-nitrogen adlayer in the environs of the {100} planes, and not the β-nitrogen adlayer as deduced from the thermal desorption experiments.

4.3.4 Ammonia interaction at 700 and 800°K under high exposure.

In Figure 25 it can be seen that the η-formation curves do not saturate but η-formation is followed by an even slower reaction. To study this reaction the emitter tip was allowed to interact with ammonia for an exposure of 10 torr-sec at 700 and 800°K. For comparison, the experiment was also carried out at 500°K. The results obtained are shown in Figure 47, 48, 49, 50 and 51. The change in work function and emission pattern upon heating the deposit obtained at 500°K (Figure 47 and 48) are identical to that obtained for a 1 torr-sec exposure as shown in Figure 42.

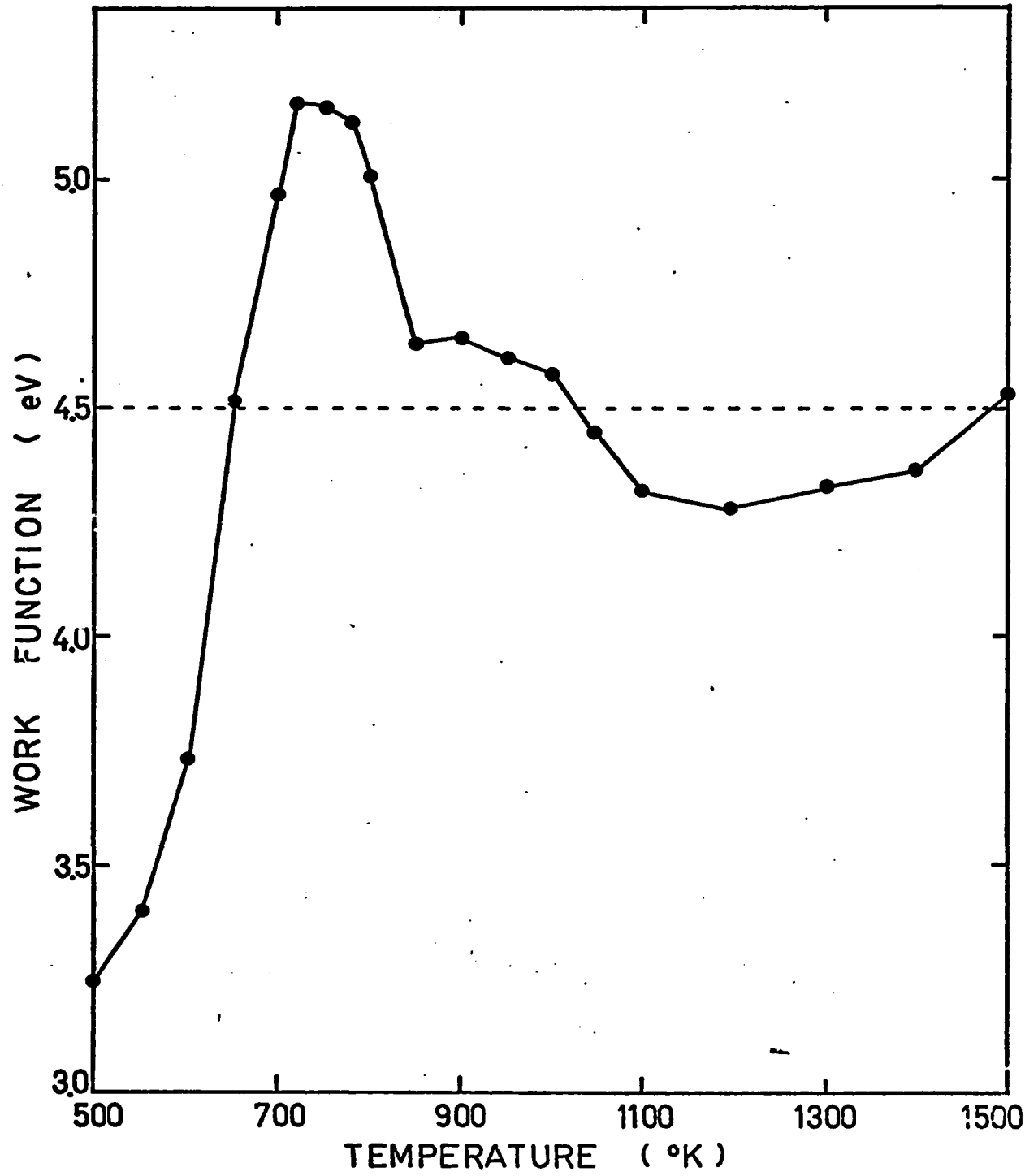

Fig. 47. The variation in work function with temperature of a tungsten emitter which had been dosed with ammonia at 500°K for 10 torr-sec.

(1) Clean W

$\bar{\phi}_0$ = 4.5 eV

(2) HN_3 dose at 500°K

$\bar{\phi}$ = 3.26 eV

(3) 600°K

3.74 eV

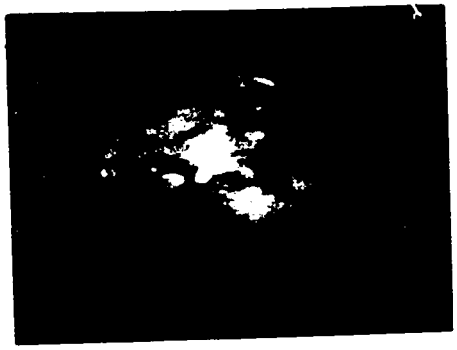

(4) 650°K

4.52 eV

(5) 700°K

4.99 eV

(6) 775°K

5.13 eV

Fig. 48. Field emission patterns obtained for ammonia interaction for 10 torr-sec at 500°K and its subsequent decomposition.

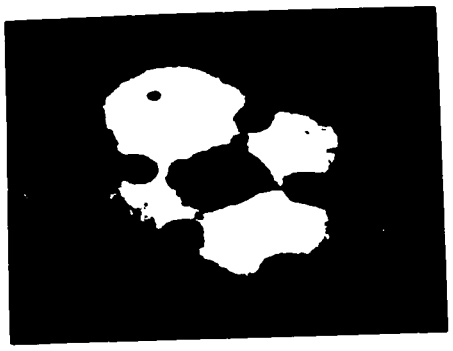

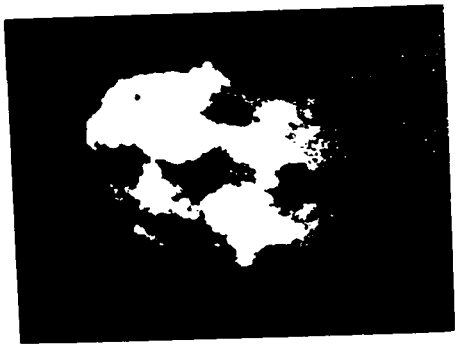

(7) 800°K
5.01 eV

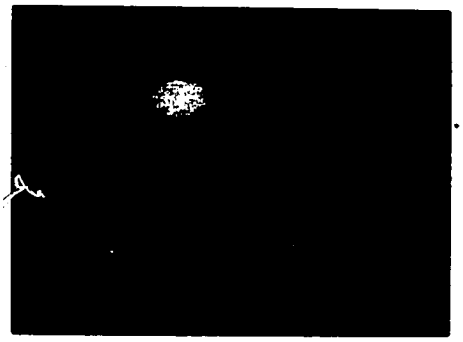

(8) 900°K
4.66 eV

(9) 1000°K
4.58 eV

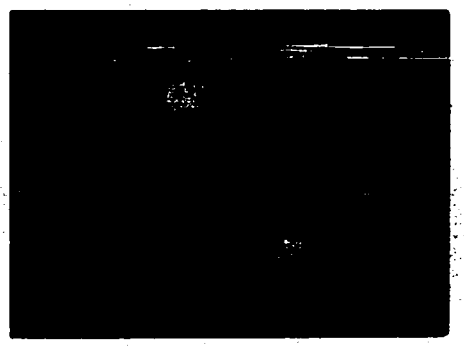

(10) 1100°K
4.33 eV

(11) 1300°K
4.34 eV

(12) 1500°K
4.54 eV

Figure 48 (continued)

[illegible]

(8) [illegible]°K

4.[illegible] eV

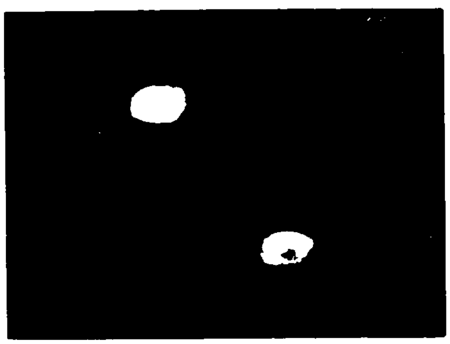

[illegible] 1[illegible]°K

4.5[illegible] eV

(10) 1100°K

4.33 eV

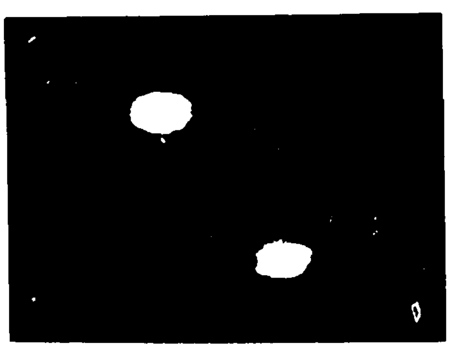

(11) 13[illegible]°K

4.34 eV

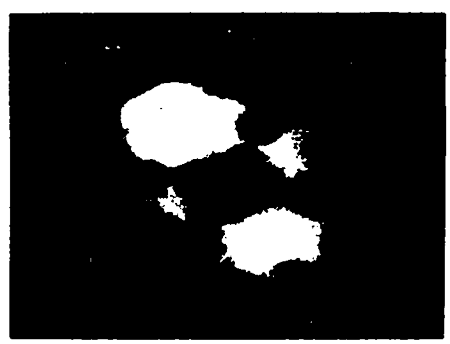

(12) 1500°K

4.54 eV

Figure [illegible] (continued)

An emission pattern with a bright ring around the {110} plane (Figure 48.2), however, indicates that yet more ammonia is adsorbed on the surface around this plane under this high exposure. For the interaction at 700°K the results obtained (Figure 50) are similar to those shown in Figure 45. However, in addition to the main pattern a few small bright spots are observed on the edges of the {110} and {111} planes (Figure 50.2). The surface which gives rise to this pattern is probably unstable in the absence of ammonia gas, since on maintaining the emitter tip at 700°K the bright spots darkened gradually and after a few minutes only the spots which had been emitting most intensely remained. During this change an increase in work function was also observed. Similar changes in work function and emission pattern as shown in Figure 45 were observed upon heating the deposit to 800°K (Figure 50.2, 50.3 and 50.4), but the work function measured at each temperature is slightly higher than that shown in Figure 45 at the corresponding temperature indicating a higher surface concentration of the η-species. The observation of the bright spots strongly suggests that extensive surface rearrangement took place during the interaction. The appearance of such an emission pattern (Figure 50.2) would appear to be the result of the formation of humps on the surface. If this is the case the work function measured would not correspond to the true work function of η-species covered surface. Since each hump has

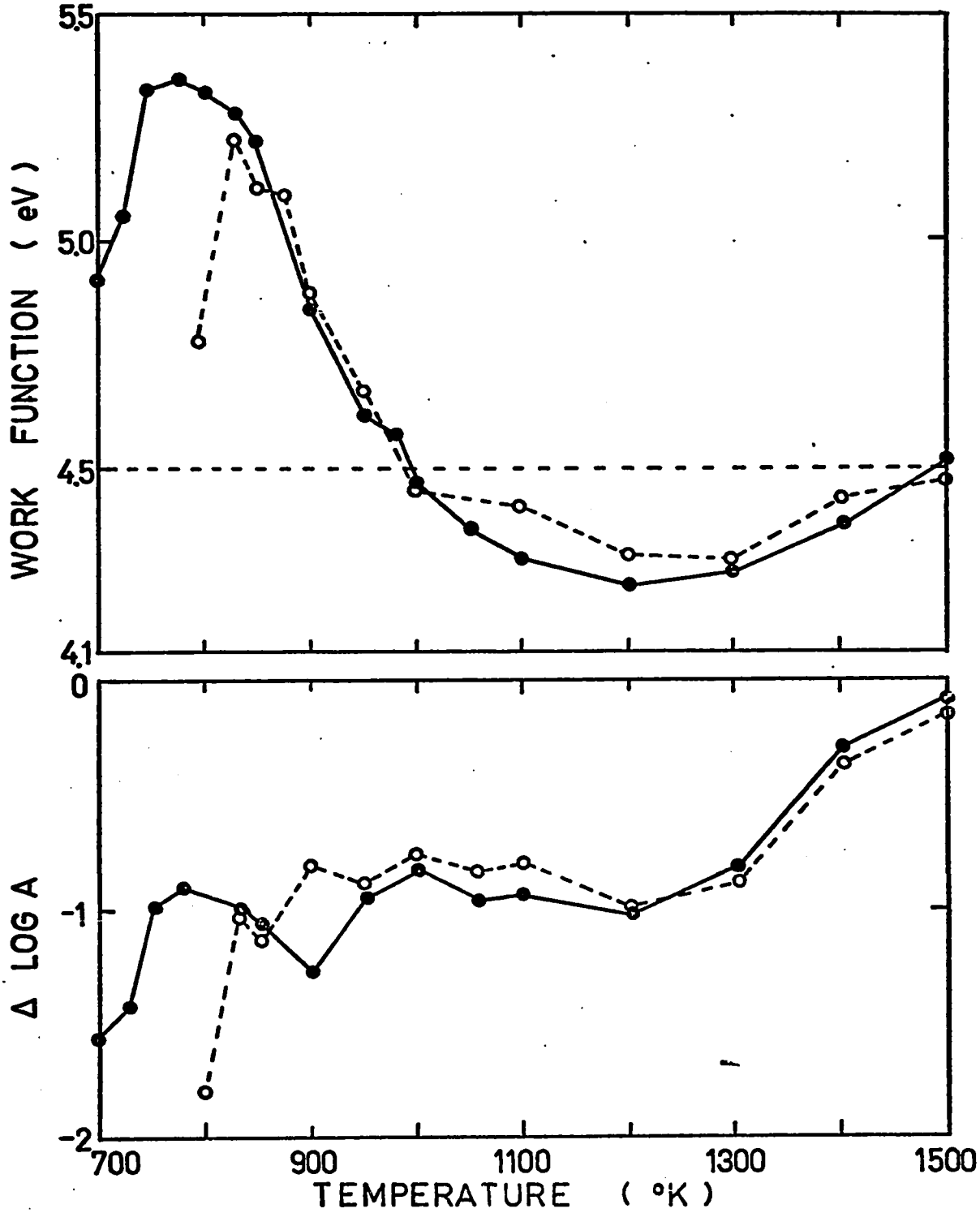

Fig. 49. The variation in work function and Δ log A, A being the pre-exponential term of equation (16), with temperature of a tungsten emitter which had been dosed with ammonia for 10 torr-sec at 700°K (filled circles) and 800°K (open circles) to form the η-species.

(1) Clean W

$\bar{\phi}_0$ = 4.5 eV

(2) NH_3 dose at 700°K

$\bar{\phi}$ = 4.92 eV

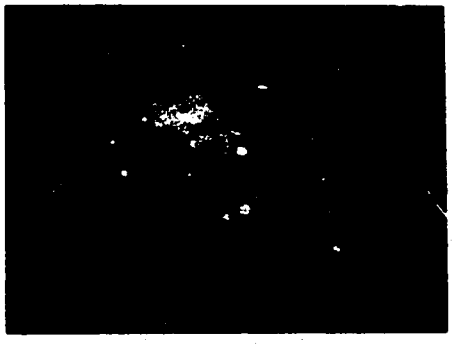

(3) 750°K

5.35 eV

(4) 800°K

5.33 eV

(5) 850°K

5.22 eV

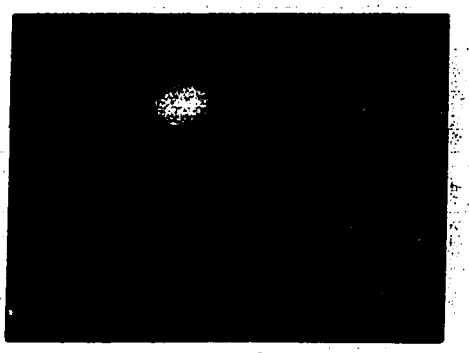

(6) 900°K

4.86 eV

Fig. 50. Field emission patterns obtained for ammonia interaction for 10 torr-sec at 700°K to form the η-species and its subsequent decomposition.

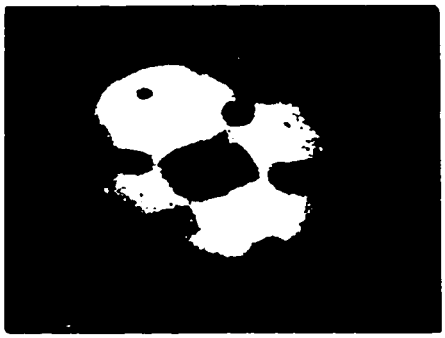

(1) Clean W

$\bar{\Phi}$ = 4.5 eV

(2) NH_3 dose at 700°K

$\bar{\Phi}$ = 4.92 eV

(3) 750°K

5.36 eV

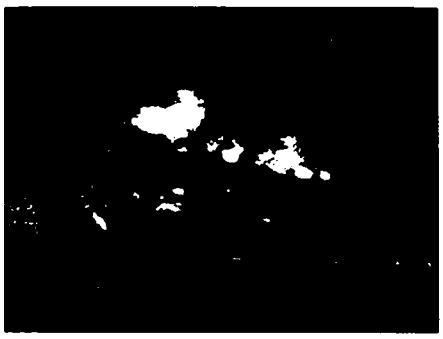

(4) 800°K

5.33 eV

(5) 850°K

5.24 eV

(6) 900°K

4.86 eV

Field emission patterns obtained for ammonia interaction for 1L torr-sec at 700°K to form the N-species and its subsequent decomposition.

(7) 1000°K
4.49 eV

(8) 1100°K
4.32 eV

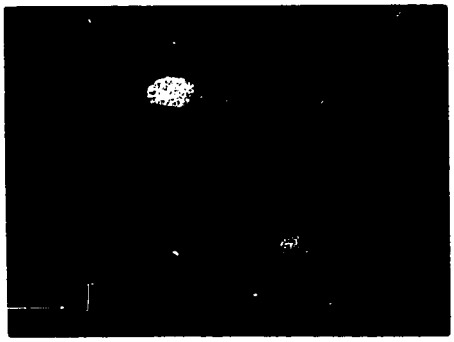

(9) 1300°K
4.28 eV

(10) 1500°K
4.52 eV

Figure 50 (continued)

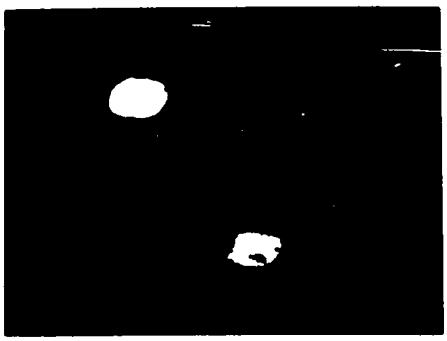

(7) 1000°K
4.49 eV

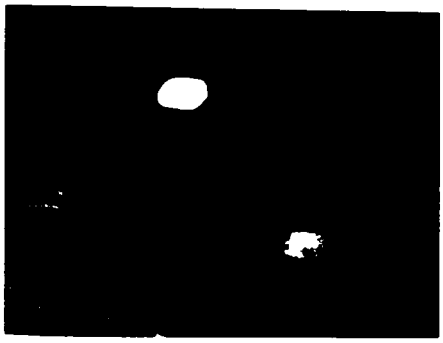

(8) 1100°K
4.32 eV

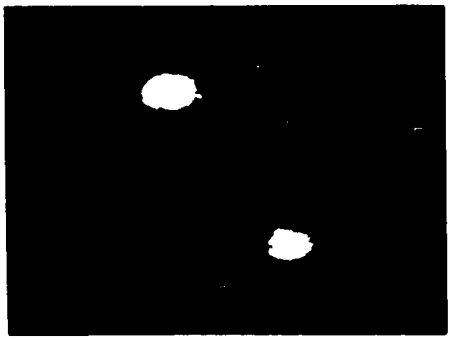

(9) 1300°K
4.28 eV

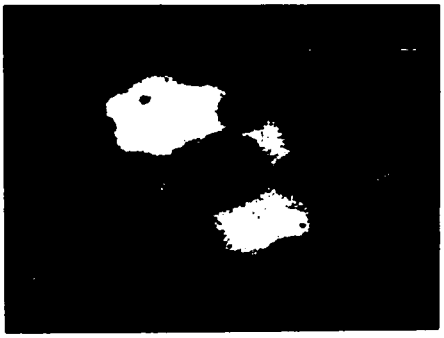

(10) 1500°K
4.52 eV

Figure 50 (continued)

a smaller radius than that of emitter tip, the local field around the hump will have higher value. If the local work function is comparable with that of the surroundings, then

$$(\phi^{3/2}/F)_{hump} < (\phi^{3/2}/F)_{tip}$$

and the humps will show up as bright spots; the emission current measured will originate mainly from the humps. Thus, the evaluation of the work function from a Fowler-Nordheim plot using the voltage/field proportionality factor, B, of the clean emitter tip will result in a lower value than the true work function. However, heating the surface in the absence of ammonia gas could cause the humps to disappear and hence the measured work function to approach the true work function value. If the disappearance of the bright spots and the increase in work function between 700 and 800°K, where η-desorption is negligible, can be taken to indicate the disappearance of the humps on the surface, the work function observed at 750°K, i.e. 5.35 eV, would correspond to the work function of η-species covered surface. On further heating, to a temperature higher than 800°K, the change in work function and emission pattern parallels that observed in Figure 45. This corresponds to the desorption of η-species, possibly the desorption of δ-nitrogen, and the desorption of β-nitrogen.

The initial deposit obtained at 800°K (Figure 51.2)

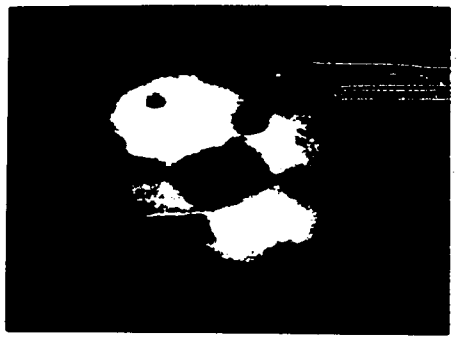

(1) Clean W

$\bar{\phi}_0$ = 4.5 eV

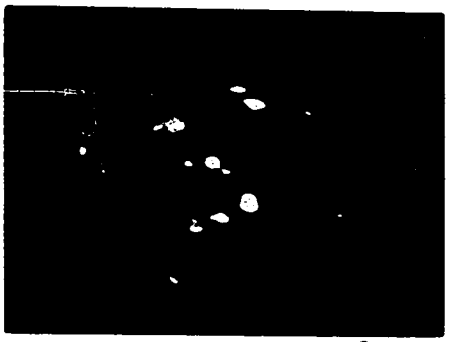

(2) NH_3 dose at 800°K

$\bar{\phi}$ = 4.78 eV

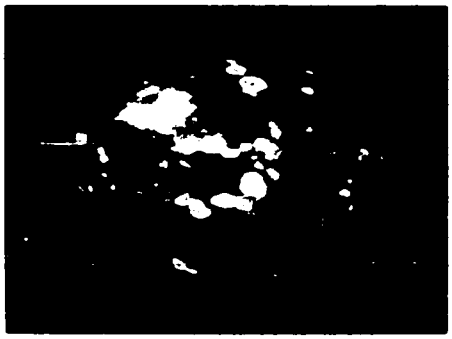

(3) 800°K

4.78 eV

(4) 850°K

5.03 eV

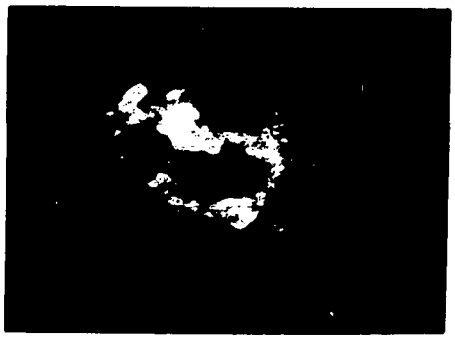

(5) 400°K

4.86 eV

(6) 950°K

4.64 eV

Fig. 51. Field emission patterns obtained for ammonia interaction for 10 torr-sec at 800°K to form the η-species and its subsequent decomposition.

(1) Clean W

$\bar{\chi}$ = 4.5 eV

(2) NH_3 dose at 800°K

$\bar{\chi}$ = 4.78 eV

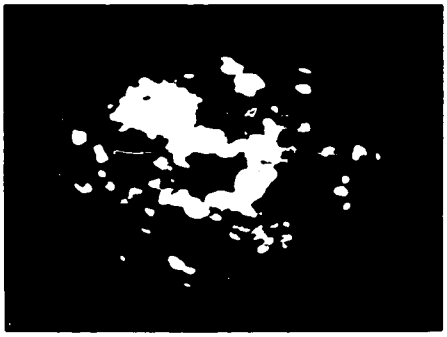

(3) 800°K

4.78 eV

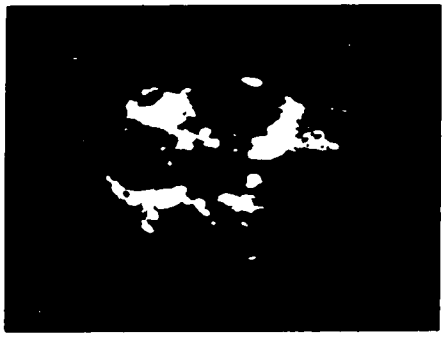

(4) 850°K

5.03 eV

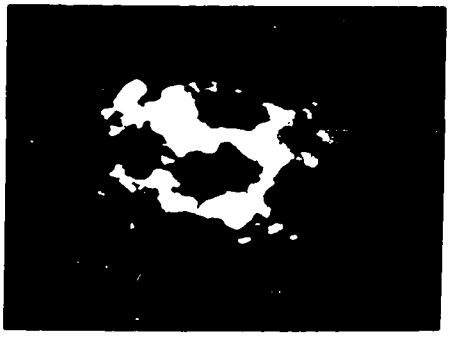

(5) 900°K

4.86 eV

(6) 950°K

4.64 eV

Fig. 51. Field emission patterns obtained for ammonia interaction for 1 torr-sec at 800°K to form the [illegible] and its subsequent decomposition.

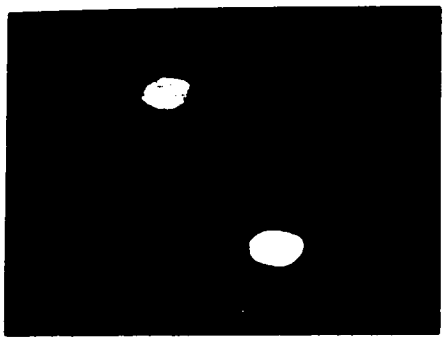

(7) 1100°K
4.36 eV

(8) 1300°K
4.24 eV

(9) 1500 °K
4.48 eV

Figure 51 (continued)

[illegible] $^{\circ}$K

4.3[illegible] eV

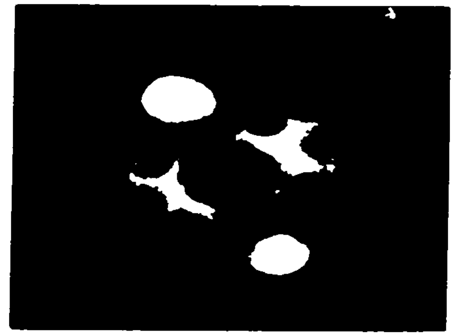

(b) 1300 $^{\circ}$K

4.24 eV

1[illegible] $^{\circ}$K

4.4[illegible] eV

Figure [illegible] (continued)

produces an extraordinarily low apparent work function, 4.78 eV, a small pre-exponential term (Figure 49) and an emission pattern consisting mainly of large bright spots around the {110} planes. These observations again indicate the formation of humps on the surface. Since the humps are the only emitting areas, the reduction in effective emitting area results in a small pre-exponential term. Heating the deposit to 825°K causes the work function and pre-exponential term to increase sharply and to reach the values corresponding to that observed upon heating the initial deposit obtained at 700°K to 825°K (Figure 49). This increase both in work function and pre-exponential term would again correspond to the smoothing out of the surface. A check of the surface coverage by the themal desorption method indicates that the deposit obtained under these dosing conditions corresponds to three monolayers of η-species. The observed extensive surface rearrangement would therefore add strong support to the possible nucleation of bulk species by penetration of nitrogen and hydrogen atoms into the surface. Upon further heating, the changes in work function and emission pattern parallel those observed for interaction at 700°K.

CHAPTER 5

DISCUSSION

The major objectives of this research are to understand the mechanism of ammonia decomposition on tungsten surfaces and to ascertain surface configurations of different species formed during the decomposition. In this section, the relevance of the flash desorption and the field emission results to these topics will be discussed. The experimental results described in this study have been obtained for a polycrystalline tungsten surface, however, it appears possible to rationalize them fairly well in terms of structures and processes on the W{100} plane. On this plane, the surface tungsten atoms are in a square array (Figure 52) with nearest neighbors separated by 3.16 Å and a surface tungsten atom density of 1.0×10^{15} cm^{-2}. The location of adsorption sites is undetermined and sites A, B and C represent three possibilities.

5.1 Mechanism and kinetics of ammonia decomposition.

Based on the present observations it is seen that ammonia decomposition on tungsten surfaces is a complicated process which involves the formation of β-nitrogen, δ-nitrogen and the η-species and the desorption of these species. An extensive surface rearrangement and the penetration of nitrogen and hydrogen atoms into the surface have also been

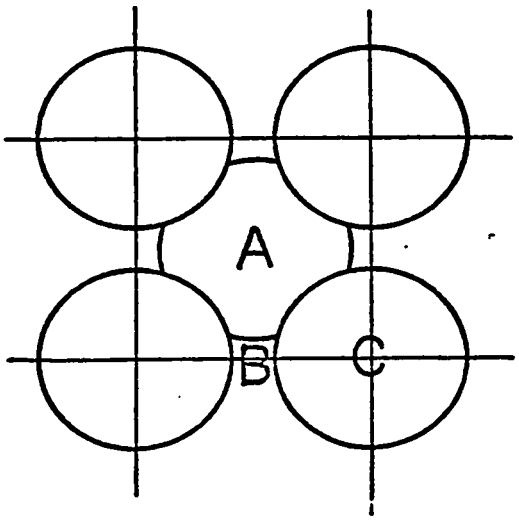

Fig. 52. Tungsten atom arrangement for a {100} plane showing three possible adsorption sites.

observed to occur during the decomposition. In Table V all of these reactions together with their rate parameters are summarized. Before considering the decomposition mechanism, it is necessary to discuss the significance of the rate equations for δ-formation, δ-desorption and η-formation. First, it was realized from Figure 14 that for δ-formation via reaction (2) hydrogen desorption is the only requirement, and since the interaction of ammonia with vacant surface sites proceeds rapidly, the rate of δ-formation is directly governed by the rate of hydrogen desorption from the surface. Since the desorption of hydrogen from such a surface occurs in the same temperature range as the desorption of hydrogen from a surface covered with hydrogen alone, between 300 and 600°K, the activation energy for δ-formation should be of the same order of magnitude as that for hydrogen desorption, ∿ 30 Kcal mole^{-1}.[37] Second, the δ-nitrogen adlayer has identical properties to that of the λ-nitrogen adlayer as will be discussed later. The rate parameters for λ-nitrogen desorption are therefore employed for δ-nitrogen desorption since the latter were not accessible from the present experiments. Finally, the kinetic analysis shown in Appendix B indicates that in the formation of the η-species via reactions (2) and (3), the rate of formation of η-species is equal to

$$\frac{dN(\eta)}{dt} = k_3 \cdot P_{NH_3} \cdot \frac{k_2}{k_3 - k_2} \cdot \left(e^{-k_2 \cdot P_{NH_3} \cdot t} - e^{-k_3 \cdot P_{NH_3} \cdot t} \right) \cdot 10^{15}$$

Table V Reactions and rate parameters for the interaction of ammonia with tungsten

Reactions	Rate equations
Adsorption	
(1) $NH_3(g) + 2W \xrightarrow{fast} W_2N(\beta) + \frac{3}{2} H_2(g)$	
(2) $NH_3(g) + W_2N(\beta) \xrightarrow{fast} 2WN(\delta) + \frac{3}{2} H_2(g)$	(2) $5.10^{-3} \exp(-31,000/RT).n_H^2$ (37)**
(3) $NH_3(g) + 2WN(\delta) \xrightarrow{slow} W_2N_3H(\eta) + H_2(g)$	(3) $3.10^{18} \exp(-12,000/RT).P_{NH_3}$
Desorption	
(4) $W_2N(\beta) \xrightarrow{1450^oK} 2W + \frac{1}{2} N_2(g)$	(4) $1.4 \cdot 10^{-2} \exp(-81,000/RT).n_\beta^2$
(5) $2WN(\delta) \xrightarrow{1100^oK} W_2N(\beta) + \frac{1}{2} N_2(g)$	(5) $10^8 \exp[-(44,700-8,000\theta)/RT].n_\delta$*
(6) $W_2N_3H(\eta) \xrightarrow{970^oK} W_2N(\beta) + N_2(g) + H(g)$	(6) $4.10^7 \exp(-35,000/RT).n_\eta$

n_H, n_β, n_δ and n_η are the surface coverages of hydrogen, β-, δ- and η-nitrogen respectively in molecules cm^{-2}.

* for the convenience of comparing with first order η-desorption, first order rate equation is used.

** Rate equation (2) is that for hydrogen desorption from an adlayer containing hydrogen alone (see page 158)

where k_2 and k_3 are the rate constants for reactions (2) and (3) respectively, and P_{NH_3} is the ammonia pressure. If the rapid δ-formation relative to η-formation, shown in Figure 25, can be taken to indicate $k_2 >> k_3$, the rate of η-formation will be given by

$$\frac{dN(\eta)}{dt} = k_3.10^{15}.P_{NH_3}.e^{-k_3 P_{NH_3}.t}$$

and the initial rate of η-formation can be approximated by

$$\frac{dN(\eta)}{dt} = k_3.10^{15}.P_{NH_3}$$

The rate constant evaluated from the initial sticking probability of the η-species (equation (20)) thus corresponds to $k_3.10^{15}$, i.e.

$$k_3.10^{15} = 3.10^{18} \exp(-12{,}000/RT)$$

and $$k_3 = 3.10^3 \exp(-12{,}000/RT) \text{ sec}^{-1} \text{ torr}^{-1}.$$

The measured activation energy for the η-formation, 12Kcal mole^{-1}, thus corresponds to that required for reaction (3). Though the activation energy for the η-formation is lower than that for the δ-formation, the former proceeds considerably more slowly than the latter as mentioned before. This behaviour is a result of the small pre-exponential term in the η-formation rate constant. This small pre-exponential term is consistent with the observation that the η-formation is a complicated process.

The formation of the δ-nitrogen adlayer, though with an activation energy of ∿30 Kcal mole^{-1}, is thus a fast

process with respect to the η-formation. The η-desorption is a first order process with an activation energy of 35 Kcal $mole^{-1}$ compared with that for δ-desorption of 44.7 Kcal $mole^{-1}$. The desorption of β-nitrogen with an activation energy of 81 Kcal $mole^{-1}$ is too slow to be considered as a step in the decomposition. The decomposition of ammonia can therefore proceed via the following competing pathways:

δ-desorption

$$2WN(\delta) \xrightarrow{1100^{o}K} W_2N(\beta) + \frac{1}{2} N_2(g)$$

or η-desorption

$$W_2N_3H(\eta) \xrightarrow{970^{o}K} W_2N(\beta) + N_2(g) + H(g)$$

The reaction path through which decomposition proceeds will be determined by the species present on the surface during the decomposition. Since δ-formation is faster than η-formation, at first sight it would appear that the surface would always be saturated with δ-nitrogen indicating decomposition via δ-desorption. However, since δ-desorption is slower than η-desorption, there will be a gradual build-up of the η-species via reaction (3), if η-formation is faster than η-desorption. The rate of η-formation depends on the ammonia pressure whereas that for η-desorption does not; thus there will be a transition pressure above which η-formation is faster than η-desorption and below which η-desorption is faster than η-formation. Thus whether δ-nitrogen or the η-species is present on the surface during decomposition will be determined

by the ammonia pressure.

The pressure at which the rate of η-formation is equal to that of η-desorption can be readily estimated. From rate equation (3), Table V, the sticking probability for ammonia in the formation of the η-species at 1000°K is found to be $\sim 10^{-5}$. The rate of formation of η-species in molecules cm^{-2} sec^{-1} at this temperature and under an ammonia pressure of P_{NH_3} is therefore equal to

$$\frac{P}{\sqrt{2\pi mkT}} \times 10^{-5} = 4.9\times10^{15}\times P_{NH_3} \text{ (in torr)}$$

whereas the rate of η-desorption is found from rate equation (6), Table V, to be 1.2×10^{15} molecules cm^{-2} sec^{-1}. Thus at an ammonia pressure of $\sim$0.2 torr the formation and desorption will have equal rates. Based on this it can be concluded that at ammonia pressures >> 0.2 torr, η-formation will be fast enough to maintain an η-species saturated surface and the decomposition will occur via η-desorption, whereas at ammonia pressures << 0.2 torr, the surface will always be saturated with δ-nitrogen indicating the decomposition via δ-desorption. In the intermediate pressure range both η-species and δ-nitrogen will be present on the surface, decomposition will occur via both δ- and η-desorption. Since η-desorption involves the breaking of an N-H bond, a hydrogen isotope effect on the rate will be observed at ammonia pressures >> 0.2 torr. The isotope effect observed by Jungers

and Taylor [6] can be accounted for satisfactorily since their experiment was carried out in the pressure range between 3 and 15 torr. The observation of an isotope effect by Barrer [7] in the pressure range between 6×10^{-3} and 6×10^{-1} torr is also consistent with the present model since in this intermediate pressure range η-formation is significant. However, the observation of an activation energy of 42.4 Kcal $mole^{-1}$ can not be accounted for by this model. Furthermore, regardless of whether decomposition occurs via δ-desorption or η-desorption, as long as the surface is saturated with the intermediate, the rate of decomposition will be independent of gas phase ammonia pressure and zero order kinetics with respect to ammonia pressure will be observed.

The δ-intermediate which is the surface species present during the decomposition at low ammonia pressures is thought to be identical to the λ-state of nitrogen obtained from activated nitrogen adsorption for the following reasons: (1) nitrogen desorption from both states commences at $\sim830^{o}K$ and both states have the same surface stoichimetry, WN, (2) the nitrogen in the β- and δ-states are adsorbed atomically on the same crystal planes [12], the complete isotopic mixing throughout the desorption process (Figure 34) indicates that nitrogen in the β- and λ-states is also adsorbed atomically on the same crystal planes, (3) the formation of λ-nitrogen [15] and δ-nitrogen both raise the work function on the {100} plane. Thus, the use of the λ-nitrogen desorption parameters for

δ-nitrogen desorption can be considered as well justified. The desorption of λ-nitrogen is an interesting process where the surface mobility of the adatoms plays an important role in the desorption mechanism. In the following section the mechanism of λ-desorption will be considered.

5.2 Desorption model for the λ-state of nitrogen.

The present experiments were carried out on a polycrystalline tungsten filament and thus any interpretation made is clouded by the possible effects of surface heterogeneity. However, since the spectra observed for nitrogen adsorption at high coverage (Figure 30) show essentially no structure the situation may not be hopeless; the situation is either exceedingly complex or relatively simple. Presumably the observations refer to only one "type" of adsorption site and one "mechanism" of desorption, with any effect of heterogeneity reflected only in a continuous energy distribution and not different modes of adsorption and different mechanisms for desorption. This is speculative and its validity will be measured by the success of a simple homogeneous model in interpreting the data. For well-annealed tungsten filaments, such as those used in the present experiments, the predominant crystal faces are the {100} and {110} planes.[38] The {110} plane appears to be inert to β-nitrogen adsorption at room temperature and above,[21] whereas the {100} plane readily adsorbs β-nitrogen and has been

extensively investigated by a variety of modern techniques. Consequently the {100} plane (Figure 52) is used as a model for the tungsten surface.

LEED observations [30] show that on the tungsten {100} plane adsorption of nitrogen to saturation of the β-state produces a C(2×2) diffraction pattern. Thus one-half of the sites are occupied and the occupied sites are next-nearest neighbours. The observed saturation surface coverage for β-nitrogen, based on the geometrical area of the filament, is 0.44×10^{15} atoms cm^{-2}, or somewhat less than the 0.5×10^{15} atoms cm^{-2} expected for half-coverage on the {100} plane. The difference could be attributed to the existence of {110} planes inactive to β-nitrogen adsorption. Clearly the tremendous drop in sticking probability for molecular nitrogen on completion of the C(2×2) β-state reflects the requirement for pairs of adjacent vacant sites for the dissociative adsorption of a diatomic gas. Isolated vacant sites surrounded by adatoms, while incapable of adsorbing molecules dissociatively, can adsorb the nitrogen atoms produced by electron impact on the gas. This process produces the λ-state with twice the surface coverage of the β-state, 0.86×10^{15} atoms cm^{-2}.

Thus, before commencing thermal desorption, the model for the λ-state at saturation is one in which every site is occupied by a nitrogen atom and that all adatoms

are identical. In the interpretation of the desorption spectra which follows, the appearance of λ- and β- "states" is attributed entirely to the mechanism of desorption and it is assumed that, prior to desorption, any separation into different binding modes is invalid.

5.2.1 The immobile limit.

Consider the completely immobile limiting case, i.e. the rate of desorption is much faster than the rate of adatom migration. Desorption will occur by combination of adjacent atom pairs and the desorption rate will be first order in the number of adjacent atom pairs,

$$\text{Rate}(\lambda) = \nu_\lambda \exp[-E_\lambda^\ddagger(\theta)/RT] \cdot N_p(\theta) \qquad (25)$$

where the functional dependence of N_p and $E_\lambda^\ddagger$ on the fractional surface coverage, θ, remains to be determined.

The dependence of N_p on θ is relatively easy to determine since the antisymmetrically equivalent case of the number of adjacent pairs of <u>vacant sites</u> in the immobile adsorption of diatomics with dissociation has been treated by J.K. Roberts.[39,40]

Consider a square array of sites, such as the {100} plane of a body centered cubic metal, in which each site has four nearest neighbour sites. If a molecule evaporates from a pair of adjacent sites and if all six sites which are neighbours of this pair of sites are occupied, the number of adjacent atom pairs, N_p, is reduced by 1 + 6. For a

surface containing N_s sites cm^{-2} and θN_s atoms cm^{-2}, when a further molecule, i.e. adjacent atom pair, evaporates then

$$d\theta = -2/N_s$$

and, on average,

$$dN_p(\theta) = -[1 + 6\gamma(\theta)]$$

where $\gamma(\theta)$ represents the average fraction which is occupied of the six sites surrounding the desorbing pair. Thus,

$$\frac{dN_p(\theta)}{d\theta} = \frac{N_s}{2}[1 + 6\gamma(\theta)] = 3.5\, N_s g(\theta)$$

where $$g(\theta) = 1/7(1 + 6\gamma(\theta))$$

and $$N_p = 3.5N_s \int_1^{\theta} g(\theta)\, d\theta + 2N_s \qquad (26)$$

since when $\theta = 1$, $N_p = 2N_s$.

For the antisymmetrical case Roberts had determined $g'(\theta)$ by an empirical method [39]

$$g'(\theta) = 1 - 0.643\theta - 0.25\theta^2 - 0.0876\theta^4$$

and therefore, for the present case we can write directly that

$$g(\theta) = 1 - 0.643(1-\theta) - 0.25(1-\theta)^2 - 0.0876(1-\theta)^4$$

Substitution in equation (26) and integration gives for the variation of N_p with θ,

$$N_p(\theta) = 3.5\, N_s(0.75\theta^2 - 0.25\theta^3 + 0.09\theta^4 - 0.02\theta^5) \quad (27)^*$$

*Equation (27) contains small rounding errors. (see Appendix C)

The success of this empirical relationship has been tested using an array of 100 sites, exactly as described by Roberts,[39,40] and counting the number of adjacent atom-pairs, N_p, as the surface is steadily depleted by desorption pairs of adjacent atoms in a random sequence. The points in Figure 53 show the results of this procedure with the curve plotted according to equation (27). The agreement is exceptionally good down to a coverage of about 0.3 and deviates slightly at lower coverage. The important point to notice is that the number of adjacent pairs drops to zero at a coverage of 0.12; this is because, in the immobile limit, evaporation of atom pairs will leave a number of isolated single atoms on the surface. The contention of the present interpretation of the desorption spectra for λ-nitrogen is that these isolated atoms will represent, in the immobile limit, the amount desorbing as β-nitrogen by bimolecular recombination. Roberts' empirical analysis suggested that the number of isolated sites remaining would be 8%, whereas an analysis based on an array of 10,000 sites by Rossington and Borst [41] suggests a figure of 9.2%. In order to interpret the desorption data in the present investigation it was found that the amount desorbing as β had to be reduced from 0.44×10^{15} atoms cm^{-2} to values varying from 0.08 to 0.20×10^{15} atoms cm^{-2} (Table III and Figure 36). This corresponds to a reduction in the amount desorbing as β from 50% to between 9 and 23%. While the agreement with the predictions of the completely

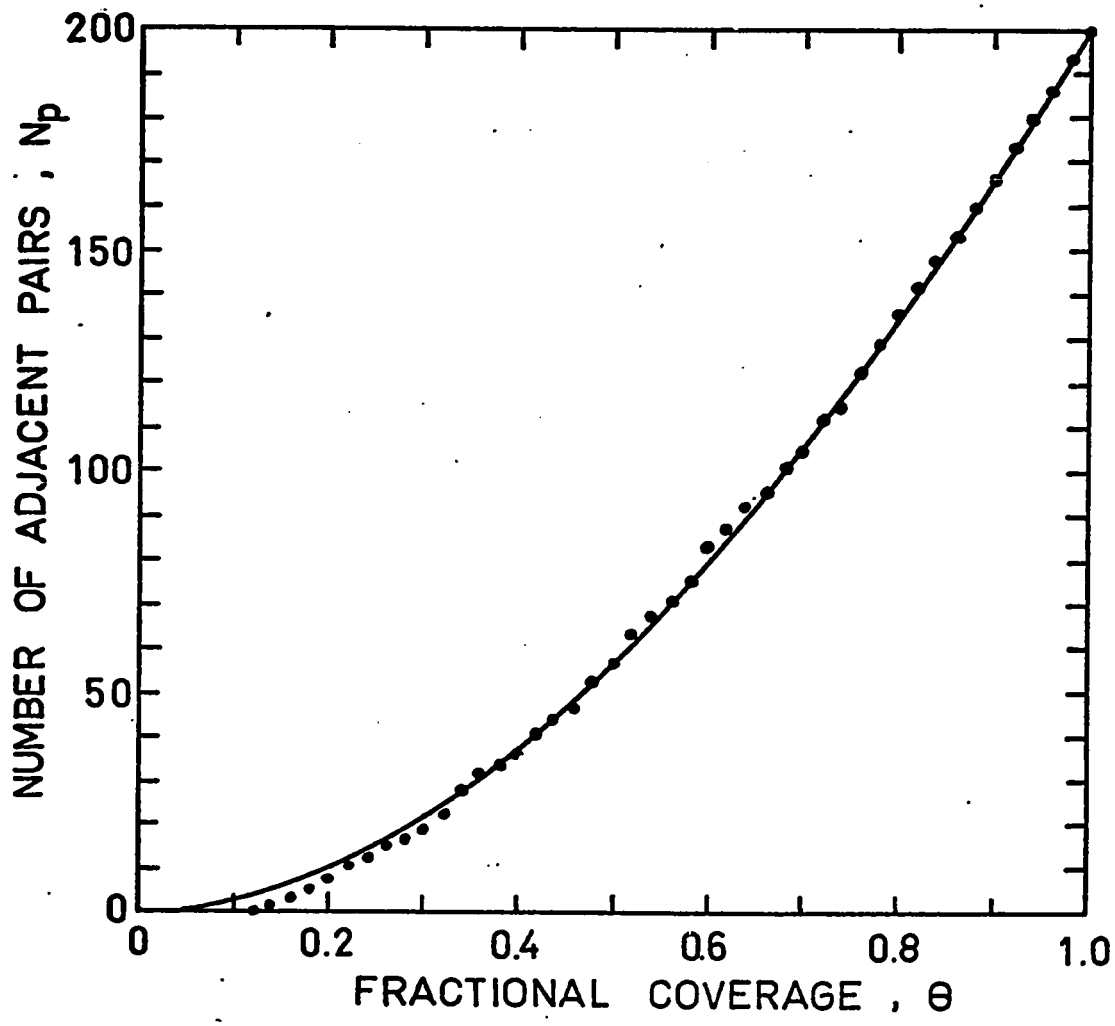

Fig. 53. The variation in the number of adjacent atom-pairs with fractional coverage for a random immobile desorption process. The points are the result of an empirical analysis using an array of 100 sites and the curve is plotted according to equation.

immobile model is reasonable, it is almost certain that some mobility exists, particularly at coverages much below $\theta=0.5$, causing the amount of depletion to be somewhat less than that for the immobile limit, i.e. 9%.

The second question pertains to the variation of activation energy for desorption, $E_\lambda^\ddagger$, on coverage. If we equate the activation energy for desorption with the energy of adsorption and assume a repulsive energy of interaction between adjacent pairs of adatoms, V, (the interaction between next-nearest neighbours being zero) then, on average,

$$E_\lambda^\ddagger(\theta) = E_o^\ddagger - [1 + 6\gamma(\theta)] \cdot V$$

where $E_o^\ddagger$ represents the activation energy for desorption for a non-adjacent pair at zero coverage or

$$E_\lambda^\ddagger(\theta) = E_o^\ddagger - 7g(\theta) \cdot V \qquad (28)$$

Again Roberts' calculations [39] suggest that a linear variation of activation energy with coverage represents a reasonable approximation.

$$E_\lambda^\ddagger(\theta) = E_o^\ddagger - \alpha\theta \qquad (29)$$

This immobile adjacent adatom-pair desorption model was also tested by computer fitting the experimental

desorption data. Using $N_p(\theta)$ defined by equation (27) and $E_\lambda^\ddagger(\theta)$ defined by equation (29) substituted in equation (25), with $E_o^\ddagger$ = 81 Kcal mole^{-1}, the best fit was determined scanning N_β, ν_λ and α. The results are shown in Table III under model (P). Standard deviations are comparable to those for the other models and cannot be used to discriminate between the models. However, the values of N_β, ν_λ and α computed are each worth some comment. First, the amount desorbing as β, N_β, must again be severely depleted to an amount close to that predicted by the model. Second, the pre-exponential, ν_λ, has a magnitude close to that expected for an ideal first order process without appreciable entropy of activation, $\sim 10^{13}$ sec^{-1}. While low first order pre-exponentials are not uncommon their interpretation is not obvious, so the observation of an ideal value is of some interest. Finally, α is rather large, $\sim$ 24 Kcal mole^{-1}. A decrease in the activation energy for desorption (or heat of adsorption) with increasing coverage can be attributed to (a) lateral interactions between the adsorbed particles, i.e. short range dipole-dipole repulsion, [39], (b) changes in the type of binding, [42] (c) changes in the work function of the surface caused by chemisorption [43,44] and (d) heterogeneity of polycrystalline surfaces. It may be tempting to dismiss the observations as a result of heterogeneity, (d), but this is contrary to the tenor of the present interpretation of the experimental observations. The immobile adjacent

adatom-pair model described here implies pairwise lateral interactions, (a), however these are only small in magnitude, contributing maybe 2 Kcal $mole^{-1}$. While such dipole-dipole interactions will make a contribution to α, the model does not exclude other contributions such as (b) or (c). The LEED observation of a (1×1) diffraction pattern for nitrogen at saturation and the complete isotope mixing (Figure 34) indicate that all the nitrogen atoms are in identical binding states and therefore possibly excluding contribution (b), however these binding states need not be identical with the initially occupied β-states at $\theta=0.5$. It is very probable that as the result of lateral interaction, the binding energy of the β-state was lowered upon populating the λ-state and at saturation all the nitrogen adatoms were identically bonded to the surface but with lower binding energy. In thermal desorption from this surface a fraction of the nitrogen adatoms would then desorb with a low activation energy and the rest with a higher activation energy. This "induced heterogeneity" has been speculated to be operative in hydrogen adsorption on tungsten single crystal planes [45,46]. Though the final possibility, (c), explains the observed change in heat of adsorption upon increasing the surface coverage straight-forwardly in several cases [47,48], it is felt that the knowledge of the variation of $\Delta\phi$ with surface coverage and single plane work function measurements upon populating the λ-state of nitrogen is required for estimating

the magnitude of this contribution, (c).

It would be unreasonable to assume that an exact demarcation exists between the immobile desorption of adjacent atom-pairs and the completely mobile bimolecular recombination between the remaining isolated adatoms. More probably the degree of mobility steadily increases as the adatom density decreases. The main claim of this immobile model as approximating the behaviour of the "λ-state" is its ability to interpret the apparent depletion of the "β-state", as evidenced by the desorption spectra in Figure 30, the computer fitting of the fast desorption data, and also the dependence of this depletion on heating rate(Figure 36).

5.2.2 Isotopic mixing.

Complete isotopic mixing throughout the desorption process(Figure 34) can be most easily interpreted as resulting from adsorption with dissociation and complete mobility before desorption. Total translational mobility (two-dimensional gas behaviour) is in contradiction to the proposed model. A solution to this conflict would be to invoke rotational freedom of molecules formed from adjacent atom pairs as a precursor to desorption. Redissociation of such ad-molecules prior to acquiring the necessary activation energy for desorption would lead to complete isotopic scrambling as observed. Again while this mechanism may be appropriate as an interpretation of the behaviour at high coverage, as the coverage decreases the mobility of individual

adatoms will become increasingly important and contribute to the isotopic scrambling.

5.3 Surface configurations of different adlayers.

Thermal desorption and field emission observations provide some information about the surface configurations of the adlayers and the possible changes of the substrate surface during adsorption. In this section the probable surface structure of δ-nitrogen adlayer and η-species will be discussed.

5.3.1 δ-nitrogen adlayer.

Field emission results indicate that the formation of β-nitrogen from ammonia causes the average work function to decrease by 0.25 eV from that of clean surface, 4.5 eV. Since the emitting area is the environs of the {100} planes (Figure 38.2) the work function of a β-nitrogen covered surface on the {100} plane can be considered to be equal to the average work function measured. The presence of β-nitrogen on this plane therefore causes a work function decrease by 0.40 eV from that of clean surface, 4.65 eV [34]. This observation is in good agreement with that measured by Delchar and Ehrlich [21] using a macroscopic method. On this plane the work function is known to decrease linearly with increasing β-nitrogen coverage [49,50], so one would expect a further decrease in the work function upon increasing the nitrogen coverage beyond the saturation coverage of β-nitrogen,

i.e. formation of δ-nitrogen. However, it is surprising to observe that populating the δ-state of nitrogen causes the work function to increase to a value larger than 4.71 eV (Figure 40.7 where $\overline{\phi}$ = 4.71 eV but the {100} plane is not emitting). This irregular behavior of work function change with increasing coverage (Figure 54) has never been observed and there is no unambiguous explanation for this observation. All the possibilities which may contribute to this observation will be discussed in following section.

First, when nitrogen is adsorbed, a covalent bond with partial ionic character is formed between the nitrogen adatom and tungsten. Though nitrogen is more electronegative than tungsten, an excess positive charge is associated with nitrogen adatoms [23]. Thus, one would expect a work function decrease upon populating the β-state of nitrogen on all crystal planes. However this is not always the case; in a study of nitrogen adsorption on tungsten [21], it was observed that nitrogen adsorption raises the work function of the {111} plane whereas it decreases the work function of the {100} plane. This different behaviour of nitrogen adatoms on different crystal planes has been explained as the result of a different location of the nitrogen adatom with respect to the surface of electroneutrality [21]; on the {100} plane, due to its densely packed surface, nitrogen adatoms can only be located above the surface, whereas on the loosely packed {111}

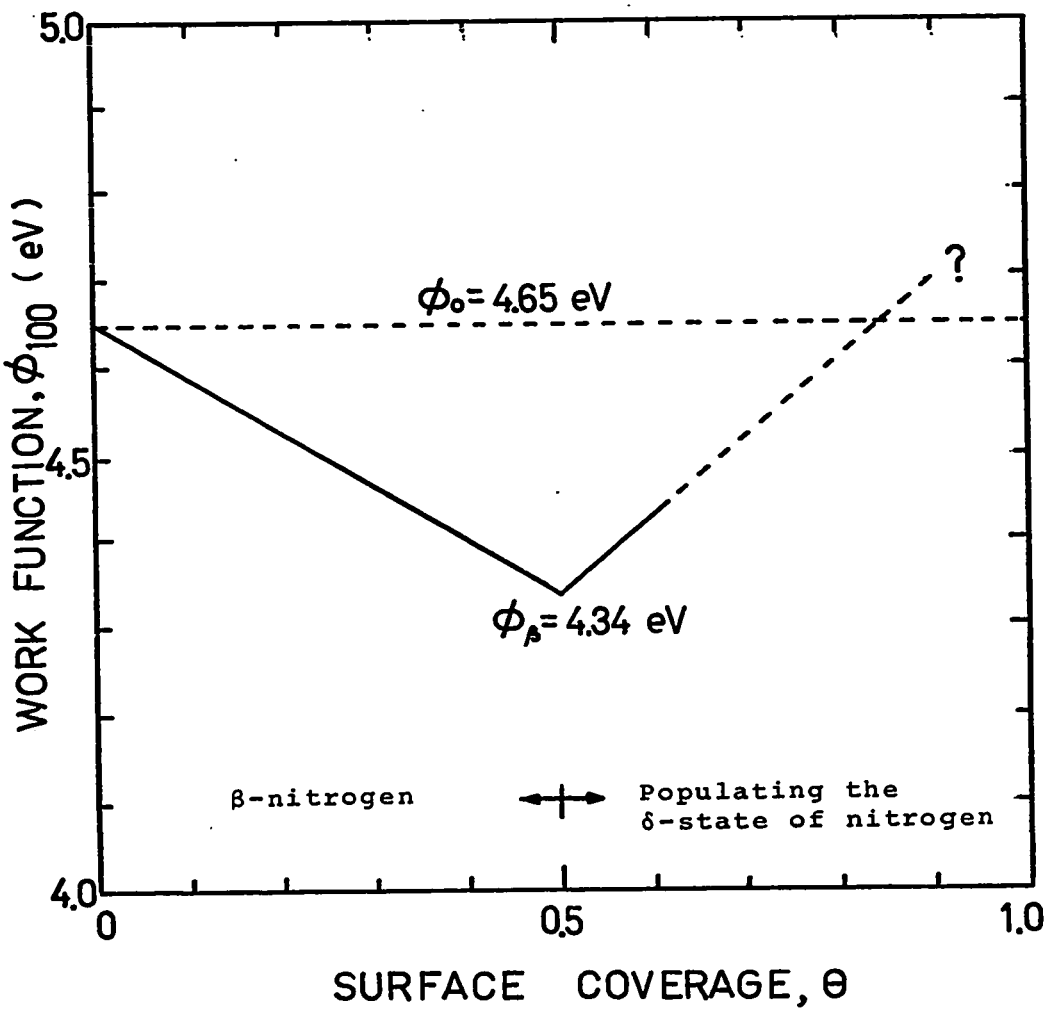

Fig. 54. The variation in work function with surface coverage upon populating the δ-nitrogen on the W{100} plane.

plane they can be located below the surface, as shown in Figure 55 (a) and (b). The effect of this different nitrogen adatom location is the formation of dipole layer with reversed polarity, which nicely explains the observed differences in sign of the work function change. Thus, if nitrogen adatoms in the δ-state would be located below the surface of electroneutrality whereas nitrogen adatoms in the β-state are located above the surface (Figure 55(c)), a reverse in direction of $\Delta\phi$ would be observed upon populating the δ-state. However, this model appears to be unlikely since if it is impossible for the β-nitrogen adatoms to be located below the surface of electroneutrality on this densely packed {100} plane, it is difficult to understand how this can become possible after more and more nitrogen is adsorbed on the surface.

Second, the original model that the nitrogen adatoms are associated with positive charges may not be correct and instead the nitrogen adatoms could be associated with negative charges and located below the surface of electroneutrality in the β-state and above the surface after the population of the δ-state (Figure 55(d) and (e)). In fact, this is the only possible surface configuration which could explain the observed change in sign of $\Delta\phi$ on the {100} plane upon formation of a complete δ-nitrogen adlayer (Figure 54). However, this model can not account for the increase in work function on the {111} plane upon populating the β-state of nitrogen.

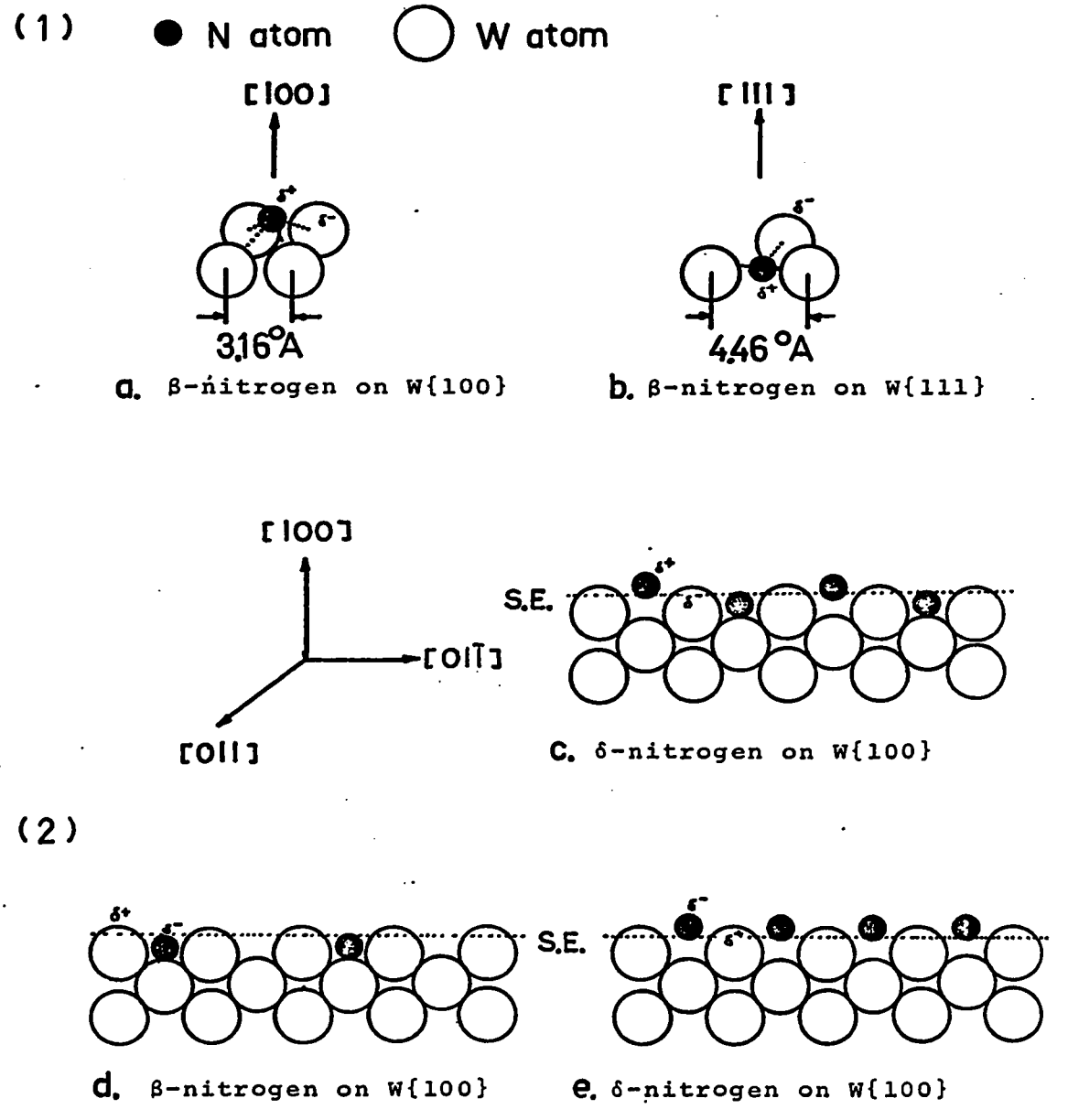

Fig. 55. Schematic diagram for possible δ-nitrogen surface configurations. The nitrogen adatoms are associated with (1) positive charges or (2) negative charges. S.E., Surface of electroneutrality.

Since the {111} plane is more loosely packed than the {100} plane and therefore the nitrogen adatoms should be able to be located under the surface of electroneutrality, a decrease in work function upon populating the β-state, as was observed on the {100} plane, should be observed. This is contrary to the observation that the formation of β-nitrogen adlayer raises the work function on the {111} plane.

Third, in a study of adsorption of potassium on tungsten surfaces using the field emission microscope, Schmidt and Gomer [51] observed irregular work function changes; the work function decreases continuously upon potassium adsorption and reaches a minimum of 1.75 eV at a coverage of about eight-tenths of a monolayer. On further increase in coverage, the work function increases slightly and reaches a value 0.5 eV higher than the minimum value. Based on a depolarization scheme they are able to explain the observed minimum in the work function-coverage plot. Though there is no such interaction between adjacent dipoles in the less densely populated β-nitrogen adlayer [50], it is very likely that dipole-dipole depolarization is operating in the more densely populated δ-nitrogen adlayer. However, its magnitude can not be possibly large enough even to account for the observed reversal in direction of $\Delta\phi$.

Finally, the closely packed nitrogen adatoms can also give rise to a repulsive interaction which would weaken the binding between nitrogen adatoms and tungsten. For the

β-state of nitrogen on the W{100} plane the C(2×2) structure is the most stable one [30], however, the observation of a (1×1) structure upon formation of a δ-nitrogen adlayer [10] does not necessarily indicate that these new binding states of δ-nitrogen are identical with the initially occupied β-states. It is probable that owing to the repulsive interaction changes in location of the adatoms, such as A, B and C sites shown in Figure 52, could take place upon formation of δ-nitrogen adlayer. This would result in a change in the amount of charge transfer, hence in $\Delta\phi$, but it is not possible to estimate its magnitude.

Thus it seems that none of these models could explain the observed change in $\Delta\phi$ satisfactorily; for a further understanding of the δ-nitrogen adlayer single plane work function measurements and measurement of the variation of $\Delta\phi$ with surface coverage are required.

5.3.2 η-species.

Formation of the η-species of overall stoichiometry W_2N_3H from δ-nitrogen, WN, requires incorporation of a further NH group for every pair of surface tungsten atoms; this does not suggest any simple surface structure. For hydrogen atoms there are two alternatives for the bonding situation; they are bonded either to tungsten atoms or to nitrogen atoms. The desorption of hydrogen from a tungsten surface is completed at temperature higher than $650^{o}K$ [9] and the presence of

nitrogen on the surface does not stabilize the hydrogen [24]. Hydrogen thus can not stay on the surface at interaction temperature as high as 700°K. It is not impossible, however, that during the interaction hydrogen atoms penetrated into the surface and were buried under the nitrogen adlayer so that they were hindered from evaporating from the surface. If this is the case, desorption of nitrogen would immediately enable the hydrogen to evaporate from the surface and give rise to the observed simultaneous desorption of hydrogen and nitrogen. However, at temperature lower than 1000°K hydrogen adatoms do not have enough energy to overcome the energy barrier of desorption as atoms, desorption can proceed only via surface recombination as molecules with second order kinetics, which is contrary to the observed hydrogen desorption in an atomic state by first order kinetics (section 4.1.2). The surface structure in which hydrogen atoms are bonded to tungsten atoms is thus not satisfactory.

It is noted that the η-species desorbs with a nitrogen to hydrogen ratio of 2 to 1 to leave a β-nitrogen surface and furthermore the nitrogen desorbs simultaneously with atomic hydrogen by first order kinetics at temperatures below those required for δ-nitrogen desorption. This strongly suggests that η-nitrogen and η-hydrogen originate from the same surface species and that a nitrogen-nitrogen bond is formed in the η-species giving it a stoichiometry WN_2H in which alternate nitrogen atoms in the δ-nitrogen structure

are converted to the η-species. Furthermore, the overcrowded surface with one and half nitrogen adatoms for each tungsten atom, which appears impossible without the N-N bond formation, also suggests the possible formation of the N-N bond.

Such an N-N bonded species need not be oriented perpendicular to the surface. Using Pauling's value of 0.7 Å for the single bond covalent radius of nitrogen [52] it can be shown that such a structure may even allow every nitrogen atom to be in contact with tungsten atoms. Figure 56 shows one possibility in which alternate rows of N atoms and N-N species are superimposed on a W{100} mesh. Such a structure allows stronger interaction with the substrate and also satisfactorily accounts for the saturation stoichiometry W_2N_3H. It has been assumed that the H atoms are bonded to the N-N species in this structure (e.g. N-NH) although it is not impossible for them to exist in imide groups, NH. This latter alternative creates the problem of understanding why α-nitrogen [53] is not accessible to the N-N species, implying desorption at about 400°K. The presence of an N-H bond in the NNH species restricts the accumulation of electron density between the nitrogen atoms and α-nitrogen may only be accessible after N-H bond breaking.

The field emission observations further complicate this picture. The observed emission pattern with small bright spots superimposed on the main pattern (Figure 50.2), the

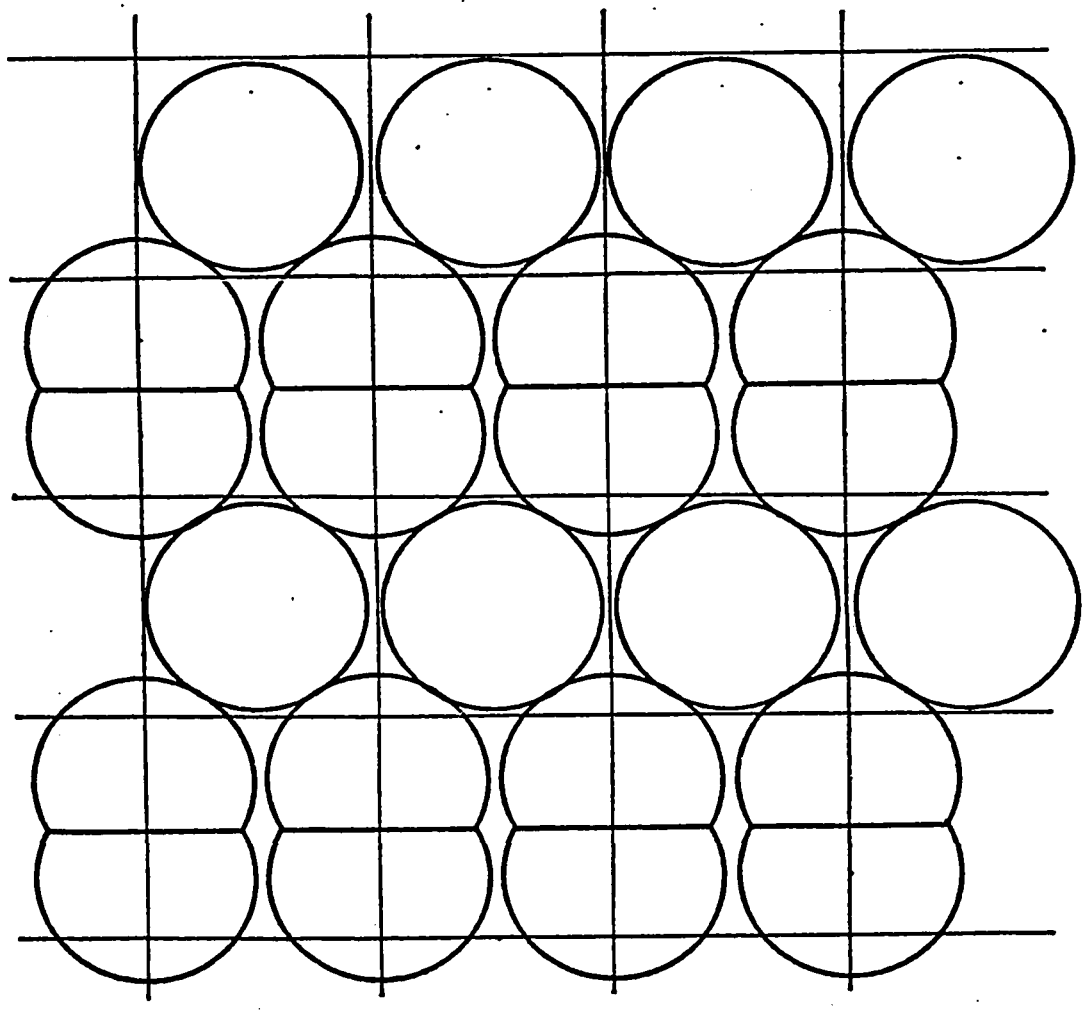

Fig. 56. A possible nitrogen arrangement for the η-species on a W{100} plane which would allow each nitrogen atom to be bonded to tungsten.

irregular work function change with increasing surface coverage, and the small pre-exponential term in the formation of η-species, all indicate the possible occurrence of surface rearrangement. In the study of self-diffusion of tungsten by field ion microscopy Ehrlich and Hudda [35] showed that surface tungsten atoms become mobile at temperature higher than 350°K. Thus this observation adds some support for such surface rearrangement. Furthermore the η-formation curves shown in Figure 25 do not saturate but η-formation is followed by an even slower reaction. This reaction probably corresponds to the formation of bulk species. The formation of interstitial tungsten "nitrides" requires an expansion of the tungsten lattice and therefore the η-species probably forms with rearrangement of the tungsten substrate. It is interesting that bulk "nitrides" of tungsten have only been formed by reaction with ammonia and not nitrogen; the η-species not only represents a surface intermediate in the decomposition of ammonia but also in the formation of bulk compounds.

In the studies of interaction of oxygen with tungsten by LEED, Tracy and Blakely [54] observed that repeated dosing of oxygen on the {100}, {111} and {112} planes at pressure between 10^{-8} and 10^{-6} torr and 300°K with intermittent heating to 750°K in vacuum for 5 sec transforms these planes to a surface with {110} facets and final work functions which are identical to that of the oxygen covered {110} plane. Based on the observed emission patterns and work function

changes, it is very likely that during the formation of η-species the surface underwent similar changes so that the rearranged surface would have similar surface structure on most of the planes giving rise to the observed patterns with uniform emission properties.

The appearance of bright-spots in the emission pattern (Figure 50.2) is undoubtedly the result of the formation of humps on the surface. Such humps have smaller radii than that of the main emitter and since the magnification is inversely proportional to the radius the resultant local magnification will exceed that of the main emitter. The small radius of the humps also causes local field enhancement and increased emission, the humps will thus show up as bright spots in the main pattern. The appearance of these bright spots at the periphery of the {110}, {111} and {100} planes may be the result of a lower binding energy of the surface atoms at the edge than in the centre of the plane, i.e. the energy required for the displacement of an atom is lower at the edges.

The observation of a pattern similar to that of δ-nitrogen (Figure 45.6) and a corresponding work function change in the sequence of η-desorption may indicate that the η-species desorbs to leave a δ-nitrogen adlayer instead of a β-nitrogen adlayer as deduced from the thermal desorption experiments. However, the lack of emission from the {100} plane does not necessarily indicate the absence of the

η-species on this plane. Without single plane work function measurement, it is not possible to draw any definite conclusion from this observation.

5.4 Interpretation of earlier experimental results based on the present understanding of ammonia decomposition.

The mechanisms proposed in earlier studies [1-4] are based almost entirely on the kinetic results, they are highly speculative and are inadequate as a description of the decomposition process at temperatures of catalytic interest. However, the present observations indicate that the results obtained by Frankenburger and Hodler [5] do indeed correctly represent the ammonia interaction with tungsten at temperatures lower than 500°K, if not at higher temperature. Thermal desorption and field emission results (Figure 12 and section 4.3.1(b)) indicate that ammonia dissociates on the surface at temperatures higher than 285°K to produce a β-nitrogen adlayer and as the nitrogen surface concentration increases so will the stability of the adsorbed NH_x intermediate. This observation is in full agreement with their observation; the formation of a surface nitride (β-nitrogen) pre-dominates on a clean surface and imide is formed to a lesser extent only at higher coverages with the concurrent adsorption of increasing amounts of undissociated ammonia. The inadequacy of their reaction scheme in interpreting the decomposition is clearly the result of the attempt to employ this low temperature result in explaining the decomposition

proceeding at much higher temperature.

It has been correctly pointed out [9] that the observation of Tamaru [8] that the rate of nitrogen desorption is equal to the rate of nitrogen production from ammonia decomposition is a misinterpretation of the experimental results. At the temperature at which the experiment was carried out η-formation is considerable; the nitrogen desorption rate measured after removing the remaining ammonia and decomposition products was therefore that of nitrogen produced by η-desorption and not that of nitrogen adsorbed from the gas phase. Though the apparent absence of any hydrogen containing species on the surface at 873°K is not understandable, the observation that nitrogen is produced in the ambient at temperatures higher than 773°K can be easily explained since η-desorption commenced at 780°K.

In more recent studies, experiments have been carried out in ultra-high vacuum systems and on clean sample surfaces, so one would expect better agreement with the present observations. However, the proposed mechanisms involving desorption of surface species such as NNH_2 [9], NH_2 [10,11] or x-nitrogen [12] as the rate limiting step obviously do not, or at best only partly, agree with the observation that η-desorption is the rate limiting step at high reactant pressure. The question why such different observations were obtained though those experiments were all carried out in clean systems and low ammonia pressures thus remains to be answered.

The interpretation of earlier field emission results by Dawson and Hansen [9] for ammonia interaction at 200°K agrees exactly with the present observations. However, the work function versus temperature plots obtained at 300, 400, and 500°K would appear to be misinterpreted as arising from the formation of species such as $W_2NN^+H_3$ and W_2NNH_2. Under the condition where those species were formed the present observations indicate that only δ-nitrogen could have been formed on the surface. Moreover, the work function versus temperature plot obtained from δ-nitrogen adlayer (curve b) is almost identical to that obtained from W_2NNH_2 adlayer (curve a) as shown in Figure 57. Though the slightly higher work function shown in curve (a) may indicate the possible formation of the η-species, it is believed that η-formation, if any, was negligible under the conditions employed in that experiment. Thus it is certain that the species observed by them were $WN.WNH_x$ and δ-nitrogen rather than W_2NNH_x. The slight disagreement in temperature scale between these two curves appears to be the result of different heating period; in curve (a) each work function was measured after heating the field emitter tip at the temperature indicated for 30 seconds whereas in curve (b) the tip was heated at the temperature indicated for only 10 seconds. Since different heating periods will give rise to different surface concentrations, the work function measured will not

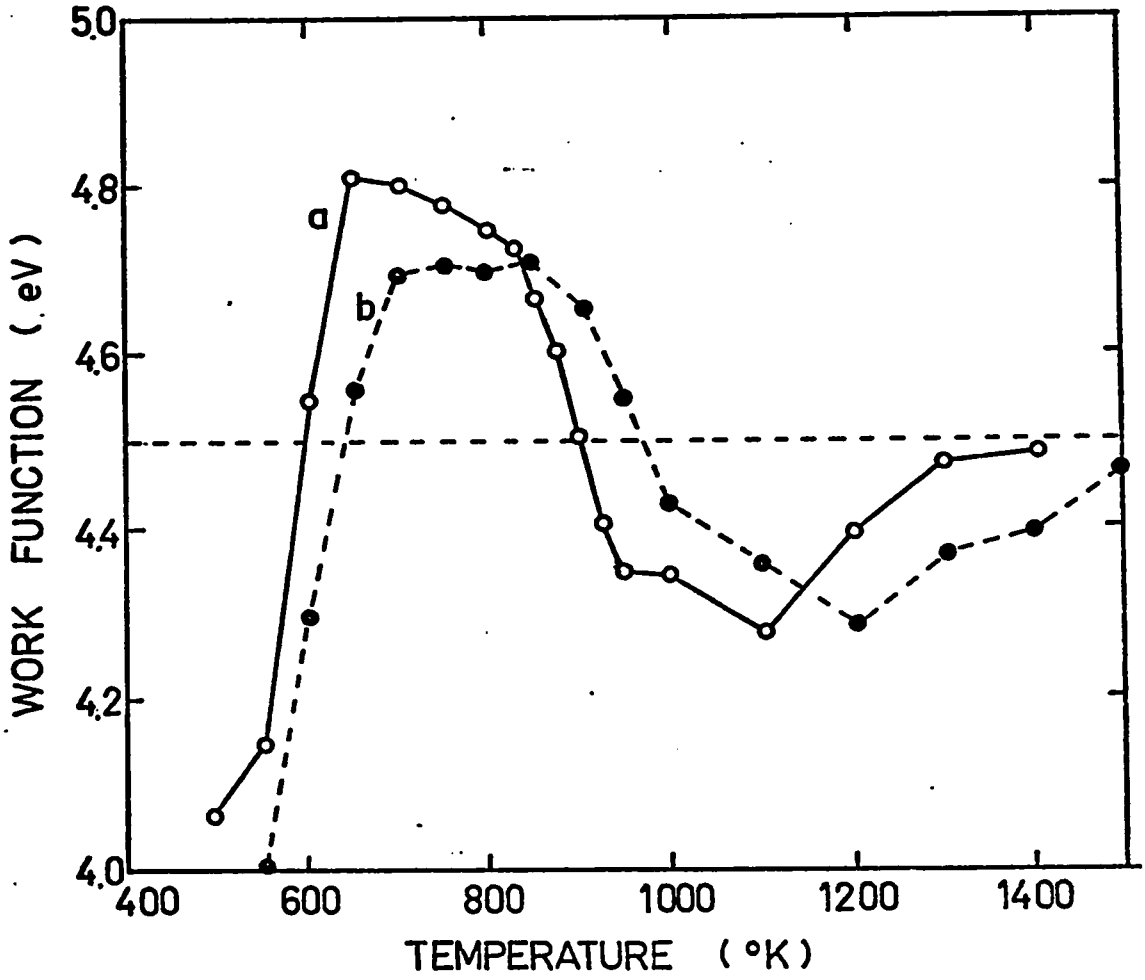

Fig. 57. Comparison of work function versus temperature plot obtained for $W_2NNH_2^{(s)}$, curve (a), with that obtained for the δ-nitrogen, curve (b).

be the same for both cases. In Figure 58 where the surface adlayer was obtained in both cases under the same dosing conditions, hence they are identical before the heating sequence was commenced, the effect of different heating periods on the measured work function is clearly illustrated.

In the thermal desorption/LEED studies by Estrup and Anderson [10] and May et al [11], the conclusion that NH_2 is the only species present on the surface during the decomposition and desorption of this species is the rate limiting step was drawn from thermal desorption results. Since these experiments were carried out with a continuous background pressure of ammonia gas and the decomposition of ammonia on the hot sample filament during the desorption interval was unavoidable, the reliability of these results has been questioned [14]. In the present experiments, if desorption was carried out with residual ammonia gas, in addition to the η-hydrogen peak a higher temperature hydrogen peak has always been observed (Figure 16) in the same temperature range as that observed in the thermal desorption/LEED experiments, namely at 1200 - 1300^{o}K. The peak occurs when the pumping of hydrogen by the hot filament at temperature higher than 1100^{o}K exceeds the rate of hydrogen production by ammonia decomposition. The high temperature hydrogen peak observed in the thermal desorption/LEED experiments would therefore appear to be spurious and the species present on the surface

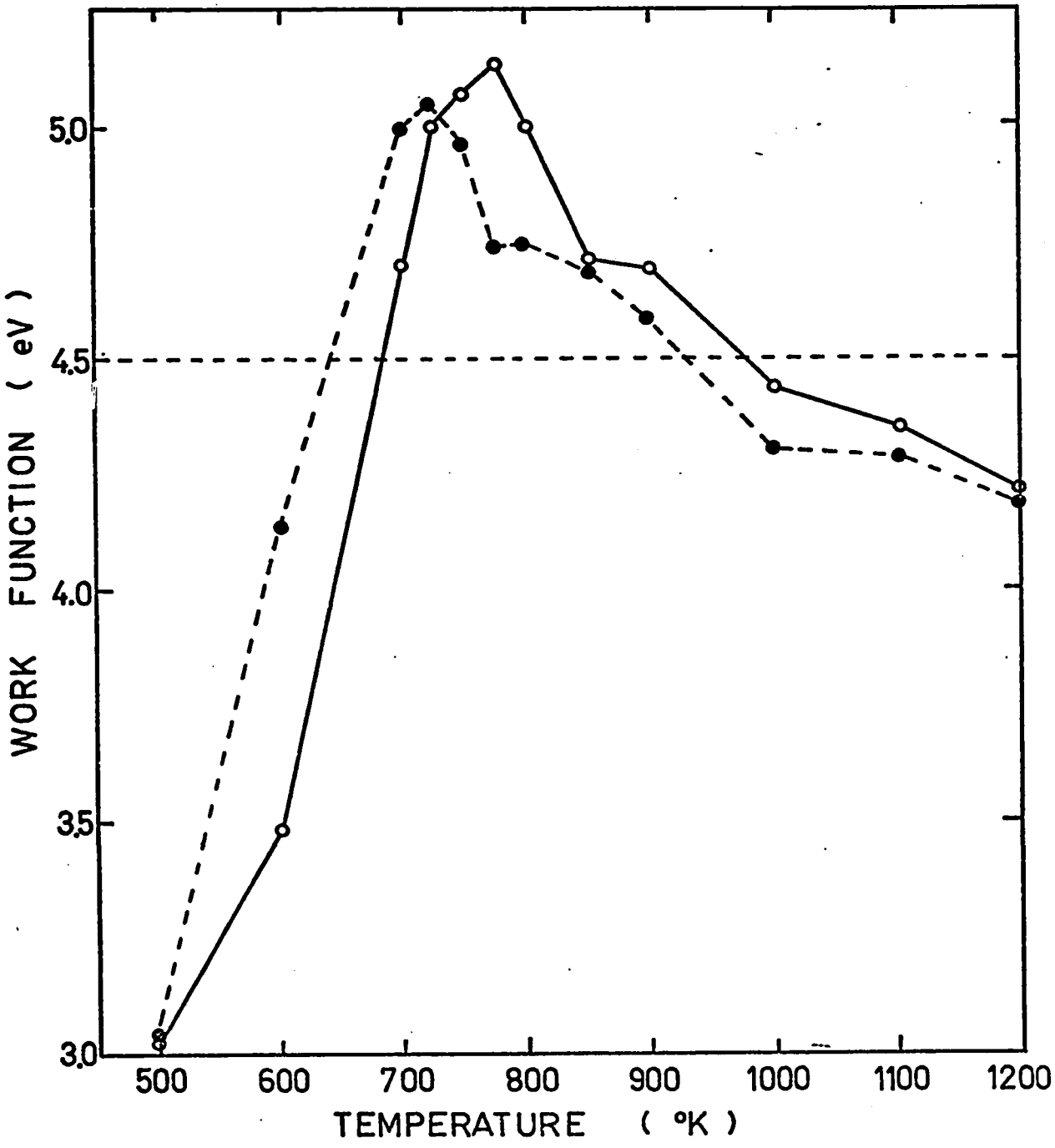

Fig. 58. Effect of different heating periods on the work function versus temperature plot. The emitters dosed under the same dosing conditions were held at the temperatures indicated for 5 seconds (open circles) and 30 seconds (filled circles).

was in fact δ-nitrogen and not NH_2 as claimed. The elimination of their hydrogen desorption observation puts most of their thermal desorption observations in agreement with the present observations for δ-desorption.

The thermal desorption results of Matsushita and Hansen [12] are in good agreement with the present observations as far as δ-nitrogen (their x-nitrogen) is concerned. However, owing to the low sticking probability for ammonia in the formation of η-species, even at 700°K, the η-formation is too slow to be detectable at room temperature and under the ammonia pressure of $\sim 10^{-8}$ torr employed in their experiments.

Present studies thus provide reasonable alternative interpretations for most of the earlier studies. The kinetic parameters for the η-desorption reaction, which is the rate limiting step at ammonia pressure >> 0.2 torr, are also in good agreement with those obtained in earlier studies as shown in Table VI, where the pre-exponential term, A, has the dimension of molecules cm^{-2} sec^{-1}. A similar comparison has been made by Matsushita and Hansen [12]. However, since their comparison was based on δ-nitrogen desorption as the rate limiting step, the agreement is not as good as that shown in Table VI.

Table VI Rates of decomposition of ammonia on tungsten

Initial ammonia pressure (torr)	Temp. at which studies were carried out (^{o}K)	Activation energy, $E^{\ddagger}$ (Kcal $mole^{-1}$)	log(Frequency factor) (Molecules $cm^{-2} sec^{-1}$)	Investigators
100-200	900-110	38.7	25.0[a]	Hinshelwood and Burk (1)
20-265	1000-1250	35.0	24.1[b]	Kunsman (3)
37	950-1150	31.1	23.1	Hailes (4)
150-350	950	35.0	25.3[a]	Jungers and Taylor (6)
$6x10^{-3}$-0.6	950-1150	42.4	24.9	Barrer (7)
7-240	548-873	48.5	23.5	Tamaru (8)
-10^{-8}	300	47.8	24.4	Matsushita & Hansen (12)
10^{-7}-10^{-2}	200-800	35.0	22.4[c]	this work
	300	44.7-80	22.7[d]	this work

(a) Assumed total surface area 1 cm^2

(b) Assumed total value 1000 ml

(c) Kinetic parameters for η-desorption

(d) Kinetic parameters for δ-desorption

CHAPTER 6

SUMMARY

Interaction of ammonia gas, at pressures between 10^{-7} and 10^{-2} torr, with tungsten surfaces, at temperatures between 200 and 800°K, has been investigated by thermal desorption mass spectrometry and field emission microscopy. Several procedures have been adopted to overcome the problems caused by the persistence of ammonia gas in ultra-high vacuum systems.

Ammonia adsorption at 200°K produces a deposit of undissociated ammonia with a surface coverage of only one half monolayer. The desorption spectrum obtained from this deposit is characterized by a low temperature hydrogen peak commencing at 285°K with peak maximum at 450°K, and a high temperature β-nitrogen peak, commencing at 1150°K with peak maximum at 1450°K. On interaction at 300°K ammonia undergoes partial decomposition and about half of the hydrogen produced desorbs leaving one half monolayer of nitrogen and ∿1.6 hydrogen atoms per each nitrogen adatom on the surface. The dissociation intermediates, NH_x, are expected to be present on the surface and the stability of these intermediates increases with increasing nitrogen surface concentration.

Repeated dosing at 300°K with intermittent heating to 800°K or interaction at temperature higher than 300°K

for an exposure less than 10^{-4} torr-sec produces a densely populated nitrogen adlayer designated as the δ-state of nitrogen. At saturation a complete δ-nitrogen adlayer with surface stoichiometry WN is formed and the surface no longer interacts with ammonia at temperature lower than 500°K. The desorption of the δ-state of nitrogen occurs at a temperature lower than that required for the desorption of the β-state of nitrogen, W_2N. Work function measurements and observed emission patterns indicate that on the {100} plane the population of δ-state of nitrogen leads to an increase of work function from that of β-nitrogen covered surface and ultimately to a change in the direction of $\Delta\phi$, whereas on the {111} plane no such change was observed.

In addition to the successive formation of the β- and δ-states of nitrogen, ammonia interaction at 500°K under an exposure higher than 5×10^{-2} torr-sec produces a small but detectable amount of a hydrogen containing species designated as the η-species. At 700°K, the initial sticking probability for the formation of this species is $\sim10^{-6}$ and a monolayer of the η-species is formed under an exposure of ∿1 torr-sec. During the η-formation the hydrogen and nitrogen surface coverages increase at an equal rate and at saturation η-species has a surface stoichiometry W_2N_3H. The η-species desorbs with a nitrogen to hydrogen ratio of 2 to 1 to leave a β-nitrogen adlayer. The desorption spectra are characterized by exactly concurred hydrogen

and nitrogen desorption which occur by first order kinetics with peak maxima at 935 and 930°K, respectively. Characteristic behavior of the η-hydrogen peak and direct observations indicate that this hydrogen desorbs as atoms. The formation of the η-species causes the average work function to increase by ∿0.68 eV from that of the clean surface. The observed emission patterns, work function measurements and the pre-exponential terms suggest that during the formation of the η-species the surface undergoes extensive surface rearrangement.

The densely populated nitrogen adlayer obtained from ammonia interaction can also be generated by the adsorption of activated nitrogen gas. The nitrogen adlayer obtained in this manner designated as the λ-state of nitrogen is thought to be identical to the δ-state of nitrogen obtained from ammonia adsorption based on several observations. The λ-state of nitrogen is thermodynamically stable with respect to gas phase nitrogen. Both λ- and β-states of nitrogen are adsorbed atomically on the same crystal planes. The kinetic studies of λ-desorption indicate that the so-called λ- and β-states actually represent different desorption mechanisms rather than different adsorption states. The evidence for the depletion of the β-state by population of the λ-state suggests that the λ-desorption mechanism is an immobile adjacent atom-pair desorption in contrast to the mobile bimolecular recombination β-mechanism. The variation in

adatom translational mobility with adatom density plays an important role in the desorption mechanism.

All these results indicate that ammonia decomposition on tungsten surfaces is a complicated process involving the formation of β-nitrogen (W_2N), δ-nitrogen (WN) and the η-species (W_2N_3H) and the desorption of these species. Quantitative kinetic measurements of these processes indicate that decomposition of ammonia can proceed via two competing pathways ; δ-desorption or η-desorption. The comparison of the rate parameters for these two processes suggests that at ammonia pressure >>0.2 torr decomposition will occur via η-desorption and a hydrogen isotope effect on rate will be observed, whereas at ammonia pressure <<0.2 torr decomposition will proceed via δ-desorption.

This study provides a new understanding for the decomposition of ammonia on tungsten surfaces and offers more reasonable interpretations for most of the earlier observations and an explanation for the failure of the earlier studies in providing a correct mechanism for this reaction.

CHAPTER 7

SUGGESTIONS FOR FUTURE RESEARCH

The proposed mechanism for the ammonia decomposition on tungsten surfaces indicates that at ammonia pressure much lower than 0.2 torr decomposition will occur via δ-desorption; the hydrogen isotope effect on the rate would thus not be observed at low ammonia pressures. The confirmation of this prediction will add strong support to the proposed mechanism, and therefore it is desirable to compare the rates of decomposition of ammonia and deutero-ammonia in the pressure range between 10^{-3} and 1 torr.

The properties of the adlayer of the δ-state of nitrogen were deduced only qualitatively from the average work function measured in this work. For further understanding single plane work function measurements, especially the variation in the work function with nitrogen surface coverage, are required.

The analysis of the desorption kinetics of the λ-state of nitrogen carried out in this work was complicated by the presence of different crystal planes such as the {100}, {111} and {110} planes on the sample surfaces. Since these planes are known to behave differently upon nitrogen adsorption from nitrogen gas at $300^{o}K$, it would be desirable to carry out this experiment by employing single crystal planes

for unambiguous measurements.

It is also worthwhile to study the relative activity for the formation and the stability of the η-adlayer on different planes by employing single crystal planes as sample.

APPENDICES

A. The fraction of η-hydrogen detected as mass 1 in the line of sight experiment.

Assuming that all the η-hydrogen desorbs as atoms and only the hydrogen which can enter the ionization chamber of the mass spectrometer directly will be detected as mass 1, the mass 2 to mass 1 ratio of the η-hydrogen peak can be estimated as follows.

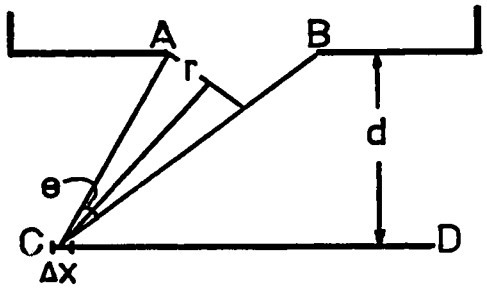

Figure A-1. Position of the sample filament

If the diameter of the ionization chamber opening is equal to AB, the length of the tungsten filament equal to CD and the distance between the ionization chamber and the filament equal to d, it can be seen that the angle θ as shown in Figure A-1 is equal to

$$\theta = \cos^{-1} \frac{AC^2 + BC^2 - AB^2}{2 \cdot AC \cdot BC}$$

The fraction F of the η-hydrogen which desorbs from the segment Δx and can enter the ionization chamber directly

can thus be set approximately equal to

$$F = \frac{\pi r^2}{4\pi \cdot AC^2}$$

Since $r = AC \cdot \sin\frac{\theta}{2}$

F is equal to $F = \frac{1}{4} \sin^2 \frac{\theta}{2}$

and the average fraction, $\overline{F}$, of η-hydrogen which desorbs from the entire filament and can enter the ionization chamber directly is thus equal to

$$\overline{F} = \frac{\sum_i F_i \Delta x_i}{\sum_i \Delta x_i}$$

The average fraction, $\overline{F}$, has been evaluated by dividing the filament into 100 segments of equal length, and calculating the F_i individually. For an ionization chamber opening with a diameter of 0.4 cm, the filament 1.2 cm in length, and the distance between the filament and the ionization chamber as 0.5 cm, the fraction of hydrogen which can enter the ionization chamber without colliding with the wall is found to be 0.021, which corresponds to a mass 2 to mass 1 ratio of ∿32.5.

B. Kinetic analysis of the η-formation.

In order to simplify the analysis, the η-formation is

assumed to proceed via

$$NH_3(g) + W \xrightarrow{k_2} WN(\delta) + 3/2\ H_2(g)$$

$$NH_3(g) + 2WN(\delta) \xrightarrow{k_3} W_2N_3H(\eta) + H_2(g)$$

Since NH_3 is in large excess, these reactions can be considered as two successive first order reactions. Let θ_δ and θ_η be the surface coverages of δ-nitrogen and η-species in fractions of a monolayer respectively, the set of differential rate equations which describes these reactions is thus

$$\frac{d(1-\theta_\delta-\theta_\eta)}{dt} = -k_2 \cdot P_{NH_3} \cdot (1-\theta_\delta-\theta_\eta) \qquad (1)$$

$$\frac{d\theta_\delta}{dt} = k_2 \cdot P_{NH_3} (1-\theta_\delta-\theta_\eta) - k_3 \cdot P_{NH_3} \cdot \theta_\delta \qquad (2)$$

$$\frac{d\theta_\eta}{dt} = k_3 \cdot P_{NH_3} \cdot \theta_\delta \qquad (3)$$

Integration of equation (1) gives for $(1-\theta_\delta-\theta_\eta)$

$$(1-\theta_\delta-\theta_\eta) = e^{-k_2 \cdot P_{NH_3} \cdot t} \qquad (4)$$

Substituting this result into equation (2) gives

$$\frac{d\theta_\delta}{dt} = k_2 \cdot P_{NH_3} \cdot e^{-k_2 \cdot P_{NH_3} \cdot t} - k_3 \cdot P_{NH_3} \cdot \theta_\delta \qquad (5)$$

This differential equation integrates to

$$\theta_\delta = \left(\frac{k_2}{k_3-k_2}\right) \cdot \left(e^{-k_2 \cdot P_{NH_3} \cdot t} - e^{-k_3 \cdot P_{NH_3} \cdot t}\right) \qquad (6)$$

The rate of η-formation is thus given by substituting (6) into (3), i.e.

$$\frac{d\theta_\eta}{dt} = k_3 \cdot P_{NH_3} \cdot \left(\frac{k_2}{k_3 - k_2}\right) \cdot \left(e^{-k_2 \cdot P_{NH_3} \cdot t} - e^{-k_3 \cdot P_{NH_3} \cdot t}\right)$$

C. The origin of the small rounding errors in equation (27).

Substitution of $g(\theta)$ in equation (26) and integration gives for the variation of Np with θ,

$$Np(\theta) = 3.5Ns(-0.0059 + 0.0194\theta + 0.747\theta^2 - 0.259\theta^3 + 0.0876\theta^4 - 0.0175\theta^5)$$

This function, $Np(\theta)$, satisfies the boundary conditions (a) $Np(\theta) = 2Ns$; $\theta=1$ and (b) $Np(\theta) = 0$; $\theta=0.08$. The second condition implies that the number of adjacent atom-pairs reduces to 0 at $\theta=0.08$ as the surface is steadily depleted by desorption of pairs of adjacent atoms in a random sequence.

Equation (27), which is obtained by neglecting the small contribution of the first and second terms in the barcket of $Np(\theta)$ function, thus no longer satisfies these boundary conditions; as $\theta=1$, $Np(\theta) = 1.95Ns$ and as $\theta=0.08$, $Np(\theta) = 0.016Ns$. However, these deviations are rather small and the agreement between the Np versus θ curve plotted according to equation (27) and the result of an empirical analysis shown in Figure 53 indicates that, except at low coverage, equation (27) is a very good approximation.

REFERENCES

1. Hinshelwood, C. N. and R. E. Burk — J. Chem. Soc. London 127, 1105 (1925).
2. Schwab, G. M. — Z. Physik. Chem. 128, 161 (1927).
3. Kunsman, C. H. — J. Am. Chem. Soc. 50, 2100 (1928).
4. Hailes, H. R. — Trans. Faraday Soc. 27, 601 (1931).
5. Frankenburger, W. and A. Hodler — Trans, Faraday Soc. 28, 229 (1932).
6. Jungers, J. C. and H. S. Taylor — J. Am. Chem. Soc. 57, 679 (1935).
7. Barrer, R. M. — Trans. Faraday Soc. 32, 490 (1936).
8. Tamaru, K. — Trans. Faraday Soc. 57, 1410 (1961).
9. Dawson, P. T. and R. S. Hansen, — J. Chem. Phys. 48, 623 (1968).
10. Estrup, P. J. and J. Anderson — J. Chem. Phys. 49, 523 (1968).
11. May, J. W., R. J. Szostak and L. H. Germer — Surface Sci. 15, 37 (1969).
12. Matsushita, K. and R. S. Hansen — J. Chem. Phys. 52, 4877 (1970).

13. Dawson, P. T. and R. S. Hansen — J. Chem. Phys. 45, 3148 (1966).
14. Matsushita, K. and R. S. Hansen — J. Chem. Phys. 51, 472 (1969).
15. Matsushita, K. and R. S. Hansen — J. Chem. Phys. 52, 3619 (1970).
16. Redhead, P. A. — Vacuum 12, 203 (1962).
17. Ehrlich, G. — Adv. in Catalysis 14, 255 (1963).
18. Gomer, R. — "Field Emission and Field Ionization" Harvard Univ. Press, Cambridge, Massachusetts (1961).
19. Herring, C. and M. H. Nichols — Revs. Modern Phys. 21, 185 (1949).
20. Smoluchowski, R. — Phys. Rev. 60, 661 (1941).
21. Delchar, T. A. and G. Ehrlich — J. Chem. Phys. 42, 2686 (1965).
22. Zimmerman D. and R. Gomer — Rev. Sci. Instr. 35, 1046 (1965).
23. Ehrlich, G. and F.G. Hudda — J. Chem. Phys. 35, 1421 (1961).
24. Yates, J. T. Jr. and T. E. Madey — J. Vac. Sci. Tech. 8, 63 (1971).
25. Hickmott, T. W. — J. Appl. Phys. 31, 128 (1960).

26. Miyahara, K., A. Ozaki and T. Kimura — J. Res. Inst. Catalysis Hokkaido Univ. 11, 124 (1963).

27. Rowland, D. G. — "Measurement of Specific Heats of Metals and Alloys at High Temperatures" Ph.D. Thesis, Iowa State Univ. (1957).

28. Yates, J. T. Jr. and T. E. Madey — "The Structure and Chemistry of Solid Surfaces" Ed. G. Somorjai (J. Wiley, New York, 1969) p.59.

29. Ehrlich, G. — J. Chem. Phys. 36, 1171 (1962).

30. Estrup, P. J. and J. Anderson — J. Chem. Phys. 46, 567 (1967).

31. Winters, H. F. and D. E. Horne, — Surface Sci. 24, 587 (1971).

32. Rigby, L. J. — Can. J. Phys. 42, 1256 (1964).

33. Becker, J. A. and C. D. Hartman — J. Phys. Chem. 57, 153 (1953).

34. van Oostrom, A. — J. Chem. Phys. 47, 761 (1967).

35. Ehrlich, G. and F. G. Hudda — J. Chem. Phys. 44, 1039 (1966).

36. Ehrlich, G. and F. G. Hudda. J. Chem. Phys. 30, 493 (1959).

37. Hickmott, T. W. J. Chem. Phys. 32, 810 (1960).

38. Johnson, R. P. Phys. Rev. 54, 459 (1938).

39. Roberts, J. K. Proc. Camb. Phil. Soc. 34, 399 (1938).

40. Roberts, J. K. "Some Problems in Adsorption" Camb. Univ. Press (1939).

41. Rossington, D. R. and E. Borst. Surface Sci. 3, 202 (1965).

42. Dowden, D. A. "Chemisorption", Ed. W. E. Garner (Butterworth, London, 1958) p.9.

43. Boudart, M. J. Am. Chem. Soc. 74, 3556 (1952).

44. Mignolet, J. C. P. Bull. Soc. Chim. Belg. 64, 126 (1955).

45. Yates, J. T. Jr. and T. E. Madey. J. Chem. Phys. 54, 4969 (1971).

46. Tamm, P. W. and L. D. Schmidt. J. Chem. Phys. 54, 4775 (1971).

47. Higuchi, I., T. Ree and H. Eyring. J. Am. Chem. Soc. 77, 4969 (1955).

48. deBoer, J. H. "Electron Emission and Adsorption Phenomena", Cambridge (1935).

49. Madey, T. E. and J. T. Yates, Jr., Nuvo Cimento Supplimento 5, 483 (1967).

50. Estrup, P. J. and J. Anderson J. Chem. Phys. 46, 567 (1967).

51. Schmidt, L. D. and R. Gomer J. Chem. Phys. 45, 1605 (1966).

52. Pauling, L. "The Nature of the Chemical Bond" (Cornell U.P., Ithaca, N.Y., 1960) 3rd. ed. p.224.

53. Ehrlich, G. J. Chem. Phys. 34, 29 (1961).

54. Tracy, J.C. and J. M. Blakely Surface Sci. 13, 313 (1968).